W72-12041

CLEAN WATER
WATER POLLUTION CONTROL RESEARCH SERIES ● 16060 ELJ 03/72

PB 211 298

DENSITY INDUCED MIXING IN CONFINED AQUIFERS

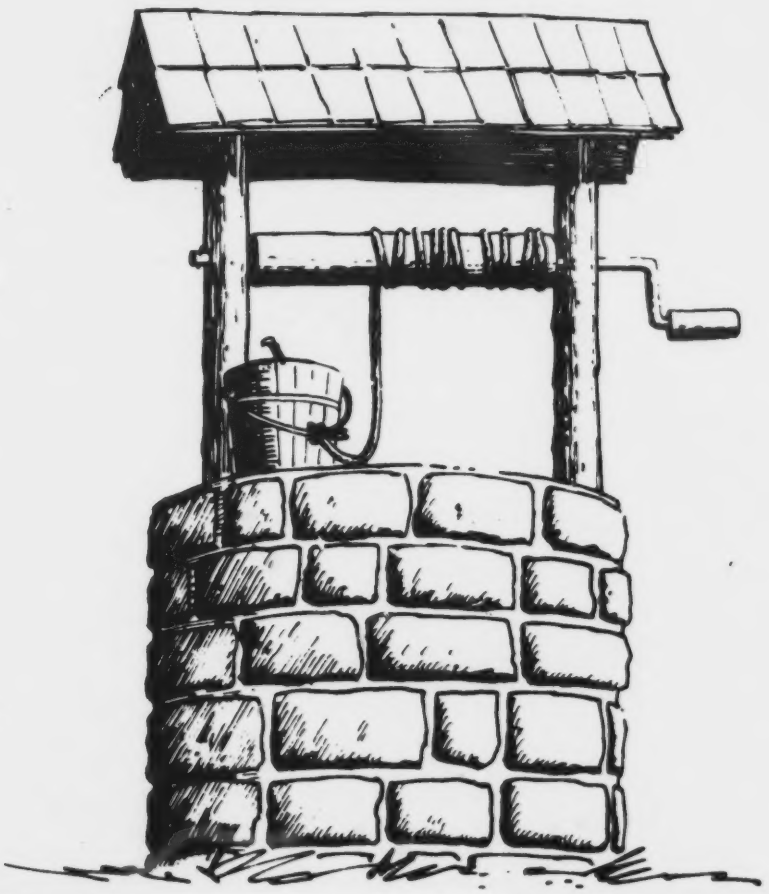

NATIONAL TECHNICAL
INFORMATION SERVICE

U.S. ENVIRONMENTAL PROTECTION AGENCY

131

WATER POLLUTION CONTROL RESEARCH SERIES

The Water Pollution Control Research Series describes the results and progress in the control and abatement of pollution in our Nation's waters. They provide a central source of information on the research, development, and demonstration activities in the water research program of the Environmental Protection Agency, through in-house research and grants and contracts with Federal, state, and local agencies, research institutions, and industrial organizations.

Inquiries pertaining to Water Pollution Control Research Reports should be directed to the Chief, Publications Branch (Water), Research Information Division, R&M, Environmental Protection Agency, Washington, D. C. 20460

SELECTED WATER RESOURCES ABSTRACTS
INPUT TRANSACTION FORM

1. Report No. W 72-12041

DENSITY INDUCED MIXING IN CONFINED AQUIFERS,

5. Report Date

8. Performing Organization Report No.

Gelhar, L. W., Wilson, J. L., Miller, J. S., and Hamrick, J. M.

Massachusetts Institute of Technology, Cambridge, Ralph M. Parsons Lab. for Water Resources and Hydrodynamics

EPA 16060ELJ 03/72

13. Type of Report and Period Covered

Environmental Protection Agency, Water Pollution Control Research Series, ~~Project Report 16060ELJ~~, 1972. 130 p, 36 fig, 7 tab, 28 ref, 3 append.

Analytical techniques are given to describe the mixing of two fluids of different density in a confined aquifer, in which one fluid is introduced to the aquifer by well recharge. The immiscible displacement process in both linear and radial flows is analyzed and the effects of longitudinal and lateral dispersion are included using a boundary layer approximation. Hydrodynamic dispersion retards gravity segregation due to density differences. During recharge excellent agreement between the theoretical predictions and experimental results was found and the predicted retarding effects of longitudinal dispersion was verified. During withdrawal some systematic differences between the theory and observation were noted. Theoretical predictions of recovery efficiency during a recharge-storage-withdrawal sequence show trends similar to those observed but are typically 5% to 10% lower than those observed. Direct theoretical predictions of recovery efficiency during single or multiple sequences of recharge-storage-withdrawal were developed for an immiscible system, and similar developments outlined for miscible displacement. (Knapp-USGS)

*Mixing, *Dispersion, *Path of pollutants, *Waste disposal wells, Density stratification, Injection wells, Stratified flow, Artificial recharge, Hydraulic models, Confined water, Artesion aquifers,

EB2.10:16060 ELJ 03/72

Copy available from GPO Sup Doc [redacted] ; microfiche from NTIS as PB , $0.95.

02F, 05B

17. Security Class. Report

21. No. of Pages

Send To:
WATER RESOURCES SCIENTIFIC INFORMATION CENTER
U S DEPARTMENT OF THE INTERIOR
WASHINGTON D C 20240

G. Knapp, 8/3/72

U.S. Geol. Survey, Water Res. Div.

DENSITY INDUCED MIXING IN CONFINED AQUIFERS

by

L. W. Gelhar
J. L. Wilson
J. S. Miller
J. M. Hamrick
Ralph M. Parsons Laboratory for Water Resources and Hydrodynamics
Department of Civil Engineering, Massachusetts Institute of Technology
Cambridge, Massachusetts 02139

for the

Office of Research and Monitoring

ENVIRONMENTAL PROTECTION AGENCY

Project #16060 ELJ

March 1972

EPA Review Notice

This report has been reviewed by the Environmental Protection Agency and approved for publication. Approval does not signify that the contents necessarily reflect the views and policies of the Environmental Protection Agency, nor does mention of trade names or commercial products constitute endorsement or recommendation for use.

ABSTRACT

Analytical techniques are developed to describe the mixing between two fluids of different density in a confined aquifer, in which one fluid is introduced to the aquifer by well recharge. The immiscible displacement process in both linear and radial flows is analyzed and the effects of longitudinal and lateral dispersion are included using a boundary layer approximation. The theoretical results demonstrate the effect of hydrodynamic dispersion in retarding gravity segregation due to density differences.

The theoretical results are compared with observations of aquifer mixing in linear and radial flow laboratory models. During recharge excellent agreement between the theoretical predictions and experimental results is found and the predicted retarding effects of longitudinal dispersion are verified. During withdrawal some systematic differences between the theory and observation are noted. Theoretical predictions of recovery efficiency during a recharge-storage-withdrawal sequence show trends similar to those observed but are typically 5 to 10% lower than those observed.

Direct theoretical predictions of recovery efficiency during single or multiple sequences of recharge-storage-withdrawal are developed for an immiscible system, and similar developments outlined for miscible displacement. The results are suggested for use in developing preliminary estimates of operating conditions in the field.

This report was submitted in fulfillment of Project Number 16060ELJ under the sponsorship of the Office of Research and Monitoring, Environmental Protection Agency.

CONTENTS

Section		Page
	Conclusions	1
	Recommendations	3
1	Introduction	5
2	Analysis of Density Induced Mixing in Linear Flow	9
3	Analysis of Density Induced Mixing in Radial Flow	31
4	Linear Flow Experiments	71
5	Radial Flow Experiments	79
	Acknowledgments	111
	References	113
	Definition of Symbols	117
	Appendices	121

Preceding page blank

FIGURES

Figure	Title	Page
2.1	Definition Sketch for Linear Flow	10
2.2	Comparison of One-Dimensional Concentration Model	10
2.3	Theoretical Horizontal Interface Projection for Linear Flow	23
2.4	δ/L as a Function of Time for the Case of No Dynamic Effects of Grain Dispersion	25
2.5	δ/L as a Function of Time for Interaction between Grain Dispersion and Density Induced Mixing	26
2.6	$g(L/\delta)$ for One-Dimensional Linear Flow	29
2.7	Total Dispersion Coefficient, E_t, as a Function of Time for Linear Flow	29
3.1	Definition Sketch of a Radial Confined Aquifer	32
3.2	Comparison of Interface Shapes for Various Values of ε_r During a Recharge Operation	37
3.3	Inverse Interface Slope, β, as a Function of Time During Recharge	56
3.4	Inverse Rate of Change of Relative Concentration, Δt, as a Function of Time During Recharge	57
3.5	$\Delta/\beta H$ as a Function of Time During Recharge for the Case of no Dynamic Effects of Grain Dispersion	59
3.6	$\Delta/\beta H$ as a Function of Time During Recharge for the Case of Interaction between Grain Dispersion and Density Induced Mixing	62
3.7	Sketch of the Interface at the End of Withdrawal	66
3.8	Recovery Ratio, R, as a Function of ε_r and ε_w ($t_s=0$)	66
4.1	View of the Linear Sand Box Model	72
4.2	Horizontal Projection of Interface, L, as a Function of Time	75

Preceding page blank

Figure	Title	Page
4.3	A Typical Linear Flow Experimental Breakthrough Curve Compared with Theory	77
5.1	View of the Radial Model	80
5.2	Photographs of the Radial Model in Operation	81
5.3	Location of Conductivity Probes	83
5.4	Detail of Well Construction	85
5.5	Calibration of Averaging Conductivity Probes	88
5.6	Media Dispersivity Calculated from the Averaging Probes	93
5.7	Piezometric Head Distribution in Radial Model	94
5.8	Comparison of Visual and Electronic Measurement of the Interface with the Immiscible Theory	97
5.9	Comparison of Theory and Experimental Time Dependent Concentration Slopes During Recharge	99
5.10	Volumetric Length of the Interface, $\beta H = \Delta W$, as a Function of Time	100
5.11	Comparison of the Coupled Theory and Experimental Time Dependent Concentration Slopes During Recharge	101
5.12	Experimental Breakthrough Curves at the Well	103
5.13	Experimental Breakthrough Curves During Recharge and Withdrawal	104
5.14	Comparison of Experimental and Theoretical Breakthrough Curves During Recharge	105
5.15	Comparison of Experimental and Theoretical Breakthrough Curves During Recharge	105
5.16	Comparison of Experimental and Theoretical Breakthrough Curves During Withdrawal	105
5.17	Δt as a Function of Time During a Recharge-Storage-Withdrawal Sequence, Run A-2	106
5.18	Δt as a Function of Time During a Recharge-Storage-Withdrawal Sequence, Run A-7	106

TABLES

Table	Title	Page
3.1	Summary of Equations Applicable to a Recharge, Storage, Withdrawal Operation	69
4.1	Range of Test Results for the Linear Model	76
5.1	Radial Model Horizontal Hydraulic Conductivity	89
5.2	Determination of Dispersivity from Averaging Probes	92
5.3	Experimental Conditions for the Radial Model	96
5.4	Observed Values of $-Q\Delta t/V_o$ during Withdrawal	108
5.5	Comparison of Theoretical Recovery Ratios with Experiments	109

CONCLUSIONS

1. Analytical techniques have been developed to describe the combined effects of density difference and hydrodynamic dispersion on mixing in linear and radial flows in confined aquifer systems. The theoretical results demonstrate the retarding effects that dispersion may have on the rate of tilting of the interface. The roles of both lateral and longitudinal dispersion in the mixing are established.

2. Laboratory experiments with linear and radial flow aquifer models confirm several aspects of the theoretical developments. During recharge operations the predictions are found to be in excellent agreement with the observed interface tilting. In most of the recharge experiments, the interface motion is dominated by immiscible dynamics but some experiments confirm the predicted retarding effects of hydrodynamic dispersion. However, during withdrawal there are significant differences between the observed and predicted interface motion. Predictions of recovery ratios showed trends similar to those observed although the predicted values were typically 5 to 10 percent lower.

3. Direct application of the analytical results in the evaluation of field operations is feasible. The results of the immiscible theory (Eq. 3.119) provide conservative estimates of the recovery ratio for a recharge-storage-withdrawal sequence in terms of aquifer and fluid properties and flow rates. Multiple recharge-storage-withdrawal sequences can be treated and improved recovery efficiency is found after a few sequences. Conditions under which dispersive effects become important can be evaluated (see Section 3.4) and these effects can be included using the computational procedure developed in Section 3.5.

RECOMMENDATIONS

1. Several additional factors of importance in field situations should be considered in future analytical and experimental studies; these include partially penetrating wells, phreatic aquifers, sloping and multilayered aquifers, and ambient flow in the aquifer.

2. Analytical or numerical solution techniques should be developed to evaluate the implicit limitations of the proposed analytical models; these should include evaluation of the effects of interface curvature during the storage and withdrawal cycles and influence of no-flux boundary conditions at the aquifer boundaries.

3. Field experiments are suggested for further evaluation of the proposed analytical techniques. This involves the development of a series of experiments in which breakthrough curves are observed at several monitoring wells and at the recharge-pumping well during a recharge-storage-withdrawal sequence. The hydraulic conductivity and dispersivity of the aquifer should be determined as part of the experimental program.

Preceding page blank

1. INTRODUCTION

1.1 General Discussion

The pressures of population and economic growth lead inevitably to problems in water resource management. One method of trying to optimize present water resources to keep up with growth involves the utilization of ground water aquifers for storage or disposal of surface or waste waters. During periods of the year when there is excess surface water available, it can be pumped into aquifers through wells for storage and use during dry periods. This use of underground aquifers for water storage is attractive because of the scarcity of natural reservoir sites, the low initial costs compared to ordinary surface reservoir construction, the elimination of evaporative losses, and the possibility of partial purification of the stored water during its passage through the aquifer.

These storage schemes can be used to either mix and dilute contaminated surface waters with naturally occuring ground water, or for storage of surface water of high quality in an aquifer initially containing water of lower quality. This latter case in which fresh water is stored, for example, in a saline aquifer could find wide application in the United States where one third of the land area has saline ground water less than 500 feet below the land surface (see Kohout, 1970). Moulder (1970) has reported field studies on the recharge of saline aquifers with fresh water and has suggested specific geographic areas where this scheme may be feasible.

Ground water aquifers are also finding wide use for disposal of liquid wastes and the trend is toward increased use of aquifers for this purpose. The number of industrial waste injection wells, for example, increased from close to 100 in 1967 to nearly 150 in 1969 (see Kohout, 1970). In addition to the disposal of normal wastes, ground water aquifers can also be used to dispose of thermally polluted waters.

When surface water is introduced into an aquifer, mixing occurs with the native ground water. Usually the surface water and native ground water differ in physical, chemical, and biological characteristics. In designing and operating recharge or disposal systems, it becomes necessary to predict and control, as much as possible, the amount of mixing between the injected and native waters.

The mixing in the aquifer is caused by the large scale convective motion of the native ground water as well as the flow from wells during recharge, disposal, or recovery. Further mixing is due to hydrodynamic dispersion which includes the effects of molecular diffusion as well as what may be termed grain dispersion. Grain dispersion is caused by the velocity variation of the fluid flowing along different paths within the pore structure of the medium. A final mixing process comes about because of differences in the physical properties of the native and injected waters. Differences in density may be a significant cause of mixing due to gravity currents

Preceding page blank

that develop. The resulting convective motion increases mixing in the aquifer. The storage of fresh surface water in saline aquifers is an example where density induced mixing is important.

1.2 Review of Previous Work

Considerable work has been done on hydrodynamic dispersion and its effects on the mixing of miscible fluids flowing in porous media. Schiedegger (1961) and Bear and Bachmat (1964) theorized a linear relationship between the dispersion tensor and the velocity of flow through porous media. Harleman and Rumer (1963) and List and Brooks (1967) gave experimental evidence that some nonlinearity between the velocity and dispersion coefficient may exist. Studies by Li and Yeh (1968) indicated that differences in viscosity and density have little or no effect on the local mixing due to dispersion at the interface. More recently Gelhar and Collins (1971) developed an analytical solution that describes the concentration of a substance at a particular radius for flow from a well. Numerical solutions of the dispersion equation have been developed by Shamir and Harleman (1967), Reddell and Sunada (1971), and Guymon, Scott, and Hermann (1970). Rose and Passioura (1971) showed that current methods for calculating the coefficient of hydrodynamic dispersion during lab tests may be profoundly affected by even seemingly negligible density differences between the original fluid and the fluid used as a tracer during tests. Furthermore Theis (1967) and Mercado (1967), demonstrated that field determinations of dispersion coefficients may be several orders of magnitude greater than those indicated by laboratory tests because of the large scale heterogeneity of natural deposits. These factors should be considered when studying and applying results from tests on hydrodynamic dispersion in the laboratory.

There has also been extensive work done on salt water intrusion in coastal aquifers. Dispersion and density induced mixing are both important in the study of salt water intrusion. Henry (1960) studied the combined effects of gravity and dispersive mixing for a steady saline wedge in a confined aquifer. Rumer and Harleman (1963) studied the effects of tidal motion on interfacial dispersion. Bear and Dagan (1964) developed an approximate analysis of the unsteady movement of a salt water wedge due to a change in the fresh water flow. They compared their results with model experiments. Shamir and Dagan (1971) developed numerical solutions for the motion of the seawater interface in coastal aquifers.

There have been a few investigations of dispersion and density induced mixing more directly related to this paper. Esmail and Kimbler (1967) and Kumer and Kimbler (1970) studied the possibility of storing fresh water in saline aquifers. Their work was derived from an "ad hoc" assumption of extending results based on the rate of interfacial tilting in a linear model with no net flow to radial flow from a well using a numerical procedure which was not explicitly described in the papers. Although their procedure involves this extrapolation from linear to radial flow, they did report good agreement between their numerical

simulations and data collected in a three dimensional radial flow model. Perrine and Gay (1964) developed numerical solutions of the problem of density induced motion during radial flow from a well with density and viscosity difference between the two fluids. Their solutions did not take into account hydrodynamic dispersion at the interface, and no comparison was made between their theory and experimental or field data.

Green and Cox (1968) developed numerical solutions of the equations of motion and mass conservation based on the method of characteristics. They analyzed miscible displacement of fluids with different density and equal viscosity in a linear model using constant dispersion coefficients in a numerical scheme. Results of the numerical analysis were compared with those from a laboratory model. Keulegan (1954) and Gardner, Downie, and Kendall (1962) reported experiments on the tilting of the interface between fluids of different density in linear laboratory models with no net flow. De Josselin de Jong (1960) developed the potential flow solution for the initial motion of a vertical interface in a linear model with no discharge. Gardner, Downie, and Kendall (1962) have also used the immiscible approximation to develop analytical descriptions of interface tilting for small and large times under conditions of no net flow.

1.3 Objectives and Scope

The primary objective of this study is to investigate the effects of hydrodynamic dispersion and density stratification on mixing in ground water systems. Of particular interest is the mixing process which occurs when a fluid whose density differs from that of the native fluid is injected into a confined aquifer. These mixing phenomena can be important in applications involving the storage of fresh water in saline aquifers or deep-well waste disposal. Methods of evaluating and predicting these mixing phenomena under field conditions are sought.

The general approach includes the development of analytical models which describe the effects of density differences and dispersion for two flow configurations. A series of laboratory experiments in also developed to evaluate the analytical predictions.

The analytical methods are first developed for mixing in a linear flow with a constant net convective velocity, and later extended to mixing in a radial flow well system. Initially, the theoretical analyses are based on immiscible displacement for the case of fluids with different density and equal viscosity. The effect of dispersion on the density induced tilting of the interface and the overall mixing is then analyzed theoretically using boundary layer type approximations. From this analysis it is possible to determine when dispersion will influence the interface tilting and the overall mixing. The analyses also reveal the conditions under which longitudinal or lateral dispersion will dominate the dispersive mixing and influence the interface tilting. The relative importance of grain dispersion and density induced mixing is characterized by a dimensionless parameter for both flow regimes.

Based on the results of the linear flow analysis, a concept of gross dispersion due to density difference is introduced and a total dispersion coefficient representing both density and grain dispersion is also derived.

The radial flow system is analyzed for the three processes of recharge, storage and withdrawal. The results are used to simulate multiple sequences of recharge, storage and withdrawal.

The results of laboratory experiments designed to evaluate the theoretical developments are presented. The linear flow case is simulated in a horizontal linear sand model. In the radial flow case a 15° radial sector model of consolidated plastic beads was constructed. Interfacial tilting and gross mixing were measured by visual and electronic means.

The application of the theoretical results to field operations is considered and predictions of recovery efficiency in a recharge-storage-withdrawal operation are developed.

2. ANALYSIS OF DENSITY INDUCED MIXING IN LINEAR FLOW

The objective in this section is to develop methods of analysis which can be used to describe the combined effects of dispersion and gravity segregation on aquifer mixing. The flow configuration considered here is a one-dimensional displacement in a confined system with horizontal boundaries, i.e., a linear flow. A theoretical analysis of immiscible displacement in a model with a net flow is developed for the case of fluids with different density but equal viscosity. Based on this analysis, a new concept of gross dispersion due to density differences is introduced. Using boundary layer approximations, the effects of grain dispersion on the tilting of the interface and the overall mixing are analyzed. The effects of both longitudinal and lateral dispersion are included in the analysis. In Section 3, these same concepts and methods of analysis are extended to the case of the radial flow system.

2.1 Immiscible Displacement in a Confined Aquifer of Constant Thickness

The problem of mixing of two liquids of different density in a homogeneous, confined aquifer may be simplified by neglecting grain dispersion and molecular diffusion. In such a case, the mixing process is described by an immiscible displacement model. Consider the displacement of a heavier liquid with density ρ_2, by a lighter liquid with density ρ_1, in a horizontal confined aquifer of constant thickness H (see Figure 2.1). If the two liquids have approximately the same kinematic viscosity, ν, (i.e., fresh and salt water), the hydraulic conductivity, K, may be taken as a constant throughout the flow.

The following analysis is based on the Dupuit approximation, which assumes hydrostatic pressure distributions and thus essentially horizontal flow. The analysis is strictly correct only when the interface slope is small and hence the vertical velocities are small.

The continuity equations for the two liquids are:

$$\frac{\partial}{\partial x}(u_1 \zeta) = - \frac{\partial \zeta}{\partial t} \tag{2.1}$$

$$\frac{\partial}{\partial x}(u_2 \eta) = - \frac{\partial \eta}{\partial t} \tag{2.2}$$

where ζ is the distance to the interface, in liquid 1, measured from the top of the aquifer, and η is the distance to the interface, in liquid 2, measured from the bottom of the aquifer. The seepage velocities of the two liquids, u_1 and u_2, are given by the Darcy equations for the two liquids,

$$u_1 = - \frac{K}{n} \frac{\partial \phi_1}{\partial x} \tag{2.3}$$

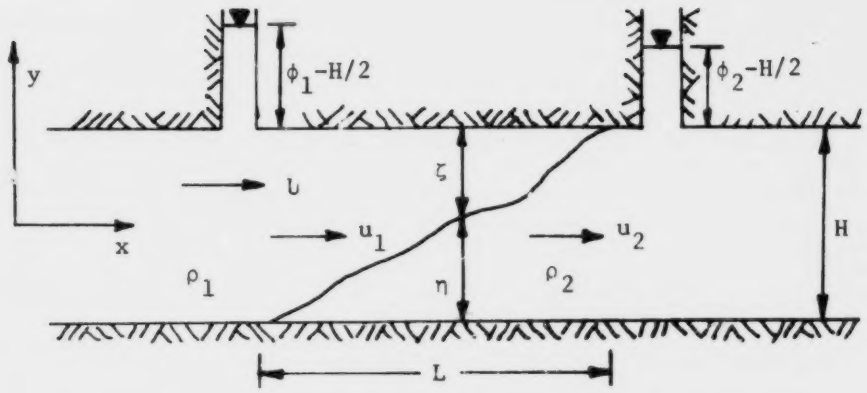

Figure 2.1 Definition Sketch for Linear Flow

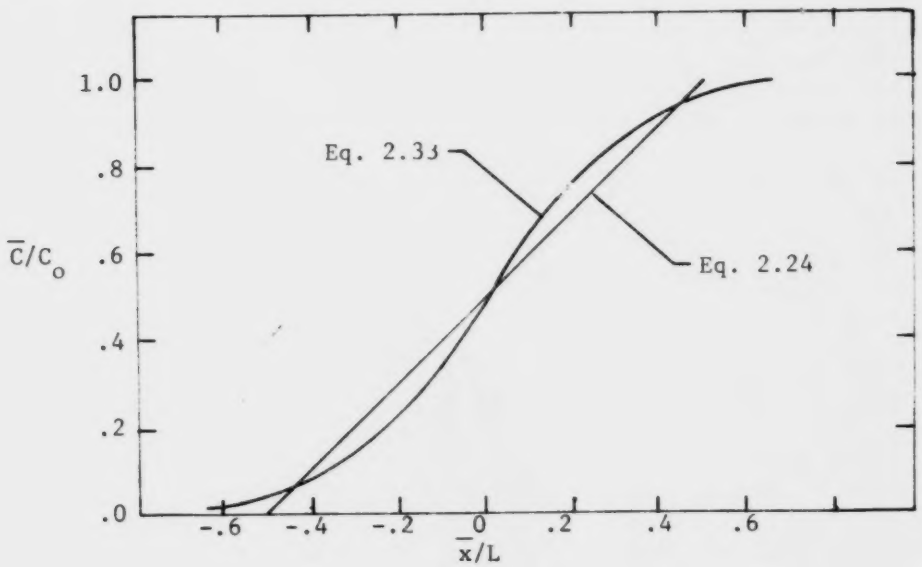

Figure 2.2 Comparison of One-Dimensional Concentration Models

$$u_2 = - \frac{K}{n} \frac{\partial \phi_2}{\partial x} \tag{2.4}$$

Vertical velocities are neglected due to the Dupuit approximation. The porosity of the aquifer is n, and the piezometric heads of the two liquids are ϕ_1 and ϕ_2. Along the interface, the fluid pressure must be continuous. The pressure continuity equation is

$$\phi_2 = \frac{\rho_1}{\rho_2} \phi_1 - \frac{\Delta\rho}{\rho_2} (\zeta - H/2) \tag{2.5}$$

$$\Delta\rho = \rho_2 - \rho_1$$

If the density difference, $\Delta\rho$, is small compared to ρ_2, and the relative density difference is identified by $\Delta\rho/\rho_2 \equiv \Delta\rho/\rho$, Eq. (2.5) becomes

$$\phi_2 = \phi_1 - \frac{\Delta\rho}{\rho} (\zeta - H/2) \tag{2.6}$$

The continuity equation for the entire flow is obtained by adding Eqs. (2.1) and (2.2) and integrating

$$u_1 \zeta + u_2 \eta = UH \tag{2.7}$$

The convection of the interface through the aquifer is due to the net seepage velocity, U.

The solution of the problem consists of determining the interface shape and location, and determining the velocities in the two liquids. Substituting Eqs. (2.3) and (2.4) into Eq. (2.7) gives,

$$\frac{\partial \phi_1}{\partial x} \zeta + \frac{\partial \phi_2}{\partial x} \eta = - \frac{nUH}{K} \tag{2.8}$$

Differentiating Eq. (2.6) and substituting into Eq. (2.8) and simplifying the results using $\zeta + \eta = H$, gives

$$\frac{\partial \phi_1}{\partial x} = - \frac{nU}{K} - \frac{\Delta\rho}{\rho} \frac{\eta}{H} \frac{\partial \eta}{\partial x} \tag{2.9}$$

Substituting Eq. (2.3) into Eq. (2.1) and eliminating ζ using $\zeta = H - \eta$ gives

$$- \frac{\partial}{\partial x} \left[\frac{K}{n} \frac{\partial \phi_1}{\partial x} (H - \eta) \right] = \frac{\partial \eta}{\partial t} \tag{2.10}$$

The partial differential equation for η is obtained by substituting Eq. (2.9) into Eq. (2.10).

$$\frac{\partial \eta}{\partial t} + U \frac{\partial \eta}{\partial x} = \frac{K}{n} \frac{\Delta \rho}{\rho} \frac{\partial^2}{\partial x^2} \left(\frac{\eta^2}{2} - \frac{\eta^3}{3H} \right) \tag{2.11}$$

Introducing a convected coordinate $\bar{x} = x - Ut$, Eq. (2.11) is simplified to

$$\frac{\partial \eta}{\partial t} = \frac{K}{n} \frac{\Delta \rho}{\rho} \frac{\partial}{\partial \bar{x}^2} \left(\frac{\eta^2}{2} - \frac{\eta^3}{3H} \right) \tag{2.12}$$

Equation (2.12) may be reduced to an ordinary differential equation using a similarity transformation.

$$\frac{\eta}{H} = F\left(\frac{\bar{x}}{H\sqrt{\tau}} \right) = F(z) \tag{2.13}$$

$$\tau = \frac{K}{n} \frac{\Delta \rho}{\rho} \frac{t}{H} \tag{2.14}$$

The resulting ordinary differential equation in z, the similarity variable, is

$$-\frac{z}{2} \frac{dF}{dz} = \frac{d^2}{dz^2} \left(\frac{F^2}{2} - \frac{F^3}{3} \right) \tag{2.15}$$

Equation (2.15) is solved for an initially vertical interface by assuming a power series in z, to give

$$\eta = \frac{1}{2} \left(H + \frac{\bar{x}}{\sqrt{\tau}} \right) \tag{2.16}$$

This solution may not apply for small times, when the interface slope is large and vertical velocities are not negligible.

The expression for the velocity in liquid 1 is obtained using Eqs. (2.3) and (2.9).

$$u_1 = U + \frac{K}{n} \frac{\Delta \rho}{\rho} \frac{\eta}{H} \frac{\partial \eta}{\partial x} \tag{2.17}$$

Using Eqs. (2.4), (2.6) and (2.9) the expression for the velocity in liquid 2 is obtained.

$$u_2 = U - \frac{K}{n}\frac{\Delta\rho}{\rho}\left(1 - \frac{\eta}{H}\right)\frac{\partial\eta}{\partial x} \tag{2.18}$$

From Eq. (2.16), the horizontal projection of the interface, L, is

$$L = 2H\sqrt{\frac{K}{n}\frac{\Delta\rho}{\rho}\frac{t}{H}} = 2H\sqrt{\tau} \tag{2.19}$$

The position of the interface is given by x_i, the distance to the interface from the x origin.

$$x_i = Ut + \frac{L}{H}y \tag{2.20}$$

Results of Eq. (2.16) indicate that the interface is a straight line, of decreasing slope, which is convected through the aquifer with a velocity U. The solution is also valid for the case of no through flow, U = 0.

If the density difference is due to the presence of some material in solution (i.e., salt), and the density is a linear function of the concentration of the material, c, then

$$\rho = \rho_1 + \Delta\rho\,\frac{c}{c_o} \tag{2.21}$$

The concentration of material in liquid 2 is c_o. To obtain a one-dimensional description of the variation of the liquid density, the concentration, c, is averaged over the aquifer thickness.

$$\bar{c} = \frac{1}{H}\int_{-\frac{H}{2}}^{\frac{H}{2}} c\,dy \tag{2.22}$$

Using the indicated concentration distribution,

$$\begin{aligned} c &= c_o \quad , -\frac{H}{2} \le y \le -\left(\frac{H}{2} - \eta\right) \\ c &= 0 \quad , -\left(\frac{H}{2} - \eta\right) \le y \le \frac{H}{2} \end{aligned} \tag{2.23}$$

The average concentration is

$$\bar{c} = c_o \frac{\eta}{H} = \frac{c_o}{L} \left(\bar{x} + \frac{L}{2} \right) \tag{2.24}$$

which indicates a linear distribution of average liquid density,

$$\bar{\rho} = \rho_1 + \Delta\rho \frac{\bar{c}}{c_o} \tag{2.25}$$

The average flux of dissolved material with respect to the convected coordinate system $(\bar{x},y)$ is

$$\bar{J} = \frac{1}{H} \int_{-\frac{H}{2}}^{\frac{H}{2}} \rho c \bar{u} \, dy \tag{2.26}$$

$$\bar{u} = u - U$$

which is evaluated, using Eqs. (2.18) and (2.23), as

$$\bar{J} = - c_o \rho_2 \frac{K}{n} \frac{\Delta\rho}{\rho} \left(1 - \frac{\eta}{H}\right) \frac{\eta}{H} \frac{\partial \eta}{\partial x} \tag{2.27}$$

Using Eq. (2.24), Eq. (2.27) is modified to the form

$$\bar{J} = - \rho_2 \frac{K}{n} \frac{\Delta\rho}{\rho} \left(1 - \frac{\eta}{H}\right) \eta \frac{\partial \bar{c}}{\partial x} \tag{2.28}$$

For a dispersive mixing process, the flux is related to the concentration gradient through a dispersion coefficient, E, as follows

$$\bar{J} = - \bar{\rho} E \frac{\partial \bar{c}}{\partial x} \tag{2.29}$$

The dispersion coefficient can thus be evaluated by equating Eqs. (2.28) and (2.29) as

$$E = \frac{K}{n} \frac{\Delta\rho}{\rho} \left(1 - \frac{\eta}{H}\right) \eta \tag{2.30}$$

for $\rho_2 \cong \bar{\rho}$. The result of Eq. (2.30) suggests that the gross characteristics of density induced mixing may be approximated by the one-dimensional dispersion equation of the form

$$\frac{\partial \bar{c}}{\partial t} + U \frac{\partial \bar{c}}{\partial x} = E_1 \frac{\partial^2 \bar{c}}{\partial x^2} \qquad (2.31)$$

where E_1 is a constant dispersion coefficient. Although Eq. (2.30) implies a parabolic distribution of the dispersion coefficient, E, over the length of the interfacial zone, satisfactory results can be obtained by using the average value.

$$E_1 = \bar{E} = \frac{H}{6} \frac{K}{n} \frac{\Delta\rho}{\rho} \qquad (2.32)$$

This dispersion coefficient, which characterizes the mixing due to density differences, will be identified as the density dispersion coefficient. This expression for $\bar{E}$ is later used to estimate the importance of the effect of the density difference on the mixing process.

The longitudinal distribution of average concentration can thus be determined approximately by solving Eq. (2.31) subject to the initial condition

$$t = 0 \quad \bar{c} = c_o \quad x>0$$

$$\bar{c} = 0 \quad x<0$$

which corresponds to an initially vertical interface at the origin x = 0. The solution is

$$\frac{\bar{c}}{c_o} = \frac{1}{2} + \frac{1}{2} \operatorname{erf}\left(\frac{x-Ut}{\sqrt{4Et}}\right) \qquad (2.33)$$

A comparison of this one-dimensional approximation with the exact result from Eq. (2.24) is shown in Figure 2.2.

In many field situations, it is the average water quality, over the aquifer thickness, which is of importance. If the mixing process is assumed to be due only to the density difference between the mixing liquids, the one-dimensional model represented by Eq. (2.33) will approximately describe the mixing process, and predict the depth-averaged water quality. The concept of a one-dimensional dispersion model to represent a two-dimensional density induced mixing process is an important simplification of this phenomenon.

2.2 Grain Dispersion Effects

The immiscible displacement model is an idealization, since there is always some degree of interfacial dispersion. The objective here is to estimate the importance of grain dispersion in comparison to the density

induced mixing.

The validity of the assumption of immiscible displacement depends on the magnitude of the density difference $\Delta\rho$. In certain cases the density difference will be large enough to completely govern the dynamics of the mixing, (i.e., the velocity field is that predicted by the immiscible model); however, the resulting model may not adequately describe the variation of density near the interface. To obtain a better description of the density variation, grain dispersion must be considered.

The mass conservation equation which describes the distribution of solute concentration c in a porous medium is [Bear, et al, 1968]

$$\frac{\partial c}{\partial t} + u \frac{\partial c}{\partial x} + v \frac{\partial c}{\partial y} = \frac{\partial}{\partial x} \left(D_1 \frac{\partial c}{\partial x}\right) + \frac{\partial}{\partial y} \left(D_2 \frac{\partial c}{\partial y}\right) \tag{2.34}$$

where u and v are the horizontal and vertical seepage velocities respectively, and D_1 and D_2 are the longitudinal and lateral dispersion coefficients respectively. To simplify the solution of Eq. (2.34), the following assumptions are made.

(i) The dispersion coefficients, D_1 and D_2, are generally velocity dependent, but for this analysis the velocity changes are assumed small and D_1 and D_2 are taken as constants and proportional to the net seepage velocity U.

(ii) The vertical convective transport may be neglected when the Dupuit approximation, which assumes negligible vertical velocities, is applicable.

(iii) The convective velocity in the dispersed region can be approximated by the velocity of the interface as determined by Eq. (2.20).

$$u \cong u_i = \frac{\partial x_i}{\partial t} \tag{2.35}$$

The interface is idealized as the line of 50% concentration.

The three assumptions simplify Eq. (2.34) to give,

$$\frac{\partial c}{\partial t} + u_i \frac{\partial c}{\partial x} = D_1 \frac{\partial^2 c}{\partial x^2} + D_2 \frac{\partial^2 c}{\partial y^2} \tag{2.36}$$

and the interface location is as given by Eq. (2.20). The interface slope, S, and its reciprocal, β, are defined as

$$\frac{L}{H} = \frac{1}{S} = \beta \tag{2.37}$$

Equation (2.20) is rewritten as

$$x_i = Ut + \beta y \tag{2.38}$$

The following coordinate transformation will be used:

$$x_1 = x - x_i(y,t) \tag{2.39}$$

Expressing the concentration c as a function of x_1, y, t, Eq. (2.36) becomes

$$\left.\frac{\partial c}{\partial t}\right|_{x_1,y} = D_1 \frac{\partial^2 c}{\partial x_1^2} + D_2\left[\left.\frac{\partial^2 c}{\partial y^2}\right|_{x_1,t} - 2\beta \frac{\partial}{\partial x_1}\left(\left.\frac{\partial c}{\partial y}\right|_{x_1,t}\right) + \beta^2 \frac{\partial^2 c}{\partial x_1^2}\right]$$

Since the lines x_1 = constant are parallel with the interface, it is reasonable to assume that

$$\left.\frac{\partial c}{\partial y}\right|_{x_1,t} = 0$$

which can be verified from the results (Eq. 2.44). The convective dispersion equation then reduces to

$$\frac{\partial c}{\partial t} = (D_1 + \beta^2 D_2) \frac{\partial^2 c}{\partial x_1^2} \tag{2.40}$$

Introducing another coordinate transformation

$$\xi = \int_0^t (D_1 + \beta^2 D_2)\, dt \tag{2.41}$$

the coefficient in Eq. (2.40) is eliminated and

$$\frac{\partial c}{\partial \xi} = \frac{\partial^2 c}{\partial x_1^2} \tag{2.42}$$

The initial conditions corresponding to a vertical interface at the origin x = 0, are

$$\begin{aligned} t = 0 \quad & c = c_o \quad x>0 \\ & c = 0 \quad x<0 \end{aligned} \tag{2.43}$$

The solution of Eq. (2.42) subject to these conditions is

$$\frac{c}{c_o} = \frac{1}{2} + \frac{1}{2}\,\mathrm{erf}\left(\frac{x_1}{\sqrt{4\xi}}\right) \tag{2.44}$$

If the dynamics of the mixing are given by the immiscible displacement model, β is given by Eq. (2.19), and hence ξ may be determined. From Eqs. (2.19) and (2.41),

$$\beta = 2\sqrt{\tau}$$

$$\xi = D_1 t + 2D_2 \tau\, t \tag{2.45}$$

$$\frac{c}{c_o} = \frac{1}{2} + \frac{1}{2}\,\mathrm{erf}\left(\frac{x - x_i}{\sqrt{4(D_1+2D_2\tau)t}}\right) \tag{2.46}$$

The result of Eq. (2.46) indicates that as time increases, the importance of lateral dispersion increases. The approximate width of the dispersed zone about the interface, δ, is defined as

$$\delta = \left[\left.\frac{\partial(c/c_o)}{\partial x}\right|_{x=x_i}\right]^{-1} = \sqrt{4\pi\xi} = \sqrt{4\pi(D_1+2D_2\tau)t} \tag{2.47}$$

As the width of the dispersed zone, δ, becomes large, dynamic effects of grain dispersion are expected, and the dynamics of the mixing are not given by the immiscible model. The ratio δ/L, where L is given by Eq. (2.19) is proposed as a criteria to estimate the importance of grain dispersion.

$$\frac{\delta}{L} = \left[\frac{\pi D_1}{6\bar{E}}\left(1 + \frac{1}{2}\left(\frac{L}{H}\right)^2 \frac{D_2}{D_1}\right)\right]^{1/2} \tag{2.48}$$

The result given by Eq. (2.46) is expected to be valid if $\delta \ll L$. As δ approaches L it becomes necessary to consider the dynamic effects of the grain dispersion. This analysis will be developed in the next section.

2.3 Interaction Between Grain Dispersion and Density Induced Mixing

In Section 2.2 the additional mixing due to grain dispersion was determined under the assumption that grain dispersion has a negligible influence upon the dynamics of the process. As mixing due to grain dispersion becomes large, the immiscible model of Section 2.1 is no

longer adequate to describe the motion. To determine the influence of grain dispersion on the fluid motion, the mass and momentum equations must be solved simultaneously. Coupling the mass and momentum equations for the entire flow field results in non-linear partial differential equations, which are extremely difficult to solve. However, a useful approximation can be developed by coupling these equations at the mean interfacial position, $x = x_i$.

The governing equations are dynamic equations (Darcy equation)

$$u = - \frac{k}{n\mu} \frac{\partial p}{\partial x} \tag{2.49}$$

$$v = - \frac{k}{n\mu} \left(\frac{\partial p}{\partial y} + \rho g\right) \tag{2.50}$$

where p is the pressure, k is the permeability, and μ is the dynamic viscosity. The equation for conservation of total mass is, under the conditions of small density difference ($\Delta\rho/\rho_1 << 1$)

$$\frac{\partial u}{\partial x} + \frac{\partial v}{\partial y} = 0 \tag{2.51}$$

Using the same assumptions made in Section 2.2, the mass conservation equation for a solute of concentration c is

$$\frac{\partial c}{\partial t} + u_i \frac{\partial c}{\partial x} = D_1 \frac{\partial^2 c}{\partial x^2} + D_2 \frac{\partial^2 c}{\partial y^2} \tag{2.52}$$

The Dupuit approximation assumes a hydrostatic pressure distribution, $\partial p/\partial y = - \rho g$, and thus from Eq. (2.49) it follows that

$$\frac{\partial u}{\partial y} = \frac{kg}{n\mu} \frac{\partial \rho}{\partial x} = \frac{K}{n} \frac{1}{\rho} \frac{\partial \rho}{\partial x} \tag{2.53}$$

where K is the hydraulic conductivity.

Equation (2.53) can be evaluated at the mean interfacial position, $x = x_i$,

$$\left.\frac{\partial u}{\partial y}\right|_{x=x_i} = \left.\frac{K}{n} \frac{1}{\rho} \frac{\partial \rho}{\partial x}\right|_{x=x_i} \tag{2.54}$$

If the width of the dispersed zone, $\delta = \sqrt{4\pi\xi}$, is large in comparison to the horizontal interface projection, L, the velocity gradient in Eq. (2.54) can be approximated by

$$\left.\frac{\partial u}{\partial y}\right|_{x=x_i} = \frac{\partial u_i}{\partial y} \tag{2.55}$$

The range of validity of this approximation is evaluated in detail in Appendix A. Using this approximation, Eq. (2.53) can be rewritten as

$$\frac{\partial u_i}{\partial y} = \frac{\partial^2 x_i}{\partial y \partial t} = \frac{K}{n}\frac{1}{\rho}\left.\frac{\partial \rho}{\partial x}\right|_{x=x_i} \tag{2.56}$$

Using Eq. (2.38), Eq. (2.56) may be rewritten in terms of β

$$\frac{d\beta}{dt} = \frac{K}{n}\frac{1}{\rho}\left.\frac{\partial \rho}{\partial x}\right|_{x=x_i} \tag{2.57}$$

The solution of Eq. (2.52) for the appropriate boundary conditions is that obtained in Section 2.2.

$$\frac{c}{c_o} = \frac{1}{2} + \frac{1}{2}\,\mathrm{erf}\left(\frac{x-x_i}{\sqrt{4\xi}}\right) \tag{2.58}$$

$$\xi = \int_o^t (D_1 + \beta^2 D_2)\, dt \tag{2.59}$$

Differentiating Eqs. (2.21) and (2.58) and combining gives

$$\frac{\partial \rho}{\partial x} = \frac{\Delta\rho}{\sqrt{4\pi\xi}} \exp - \frac{(x-x_i)^2}{4\xi} \tag{2.60}$$

To couple the mass and momentum equations at the mean interfacial position, Eq. (2.60) is evaluated at $x = x_i$, and substituted into Eq. (2.57).

$$\frac{d\beta}{dt} = \frac{K}{n}\frac{\Delta\rho}{\rho}\frac{1}{\sqrt{4\pi\xi}} \tag{2.61}$$

Equation (2.61) must be solved simultaneously with Eq. (2.59) in differential form.

$$\frac{d\xi}{dt} = D_1 + \beta^2 D_2 \tag{2.62}$$

The solutions of Eqs. (2.61) and (2.62) with the initial conditions

$$\beta = \xi = 0 \quad \text{at} \quad t = 0$$

are, for the reciprocal slope β,

$$\beta^2 + \frac{D_2}{D_1}\frac{\beta^4}{6} = \frac{6}{\pi}\frac{\bar{E}}{D_1}\tau \tag{2.63}$$

and for the dispersed zone width, δ,

$$\delta = \sqrt{4\pi\xi} = \frac{2\pi n\rho}{K\Delta\rho}\left(\beta D_1 + \frac{\beta^3}{3} D_2\right) \tag{2.64}$$

The ratio of the dispersed zone width to the horizontal projection of the mean interface is, from Eqs. (2.63) and (2.64),

$$\frac{\delta}{L} = \frac{\pi}{3}\frac{D_1}{E}\left(1 + \frac{4}{\pi}\frac{D_2}{D_1}\frac{\bar{E}}{D_1}\tau\right)^{1/2} \tag{2.65}$$

Equations (2.63) and (2.65) may be approximated for both large and small interface slopes, noting that D_1 is usually an order of magnitude larger than D_2. For large slopes, the lateral dispersion term is negligible and Eqs. (2.63) and (2.65) reduce to

$$\beta = \frac{L}{H} = \left(\frac{6}{\pi}\frac{\bar{E}}{D_1}\tau\right)^{1/2} \tag{2.66}$$

$$\frac{\delta}{L} = \frac{\pi}{3}\frac{D_1}{\bar{E}} \tag{2.67}$$

If the interface slope is small (large β), longitudinal dispersion is negligible and Eqs. (2.63) and (2.65) become

$$\beta = \frac{L}{H} = \left(\frac{36}{\pi}\frac{\bar{E}}{D_2}\tau\right)^{1/4} \tag{2.68}$$

$$\frac{\delta}{L} = \left(\frac{4\pi}{9}\frac{D_2}{\bar{E}}\tau\right)^{1/2} \tag{2.69}$$

It should be noted that, in the analyses of grain dispersion in Sections 2.2 and 2.3, the boundary conditions of no mass flux at the upper and lower aquifer limits were not explicitly applied. The resulting solutions are therefore strictly valid only for aquifers which are of infinite vertical extent. It can be seen by direct evaluation of the vertical

mass flux at the boundaries ($y = \pm H/2$) that the boundary conditions are not exactly satisfied. In Appendix B, some possible effects of this boundary condition are explored. However, no explicit evaluation of the effects was obtained, other than an indication that the boundary effects may become important when δ/L is large.

2.4 Discussion of Theoretical Results

In the previous sections, theoretical models were presented to describe, for a one-dimensional linear flow in a confined aquifer, the mixing of two fluids due to the effects of density difference and grain dispersion. Also introduced was the concept of the density dispersion coefficient, $\overline{E}$, the magnitude of which may be used to estimate the relative importance of density difference in the mixing process.

In the first model (Section 2.1) only the effect of density difference is included. An immiscible displacement process is assumed and results describing the tilting of an interface as it is being convected through the aquifer at the net seepage velocity are obtained. One characteristic of this model is the horizontal projection of the interface, L, given by Eq. (2.19). Previous investigators have obtained expressions for L, for immiscible displacement in enclosed systems with no net flow. For the case of no net flow, Gardner, et al., (1962) obtained for small and large time respectively

$$L/H = \sqrt{3}\,\tau \tag{2.70}$$

$$L/H = 2\sqrt{\tau} \tag{2.71}$$

The second result (Eq. 2.71) was originally developed by Dietz (1953) and also agrees with that found in this study (Eq. 2.19). Gardner, et al., (1962) also suggested an interpolation formula which encompasses Eqs. (2.70) and (2.71) in the form

$$\left(\frac{L}{H}\right)^2 = \frac{12\tau^2}{4+3\tau} \tag{2.72}$$

In the development leading to Eq. (2.19) it was noted that the result was independent of the net seepage velocity and thus the agreement between Eqs. (2.19) and (2.71) is expected. The results of the immiscible displacement theory (Eq. 2.19) and Gardner's interpolation formula (Eq. 2.72) are shown in Figure 2.3.

In the second model (Section 2.2), the effects of grain dispersion were considered under the assumption that grain dispersion has no influence upon the dynamics of the flow. Under this assumption, the horizontal projection of the interface, now idealized as the line of 50 per cent concentration, is the same as the immiscible displacement result,

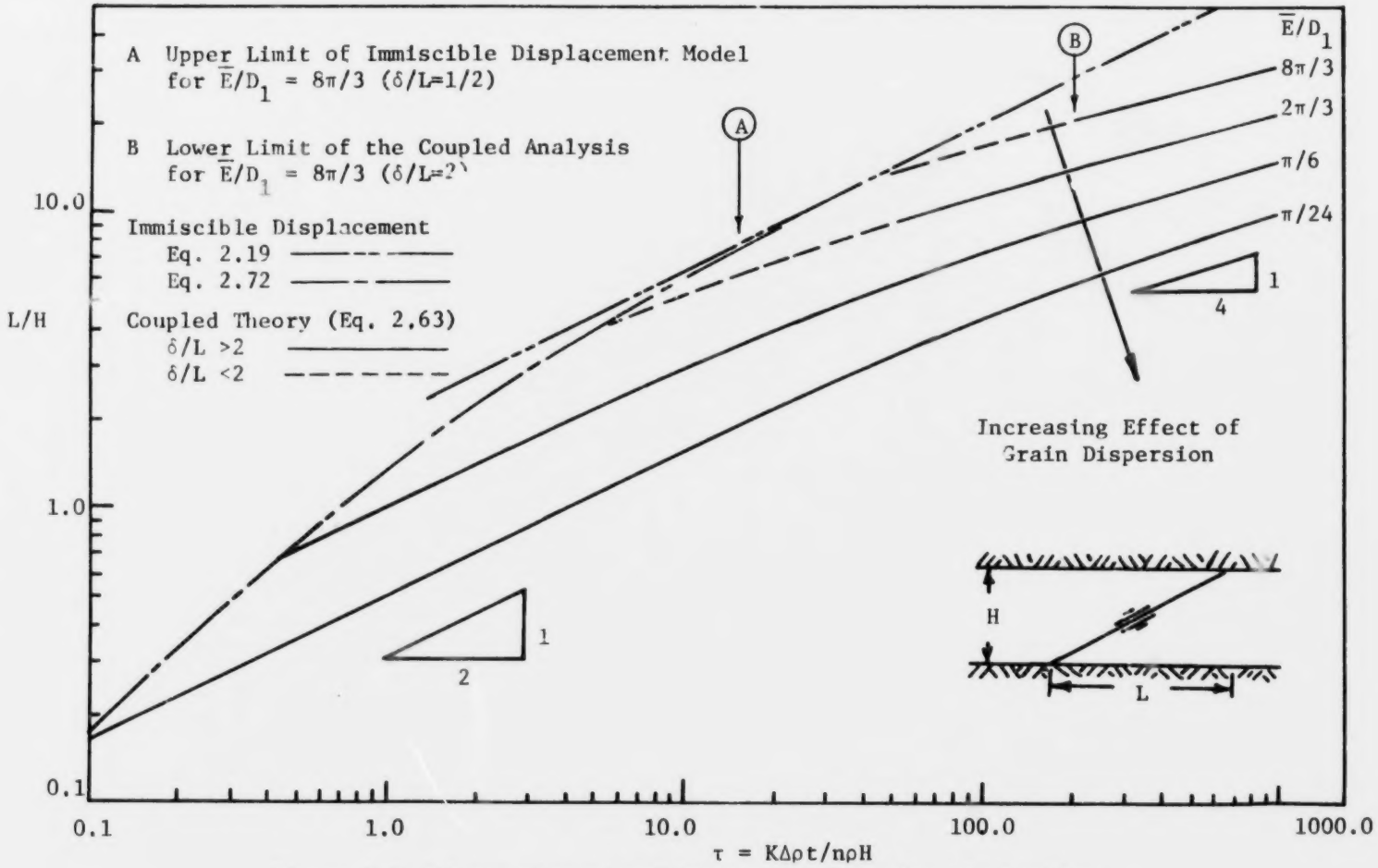

Figure 2.3 Linear Theoretical Horizontal Interface Projection

Eq. (2.19). An estimate of the width of the dispersed zone, δ, about the interface is given by Eq. (2.47). As indicated in Section 2.2, the immiscible model (Eq. 2.19) is valid when δ/L is small compared to unity. The ratio δ/L, as evaluated from Eq. (2.48) for three values of $\bar{E}/D$, is shown in Figure 2.4 as a function of the dimensionless time, τ. From Figure 2.4, it is seen that even for large values of $\bar{E}/D_1$, mixing due to grain dispersion will eventually become as important and influence the rate of interface tilting. The exact limits of applicability of the immiscible model can not be specified but reasonable estimates are obtained by assuming that the limiting value of δ/L is a fixed number less than one, say $\delta/L = 1/2$. For a given value of $\bar{E}/D_1$, the indicated maximum value of dimensionless time, τ, for which the immiscible solution applies, is found from Figure 2.4 or Eq. (2.48). For example, when $\bar{E}/D_1 = 8\pi/3$ the maximum $\tau = 15$, as shown in Figure 2.3.

In the third model (Section 2.3), effects of density difference and grain dispersion are analyzed by an approximate coupling of the mass and momentum equations based on large δ/L. The solution is given by Eq. (2.63), which represents a family of curves relating β, the inverse interface slope ($\beta=L/H$), and τ for various values of $\bar{E}/D_1$ and D_1/D_2. Equation (2.63) has two asymptotes, Eqs. (2.66) and (2.68), for large and small interfacial slopes or small and large times, respectively. In Figure 2.3, Eq. (2.63) is shown for four values of $\bar{E}/D_1$, with D_1/D_2 constant and equal to 10. As noted in Section 2.3, the coupled analysis (Eq. 2.63) is valid for $\delta/L \gg 1$. The ratio δ/L from Eq. (2.65) is shown in Figure 2.5 for four values of $\bar{E}/D_1$. An approximate limit on the range of application of Eq. (2.63) can be found by taking $\delta/L = 2$ in Eq. (2.65) or Figure 2.5. For example, when $\bar{E}/D_1 = 8\pi/3$, the limiting value is $\tau = 200$ and the coupled analysis (Eq. 2.63) should be valid for times greater than this value as indicated in Figure 2.3. It can be seen that the regions of validity of the immiscible theory (Eq. 2.19) and the coupled analysis (Eq. 2.63) are mutually exclusive for a given value of $\bar{E}/D_1$. In general, there will be an intermediate time range in which neither theory is applicable. In the example $\bar{E}/D_1 = 8\pi/3$, the range is $15 < \tau < 200$. The actual behavior in this range is not known, but a smooth transition between the models is expected. The portions of the curves representing Eq. (2.63) for $\delta/L < 2$ are shown as dashed lines in Figure 2.3. It is seen that, even for large values of $\bar{E}/D_1$, lateral grain dispersion will eventually influence the interface tilting. From Figure 2.3, it is seen that as $\bar{E}/D_1$ decreases, interface tilting becomes less and as lateral dispersion becomes important, the rate of tilting decreases.

The ratio δ/L indicates the relative importance of the two mixing mechanisms, grain dispersion and density difference. When δ/L is small (Section 2.2), the grain dispersion has no effect on the interface tilting and mixing dynamics are governed by the immiscible solution. When δ/L is large the combined effects of the two mixing mechanisms are important and the coupled analysis governs the mixing. The coupled solution does not reduce to the immiscible solution as $D_1, D_2 \to 0$, because the regions of validity for the two analyses do not overlap.

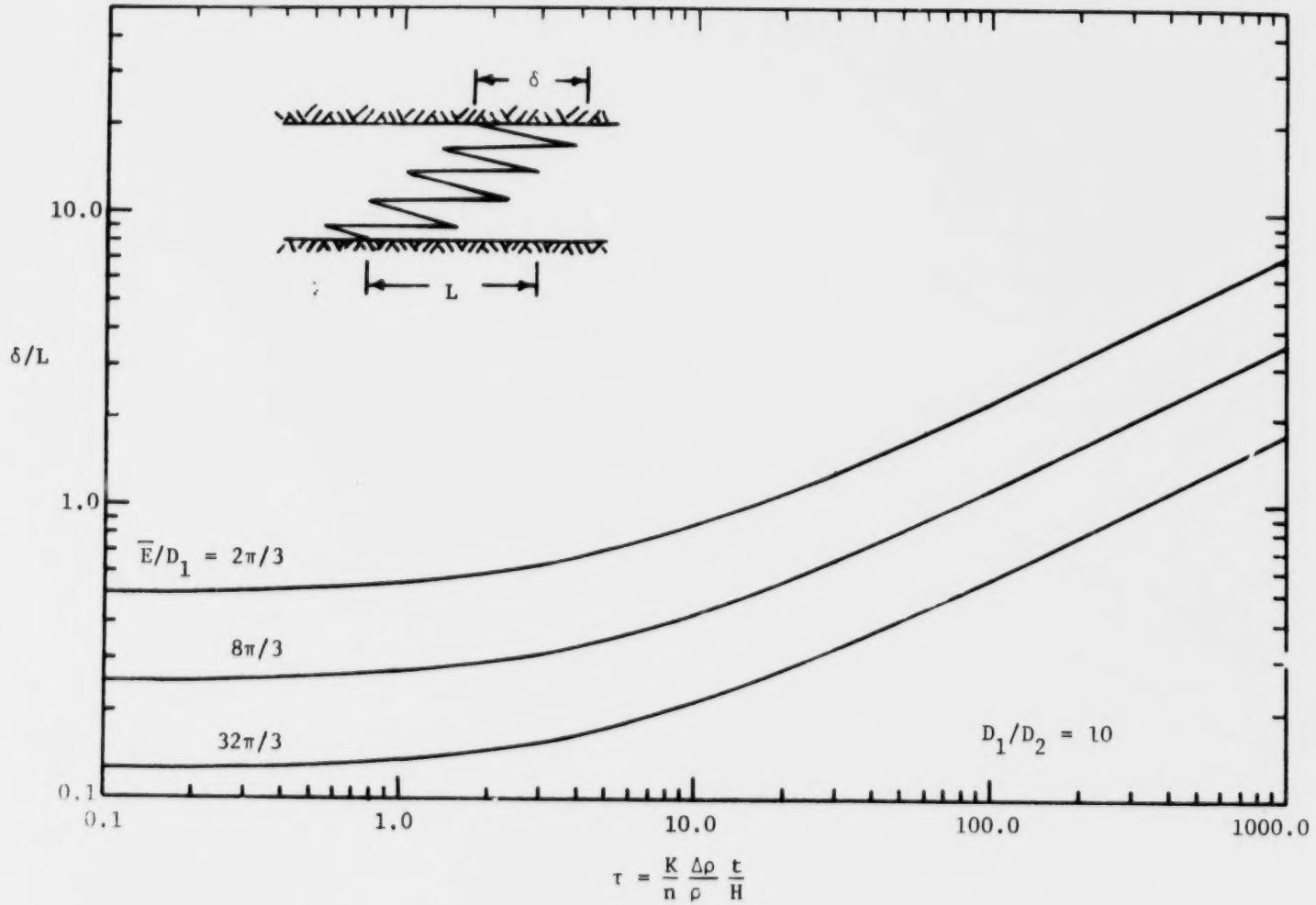

Figure 2.4 δ/L as a Function of Time for the Case of No Dynamic Effects of Grain Dispersion

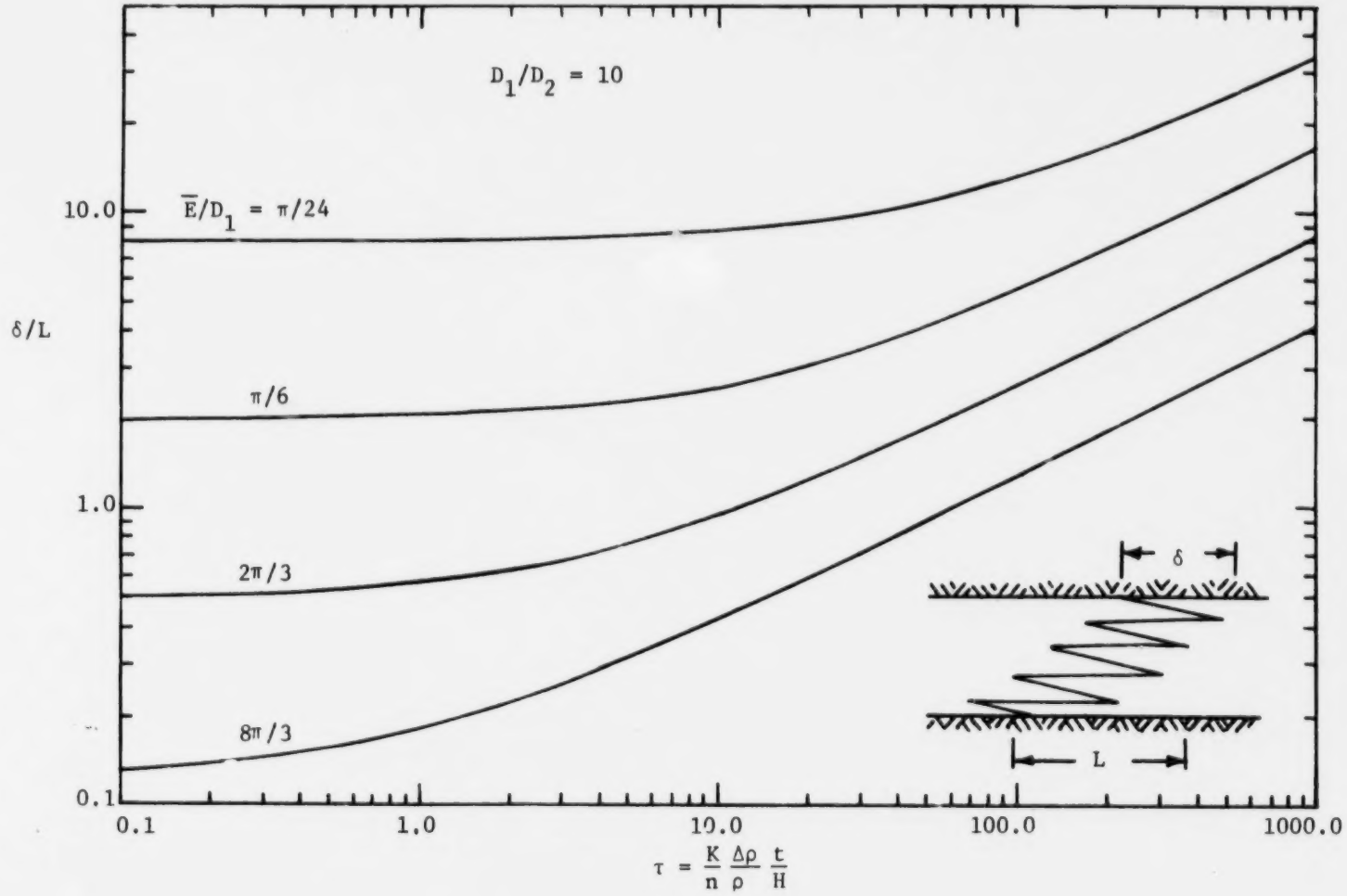

Figure 2.5 δ/L as a Function of Time for Interaction Between Grain Dispersion and Density Induced Mixing

A numerical example for some typical field conditions will illustrate the importance of the different mixing phenomena. Consider a sandy aquifer 50 feet thick having a hydraulic conductivity, K, of 0.03 ft/sec and a porosity, n, of 0.35. For a one percent density difference, the density dispersion coefficient is $\bar{E} = 7.15 \times 10^{-5}$ ft^2/sec. For a hydraulic gradient of 0.01, the net seepage velocity from Darcy's law is $U = 8.6 \times 10^{-4}$ ft/sec. The longitudinal dispersion coefficient is estimated to be $D_1 = 2.8 \times 10^{-6}$ ft/sec from results by Harleman, Melhorn and Rumer (1963) and $D_1/D_2 = 10$ is assumed. The ratio $\bar{E}/D_1$ is approximately 26, indicating that the mixing process is initially one of immiscible displacement. The immiscible model (Eq. 2.19) will be valid up to a dimensionless time $\tau = 57$ which is determined from Eq. (2.48). Thus a period of somewhat over one month would be required before the interface tilting would be influenced by grain dispersion. After one month, the horizontal projection of the interface, L, is 670 feet and the width of the dispersion zone about the interface, as given by Eq. (2.48), is 300 feet.

The results of the analyses of the combined effects of grain dispersion and density-induced motion can also be interpreted in terms of a total dispersion coefficient, E_t, defined by

$$j_x = - \rho E_t \frac{\partial \bar{c}}{\partial x} \tag{2.73}$$

where j_x is the mass flux relative to the mean flow U, and $\bar{c}$ is the depth-averaged concentration given by

$$\bar{c} = \frac{1}{H} \int_{-H/2}^{H/2} c \, dy \tag{2.74}$$

The total dispersion coefficient, E_t, can be evaluated directly from the results of Sections 2.2 or 2.3 in the general form

$$\frac{c}{c_o} = \frac{1}{2} + \frac{1}{2} \operatorname{erf} \frac{x - x_i}{\sqrt{4\xi}} \tag{2.75}$$

where $x_i = Ut + \beta y$ (Eq. 2.38), β is given by Eqs. (2.19) or (2.63) and ξ by Eqs. (2.45) or (2.64). The average concentration is determined using Eq. (2.75) in Eq. (2.74) with the result

$$\frac{\bar{c}}{c_o} = \frac{1}{2} + \frac{\sqrt{4\xi}}{2\beta H} \left[\theta_2 \operatorname{erf}\theta_2 - \theta_1 \operatorname{erf}\theta_1 + (e^{-\theta_2^2} - e^{-\theta_1^2})/\sqrt{\pi}\right] \tag{2.76}$$

where $\theta_2 = (\bar{x} + \beta H/2)/\sqrt{4\xi}$, $\theta_1 = (\bar{x} - \beta H/2)/\sqrt{4\xi}$ and $\bar{x} = x - Ut$. The gradient of the depth-averaged concentration is then

$$\frac{\partial}{\partial x}\left(\frac{\bar{c}}{c_o}\right) = \frac{1}{2\beta H}(\mathrm{erf}\theta_2 - \mathrm{erf}\theta_1) \tag{2.77}$$

The mass flux, j_x, is expressed as

$$j_x = -\frac{1}{H}\int_{-H/2}^{H/2} \rho D_1 \frac{\partial c}{\partial x}\, dy + \frac{1}{H}\int_{-H/2}^{H/2} \rho c\bar{u}\, dy \tag{2.78}$$

where $\bar{u} = u - U$. Assuming small density changes, Eq. (2.78) is adequately approximated by

$$j_x = -\rho D_1 \frac{\partial \bar{c}}{\partial x} + \frac{\rho}{H}\int_{-H/2}^{H/2} c\bar{u}\, dy \tag{2.79}$$

Using Eqs. (2.73) and (2.79), the total dispersion coefficient becomes

$$E_t = D_1 - \left(\frac{1}{H}\int_{-H/2}^{H/2} c\bar{u}\, dy\right) / \frac{\partial \bar{c}}{\partial x} \tag{2.80}$$

The convective flux integral in Eq. (2.80) was evaluated at $x=Ut$ ($\bar{x}=0$) in Appendix B (Eq. B.6) as

$$-\frac{1}{H}\int_{-H/2}^{H/2} c\bar{u}\, dy = \frac{3c_o D_1}{2\beta H}\frac{\bar{E}}{D_1}\Phi\left(\frac{L}{\delta}\right) \tag{2.81}$$

in which $L = \beta H$, $\delta = \sqrt{4\pi\xi}$ and Φ is defined in Eq. (B.7). Introducing Eq. (2.77) with $\bar{x} = 0$ and Eq. (2.81) in Eq. (2.80),

$$\frac{E_t - D_1}{D_1} = \frac{3}{2}\left(\frac{\bar{E}}{D_1}\right) g\left(\frac{L}{\delta}\right) \tag{2.82}$$

where $g(L/\delta) = \Phi(L/\delta)/\mathrm{erf}(\sqrt{\pi}L/2\delta)$. The right hand side of Eq. (2.82) represents the relative increase of the total dispersion coefficient over the longitudinal dispersion coefficient for the medium. The function $g(L/\delta)$ was evaluated numerically and is shown in Figure 2.6. For a given value of the parameter $\bar{E}/D_1$, L/δ is determined by the appropriate model from Section 2.2 or 2.3 (Eqs. 2.48 or 2.65) as discussed earlier in this section. The results of this computation for three values of $\bar{E}/D_1$ are shown in Figure 2.7. The dashed portion of the curves represent an estimated interpolation in the region where neither of the two theories for δ/L is strictly valid. It is seen from Figure 2.7 that the total

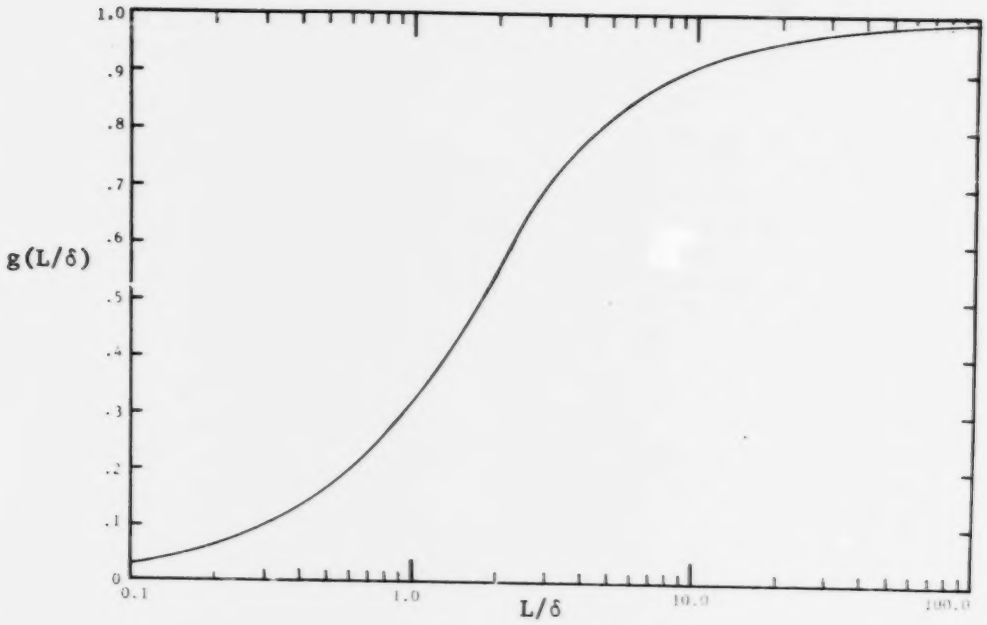

Figure 2.6 g(L/δ) for One Dimensional Linear Flow

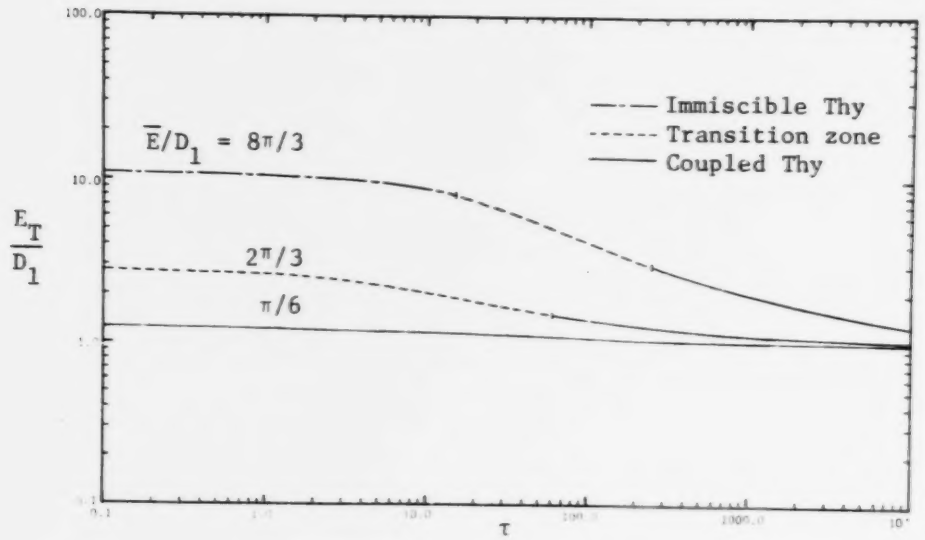

Figure 2.7 Total Dispersion Coefficient, E_T, as a Function of Time for Linear Flow

dispersion coefficient, E_t, decreases with increasing time and that eventually the additional dispersion due to density differences becomes negligible.

Rose and Passioura (1971) reported experiments in which the additional dispersion associated with density differences was determined from breakthrough curves. These experiments were done with columns of circular cross-section and therefore are not directly comparable with the present results. However, the increase in dispersion coefficient indicated from Eq. (2.82) for these experimental conditions is found to be of the same order of magnitude as that observed.

3. ANALYSIS OF DENSITY INDUCED MIXING IN RADIAL FLOW

In this section the methods of analysis developed for linear flow in Section 2 are extended to the more practical case of radial flow from a fully penetrating well in a horizontal confined aquifer. The approach generally parallels that for linear flow including first an analysis of immiscible displacement, next a superposition of dispersive effects on that result and finally a consideration of the combined effects of density differences and grain dispersion. The analysis is generalized to treat a recharge-storage-pumping sequence that would be typical of field well operations.

3.1 Immiscible Displacement

As in Section 2.1, the problem of mixing two liquids of different density in a homogeneous, confined aquifer may be simplified by neglecting grain dispersion and molecular diffusion. In such a case, the mixing process is described by an immiscible displacement model. Figure 3.1 illustrates the displacement of a heavier fluid of density, ρ_2, by a lighter fluid of density, ρ_1, in a horizontal confined aquifer of constant thickness H. If the two liquids have approximately the same kinematic viscosity, ν, the hydraulic conductivity, K, may be taken as a constant throughout the flow.

The following analysis is based on the Dupuit approximation, which assumes hydrostatic pressure distributions and thus essentially horizontal flow. The analysis is strictly correct only when the interface slope is small and hence the vertical velocities are small.

The continuity equations for the two fluids are

$$\frac{1}{r}\frac{\partial}{\partial r}(u_1 \zeta r) = -\frac{\partial \zeta}{\partial t} \tag{3.1a}$$

$$\frac{1}{r}\frac{\partial}{\partial r}(u_2 \eta r) = -\frac{\partial \eta}{\partial t} \tag{3.1b}$$

where ζ is the vertical distance to the interface, in liquid 1, measured from the top of the aquifer, and η is the vertical distance to the interface, in liquid 2, measured from the bottom of the aquifer. The seepage velocities of the two fluids are given by the Darcy equation,

$$u_1 = -\frac{K}{n}\frac{\partial \phi_1}{\partial r} \tag{3.2}$$

$$u_2 = -\frac{K}{n}\frac{\partial \phi_2}{\partial r} \tag{3.3}$$

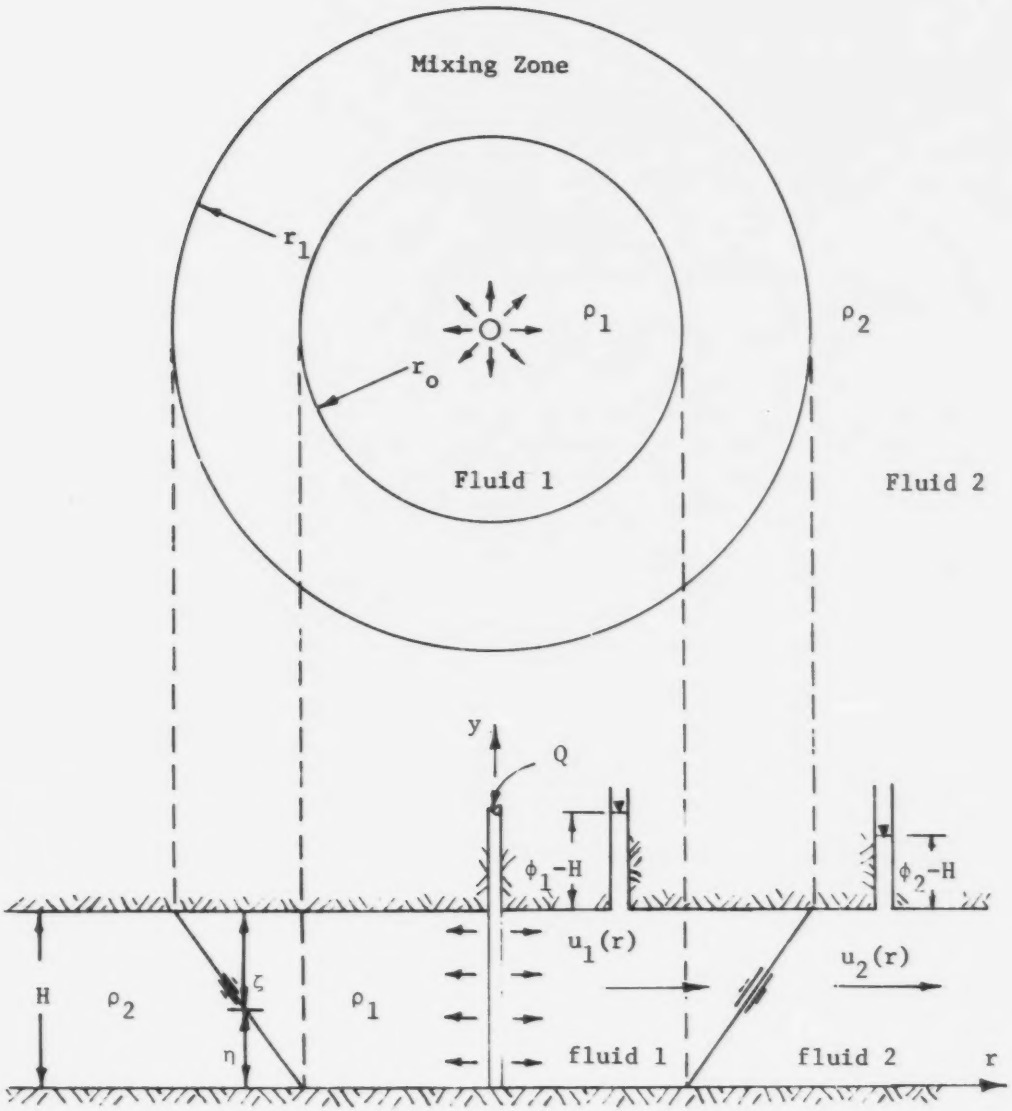

Figure 3.1 Definition Sketch of a Radial Confined Aquifer

Vertical velocities are neglected due to the Dupuit approximation. The porosity of the aquifer is n, and the piezometric heads of the two liquids are ϕ_1 and ϕ_2. The continuity expression for the entire flow field is obtained by adding Eqs. (3.1) and integrating,

$$\zeta u_1 + \eta u_2 = \frac{Q}{2\pi nr} = \frac{A}{r} H \tag{3.4}$$

where $A = Q/2\pi nH$. The convection of the interface through the aquifer is due to the net seepage velocity, A/r.

Along the interface, the fluid pressure must be continuous ($p_1 = p_2$), or

$$\phi_2 = \frac{\rho_1}{\rho_2} \phi_1 - \frac{\Delta\rho}{\rho_2}(\zeta - H) \tag{3.5}$$

where

$$\Delta\rho = \rho_2 - \rho_1 \tag{3.6}$$

For small density differences Eq. (3.5) becomes

$$\phi_2 = \phi_1 - \frac{\Delta\rho}{\rho}(\zeta - H) \tag{3.7}$$

in which the relative density difference is identified by $\Delta\rho/\rho_2 = \Delta\rho/\rho$.

The problem involves the determination of the interface shape and location. Substituting Eqs. (3.2) and (3.3) into Eq. (3.4) gives

$$\frac{\partial\phi_1}{\partial r} \zeta + \frac{\partial\phi_2}{\partial r} \eta = - \frac{Q}{2\pi rK} \tag{3.8}$$

Differentiating Eq. (3.5) and substituting into Eq. (3.8) with $H = \eta + \zeta$ results in the expression

$$\frac{\partial\phi_1}{\partial r} = - \frac{An}{rK} - \frac{\Delta\rho}{\rho} \frac{\eta}{H} \frac{\partial\eta}{\partial r} \tag{3.9}$$

Substituting Eq. (3.2) into Eq. (3.1a) and eliminating ζ using $\zeta = H - \eta$, gives

$$- \frac{\partial\eta}{\partial t} = \frac{K}{n} \frac{1}{r} \frac{\partial}{\partial r}\left[(H-\eta) \frac{r\partial\phi_1}{\partial r}\right] \tag{3.10}$$

Replacing the derivative of ϕ_1 with Eq. (3.9), the partial differential equation for η is found to be

$$\frac{\partial \eta}{\partial t} + \frac{A}{r}\frac{\partial \eta}{\partial r} = D\,\frac{1}{r}\frac{\partial}{\partial r}\left[\left(1 - \frac{\eta}{H}\right)\frac{\eta}{H}\,r\,\frac{\partial \eta}{\partial r}\right] \tag{3.11}$$

where $D = \frac{K}{n}\frac{\Delta\rho}{\rho}H$.

Recharge Cycle Because of the nature of the flow geometry, it is helpful to express Eq. (3.11) in a volumetric coordinate system. During recharge, with a positive flow rate Q_r into the aquifer, the transformations are,

$$\Psi = (\pi n H) r^2 \tag{3.12a}$$

$$\Psi_* = Q_r t \tag{3.12b}$$

which represent, respectively, transformed space and time coordinates. Using these transformations, Eq. (3.11) becomes

$$\frac{\partial \eta}{\partial \Psi_*} + \frac{\partial \eta}{\partial \Psi} = \frac{2D}{A}\left[\frac{\eta}{H}\left(1 - \frac{\eta}{H}\right)\Psi\,\frac{\partial \eta}{\partial \Psi}\right] \tag{3.13}$$

Note that this substitution transforms the radially dependent coefficient of the convective term into a constant. The equation can be simplified further by transforming to a convective coordinate system:

$$\bar{\Psi} = \Psi - \Psi_* \tag{3.14}$$

Eq. (3.13) now becomes

$$\frac{\partial \eta}{\partial \Psi_*} = \frac{2D}{A}\,\frac{\partial}{\partial \bar{\Psi}}\left[\frac{\eta}{H}\left(1 - \frac{\eta}{H}\right)(\bar{\Psi}+\Psi_*)\,\frac{\partial \eta}{\partial \bar{\Psi}}\right] \tag{3.15}$$

This recharge equation can be reduced to an ordinary differential equation using a similarity transformation

$$\begin{aligned} f &= \eta/H = F(z) \\ z &= \bar{\Psi}/\varepsilon_r \Psi_* \end{aligned} \tag{3.16}$$

where

$$\varepsilon_r = \sqrt{D/A_r} \tag{3.17}$$

$$A_r = Q_r/2\pi nH \tag{3.18}$$

and the subscript "r" refers to the recharge cycle. The resulting ordinary differential equation in z, the similarity variable, is

$$-\frac{z}{2}\frac{df}{dz} = \frac{d}{dz}[f(1-f)(1+\varepsilon_r z)\frac{df}{dz}] \tag{3.19}$$

The parameter ε_r indicates the relative importance of the density difference, represented by D, as compared to convection, represented by A. For increasing ε_r, the relative rate of tilting of the interface should increase.

For small ε_r, a perturbation solution for Eq. (3.19) of the form

$$f = f_o + \varepsilon_r f_1 + \varepsilon_r^2 f_2 + \cdots \tag{3.20}$$

is assumed. For equations of $O(1)$ this results in a nonlinear equation in f_o and z

$$-\frac{z}{2}\frac{df_o}{dz} = \frac{d}{dz}[f_o(1-f_o)\frac{df_o}{dz}] \tag{3.21}$$

This equation is solved for an initially vertical interface by assuming a power series in z, to give

$$f_o = \frac{1}{2}(1+z) \tag{3.22}$$

The equations for higher orders, ε_r^n, are of the general linear form

$$(1-z^2)\frac{d^2f_n}{dz^2} - 2z\frac{df_n}{dz} - 2f_n = F(f_{n-1}, f_{n-2}, \cdots f_o, z) \tag{3.23}$$

$$n = 1,2,3,\cdots\cdots$$

For n = 1 the equation is

$$(1-z^2)\frac{d^2f_1}{dz^2} - 2z\frac{df_1}{dz} - 2f_1 = -\frac{1}{2}(1-3z^2) \tag{3.24}$$

and the particular solution is

$$f_1 = \frac{1}{16}(1-3z^2) \tag{3.25}$$

Similarly, the equation for n = 2 is

$$(1-z^2)\frac{d^2f_2}{dz^2} - 2z\frac{df_2}{dz} - 2f_2 = \frac{z}{32}(23-51z^2)$$

for which the particular solution is

$$f_2 = \frac{-z}{112}(1 - \frac{51}{4}z^2) \tag{3.26}$$

Therefore, during recharge, the interface behaves as

$$\frac{\eta}{H} = \frac{1}{2}(1+z) + \frac{\varepsilon_r}{16}(1-3z^2) - \frac{\varepsilon_r^2 z}{112}(1 - \frac{51}{4}z^2)+\cdots \tag{3.27}$$

The solutions of Eq. (3.23) will, in general, include two solutions of the linear homogeneous equation and a particular solution which depends on F. However, the homogeneous equation, which is closely related to the Legendre equation, can be shown to have mathematical singularities at z = ±1 and therefore the solutions of the homogeneous equation must be excluded on physical grounds. The result represented by Eq. (3.27) is shown in Figure 3.2 for two values of ε_r. It can be seen that, even for the relatively large value $\varepsilon_r = .65$, the departure from the linear interface shape of the zero order solution is not large. Note that the upper and lower limits of the interface (f = 1 and f = 0) advance as ε increases, but that the arrival time of f = 1/2 has been delayed relative to the average displacement.

The length of the interface in volumetric coordinates is expressed as

$$\Delta\Psi = \bar{\Psi}\big|_{f=1} - \bar{\Psi}\big|_{f=0} = \pi nH(r^2\big|_{f=1} - r^2\big|_{f=0}) \tag{3.28}$$

which can be determined from Eq. (3.27) by evaluating the end points of the interface,

$$z_1 = 1 + \frac{1}{4}\varepsilon_r - \frac{5}{224}\varepsilon_r^2 + \cdots \tag{3.29}$$

$$z_o = -1 + \frac{1}{4}\varepsilon_r + \frac{5}{224}\varepsilon_r^2 + \cdots \tag{3.30}$$

Thus from Eqs. (3.16), (3.28), (3.29) and (3.30)

$$\Delta\Psi = 2\varepsilon_r\Psi_*[1 - \frac{5}{224}\varepsilon_r^2 + \cdots] \tag{3.31}$$

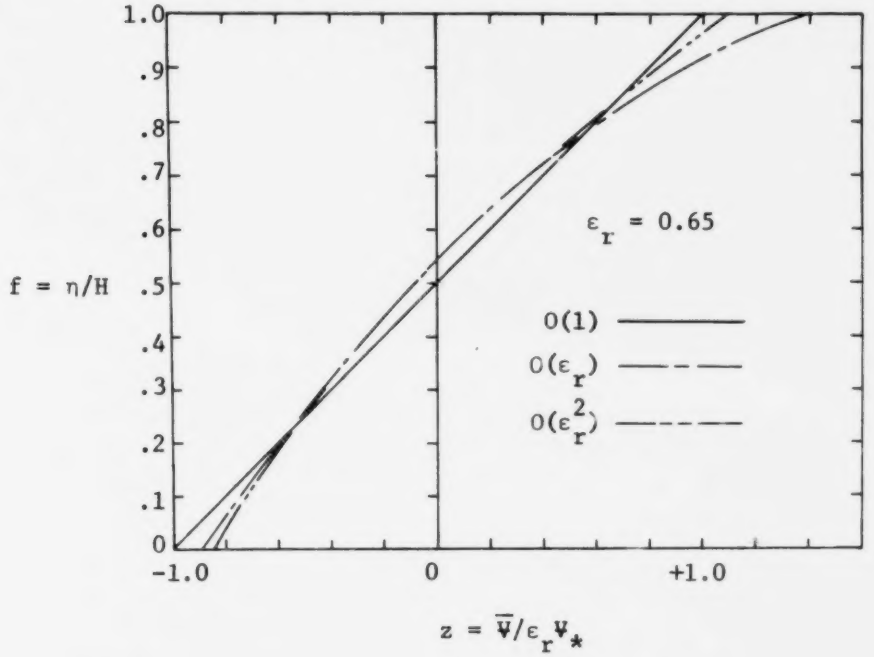

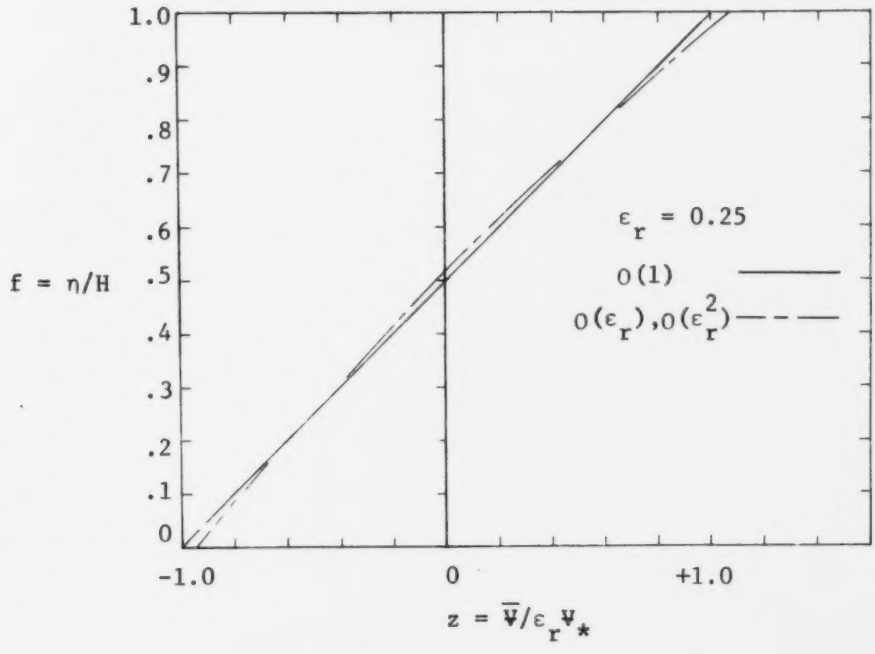

Figure 3.2 Comparison of Interface Shapes for Various Values of ε_r During a Recharge Operation

The interface location can be described by a coordinate Ψ_i, the volumetric distance from the origin. For the zero order solution (Eq. 3.27 with $\varepsilon_r = 0$) the interface position is given by

$$\Psi_i = \Psi_*(1+g) \tag{3.32}$$

where

$$g = 2\varepsilon_r\left(\frac{y-H/2}{H}\right)$$

and y is the vertical distance from the bottom of the aquifer. The radius to the interface is expressed as r_i and the interfacial velocity, u_i, is

$$u_i = \frac{\partial r_i}{\partial t} = \frac{A_r}{r_*}\sqrt{1+g} \tag{3.33}$$

where

$$r_i = \sqrt{\Psi_i/\pi n H} = r_*\sqrt{1+g} \tag{3.34}$$

$$r_* = \sqrt{\Psi_*/\pi n H} = \sqrt{2A_r t} \tag{3.35}$$

Storage Cycle During storage of liquid 1 in the aquifer, there is no net flow (Q=0) and the convective term of Eq. (3.11) becomes zero, thus

$$\frac{\partial \eta}{\partial t} = D\,\frac{1}{r}\,\frac{\partial}{\partial r}\left[(1-\frac{\eta}{H})\frac{\eta}{H}\,r\,\frac{\partial \eta}{\partial r}\right]$$

This equation may be transformed to volumetric form using Eq. (3.12a)

$$\frac{\partial \eta}{\partial t} = 2D(2\pi n H)\,\frac{\partial}{\partial \Psi}\left[\frac{\eta}{H}(1-\frac{\eta}{H})\,\Psi\,\frac{\partial \eta}{\partial \Psi}\right] \tag{3.36}$$

and may be further simplified by introducing the coordinate system

$$\bar{\Psi} = \Psi - \Psi_o$$

where Ψ_o is the volume of liquid of density ρ_1 which was injected during recharge. Equation (3.36) then transforms to

$$\frac{\partial \eta}{\partial t} = 2D(2\pi n H)\,\frac{\partial}{\partial \bar{\Psi}}\left[\frac{\eta}{H}(1-\frac{\eta}{H})(\bar{\Psi}+\Psi_o)\frac{\partial \eta}{\partial \bar{\Psi}}\right] \tag{3.37}$$

When the length of the wedge is small compared to the distance from the well, $\Psi_1 << \Psi_o$, Eq. (3.37) is approximated by

$$\frac{\partial \eta}{\partial t} = 2D(2\pi nH)\Psi_o \frac{\partial}{\partial \Psi}[\frac{\eta}{H}(1 - \frac{\eta}{H}) \frac{\partial \eta}{\partial \Psi}] \tag{3.38}$$

This equation may be reduced to an ordinary differential equation using the similarity transformation

$$\frac{\eta}{H} = f = F(z')$$

$$z' = \frac{\Psi_1}{\sqrt{4\pi nHD\Psi_o t + C_1}} \tag{3.39}$$

where C_1 is an arbitrary constant added in order to fit the initial interface shape at the start of the storage period. The resulting ordinary differential equation is

$$-\frac{z'}{2}\frac{df}{dz'} = \frac{d}{dz'}[f(1-f)\frac{df}{dz'}] \tag{3.40}$$

which has the solution (see Eqs. 3.21 and 3.22)

$$f = \frac{1}{2}(1+z') \tag{3.41}$$

The result of Eq. (3.41) represents a linear interface in volumetric coordinates and is implicitly limited to cases in which the volumetric length of the interface is small compared to the initial volume Ψ_o. The explicit features of this limitation will be discussed in sections 3.4 and 3.5, but it can be seen from Eqs. (3.39) and (3.41) that this solution will become invalid for large times. It is also implied that the initial condition for the storage cycle should correspond to a linear interface at the end of the recharge cycle and thus that ε_r be small.

It would be desirable to obtain solutions during the storage cycle which are not limited by the approximation in Eq. (3.38), i.e., small ε_r during recharge. Although the equation governing the storage cycle (Eq. 3.37) is similar to that for the recharge cycle (Eq. 3.15), the method of solution used for the recharge cycle does not apply because a similarity form of Eq. (3.37) can not be obtained.

Withdrawal Cycle During withdrawal, fluid is pumped from the aquifer at a rate Q_w and the governing equation becomes, from Eq. (3.11),

$$\frac{\partial \eta}{\partial t} - \frac{A_w}{r}\frac{\partial \eta}{\partial r} = D\,\frac{1}{r}\left[\left(1 - \frac{\eta}{H}\right)\frac{\eta}{H}\, r\,\frac{\partial \eta}{\partial r}\right] \qquad (3.42)$$

where $A_w = Q_w/2\pi nH$. This equation may be transformed to a volumetric convective coordinate system using Eq. (3.12a) and

$$\Psi_* = \Psi_o - Q_w(t-t_o)$$

$$\bar{\Psi} = \Psi - \Psi_*$$

where

t_o = time at the start of withdrawal

Ψ_o = net injected volume at t_o

Equation (3.42) then reduces to

$$\frac{\partial f}{\partial \Psi_*} = -\,2\varepsilon_w^2\,\frac{\partial}{\partial \bar{\Psi}}\left[f(1-f)(\bar{\Psi} + \Psi_*)\,\frac{\partial f}{\partial \bar{\Psi}}\right] \qquad (3.43)$$

with $\varepsilon_w = \sqrt{D/A_w}$. When the length of the interface is relatively small compared to the distance from the origin to the front, $\Psi_* >> \bar{\Psi}$, Eq. (3.43) is approximated by

$$\frac{\partial f}{\partial (C_2 - \Psi_*^2)} = \varepsilon_w^2\,\frac{\partial}{\partial \bar{\Psi}}\left[f(1-f)\,\frac{\partial f}{\partial \bar{\Psi}}\right] \qquad (3.44)$$

This equation has the solution

$$f = \frac{1}{2}\left(1 + \frac{\bar{\Psi}}{\varepsilon_w\sqrt{C_2 - \Psi_*^2}}\right) \qquad (3.45)$$

where C_2 is a constant to be determined from the initial conditions for the withdrawal cycle. The length of the interface in volumetric coordinates will be given by

$$\Delta\Psi = 2\varepsilon_w\sqrt{C_2 - \Psi_*^2} \qquad (3.46)$$

and the location of the interface is expressed as

$$\Psi_i = \Psi_* + \frac{2\varepsilon_w}{H}\sqrt{C_2 - \Psi_*^2}\;(y - H/2) \qquad (3.47)$$

The solution for the withdrawal cycle, as given in Eq. (3.45), represents a linear interface in volumetric coordinates. The range of applicability of this solution will, as discussed in Sections 3.4 and 3.5, depend on the initial condition from a storage or recharge cycle. It can be seen from Eq. (3.46) that as Ψ_* approaches zero (i.e., the entire stored volume is withdrawn), the ratio $\Delta\Psi/\Psi_*$ becomes large and the approximation implied in Eq. (3.44) becomes invalid. A perturbation solution of the exact equation (Eq. 3.43) was attempted using the method employed for the recharge cycle. A similarity form of Eq. (3.43) can be found, but in the withdrawal case, the initial conditions can not be satisfied by the similarity form.

Matching Between Cycles The solutions for the storage and withdrawal cycles (Eqs. 3.41 and 3.45) can be combined with the zero order solution for recharge (Eq. 3.22) to represent general recharge-storage-pumping sequences. The general approach in matching between the cycles will be outlined here and explicit applications to aquifer operations will be developed in Section 3.5. Because each of the three solutions represents a linear interface in volumetric coordinates, the matching between the cycles can be expressed conveniently in terms of the inverse slope of the interface in volumetric coordinates, β, which is given by

$$\beta \equiv \frac{\partial \Psi_i}{\partial y} = \left(\frac{\partial \eta}{\partial \Psi}\right)^{-1} = \frac{\Delta\Psi}{H} \tag{3.48}$$

The constants C_1 and C_2 appearing in the storage and withdrawal solutions can be expressed in terms of the initial inverse slope, β_o, at the start of the cycle. From Eq. (3.41) for the storage cycle

$$\beta = 2\sqrt{4\pi nHD\Psi_o t + C_1}/H$$

and if the time t is measured from the start of the cycle, the constant C_1 can be determined in terms of β_o. The resulting expression for the inverse slope during storage is therefore

$$\beta = \beta_o\left(1 + \frac{16\pi nD\Psi_o t}{\beta_o^2 H}\right)^{1/2} \tag{3.49}$$

Likewise for the withdrawal cycle the inverse slope is, using Eq. (3.46),

$$\beta = \beta_o\left[1 + \left(\frac{2\varepsilon_w}{\beta_o H}\right)^2 (\Psi_o^2 - \Psi_*^2)\right]^{1/2} \tag{3.50}$$

where β_o is the initial inverse slope when $\Psi_* = \Psi_o$, the initial net injected volume.

The zero order solution for recharge may also be generalized to include

initial conditions corresponding to an interface of inverse slope β_o and initial injected volume Ψ_o. Noting that the zero order solution during recharge is represented by Eq. (3.15) with $\bar{\Psi} << \Psi_*$, and defining $\Psi_* = Q_r t + V_o$ with t measured from the start of this recharge cycle,

$$\frac{\partial f}{\partial \Psi_*} = \frac{2D}{A_r} \frac{\partial}{\partial \bar{\Psi}} [f(1-f)\Psi_* \frac{\partial f}{\partial \bar{\Psi}}]$$

the solution can be written

$$f = \frac{1}{2}[1 + \frac{\bar{\Psi}}{\varepsilon_r \sqrt{\Psi_*^2 + C_3}}] \tag{3.51}$$

The constant, C_3, is again evaluated in terms of β_o and Ψ_o to yield

$$\beta = \beta_o [1 + (\frac{2\varepsilon_r}{\beta_o H})^2 (\Psi_*^2 - \Psi_o^2)]^{1/2} \tag{3.52}$$

The inverse slope, β, determined from any of the three cases can provide the initial value β_o for any subsequent cycle.

Using the above notation, the solutions in all three cycles (Eqs. (3.22), (3.41) and (3.45)) can be represented in the general form

$$f = \frac{1}{2} + \frac{\bar{\Psi}}{\beta H} \tag{3.53}$$

where β is given by Eq. (3.49), (3.50) or (3.52).

3.2 Effects of Grain Dispersion

The immiscible displacement models of section 3.1 are an idealization of the actual situation, since there will always be some degree of interfacial dispersion. The objective of this section is to estimate the importance of grain dispersion, under the assumption that the dispersion does not attenuate the rate of interfacial tilting. This corresponds to the case in which the density difference, $\Delta\rho$, is large enough to completely govern the dynamics of mixing (i.e., the velocity field is predicted by the immiscible model), but in which the resulting model does not adequately describe the variation of density near the interface. To obtain a better description of the density variation, grain dispersion must be considered. The analysis of the recharge cycle will be developed in detail, and the results for the other cycles will be obtained as a simple extension of this case.

Recharge Cycle The convective-dispersion equation, neglecting molecular diffusion, is, during the recharge cycle,

$$\frac{\partial c}{\partial t} + v_r \frac{\partial c}{\partial r} = \frac{1}{r} \frac{\partial}{\partial r}(D_1 r \frac{\partial c}{\partial r}) + \frac{\partial}{\partial y}(D_2 \frac{\partial c}{\partial y}) \qquad (3.54)$$

where v_r is the convective radial velocity, and D_1 and D_2 are the longitudinal and lateral grain dispersion coefficients, respectively. The vertical convective transport term is neglected since the Dupuit assumption, which assumes negligible vertical velocities, is assumed to be applicable. Equation (3.54) can be simplified by the following assumptions:

(i) The dispersion coefficients, D_1 and D_2, are generally velocity dependent. For this analysis, velocity variations from the depth averaged velocity, A/r, will be assumed small and D_1 and D_2 are taken as

$$D_1 = \alpha_1 \frac{|A|}{r} \qquad D_2 = \alpha_2 \frac{|A|}{r}$$

where α_1 and α_2 are the longitudinal and lateral grain dispersivities respectively.

(ii) The convective velocity in the dispersed region can be approximated by the velocity of the interface, u_i. For the case of recharge with the approximate interfacial solution given by Eq. (3.32), u_i is given by Eq. (3.33).

The interface is idealized as the line of 50% concentration. Under these assumptions, Eq. (3.54) simplifies to

$$\frac{\partial c}{\partial t} + u_i \frac{\partial c}{\partial r} = \alpha_1 \frac{|A|}{r} \frac{\partial^2 c}{\partial r^2} + \alpha_2 \frac{|A|}{r} \frac{\partial^2 c}{\partial y^2} \qquad (3.55)$$

Recharge Cycle During recharge A is identically equal to A_r and Eq. (3.55) can be further simplified by a transformation to a volumetric coordinate system (Eq. 3.12)

$$\frac{\partial c}{\partial \Psi_*} + \frac{u_i}{A_r/r} \frac{\partial c}{\partial \Psi} = \frac{\alpha_1}{A_r/r}[Q_r \frac{\partial^2 c}{\partial \Psi^2} - \frac{\partial (A_r/r)}{\partial r} \frac{\partial c}{\partial \Psi}] + \alpha_2 \frac{A_r/r}{Q_r} \frac{\partial^2 c}{\partial y^2} \qquad (3.56)$$

Introducing a new coordinate transformation,

$$\Psi_\ell = \Psi - \Psi_i(y, \Psi_*) \qquad (3.57)$$

in which Ψ_i is given by Eq. (3.32) or

$$\Psi_i = \Psi_* + \beta(y - H/2) \qquad (3.58)$$

and $\beta = 2\varepsilon_r \Psi_*/H$, the concentration is expressed as a function of Ψ_*, Ψ_ℓ and y.

$$\frac{\partial c}{\partial \Psi_*} + \frac{u_i}{A/r}\frac{\partial c}{\partial \Psi_\ell} - \frac{u_i}{A/r_i}\frac{\partial c}{\partial \Psi_\ell} = \frac{\alpha_1}{A/r}\left[Q_r \frac{\partial^2 c}{\partial \Psi_\ell^2} - \frac{\partial A/r}{\partial r}\frac{\partial c}{\partial \Psi_\ell}\right]$$

$$+ \alpha_2 \frac{A_r/r}{Q_r}\left[\left.\frac{\partial^2 c}{\partial y^2}\right|_{\Psi_\ell,t} - 2\beta\frac{\partial}{\partial \Psi_\ell}\left(\left.\frac{\partial c}{\partial y}\right|_{\Psi_\ell,t}\right) + \beta^2 \frac{\partial^2 c}{\partial \Psi_\ell^2}\right] \qquad (3.59)$$

Since the coordinates, Ψ_ℓ = constant, are parallel with the interface, it is reasonable to assume that

$$\left.\frac{\partial c}{\partial y}\right|_{\Psi_\ell,t} \cong 0$$

The convective dispersion equation then reduces to

$$\frac{\partial c}{\partial \Psi_*} = \left(\alpha_1 \frac{Q_r}{A_r/r_*} + \alpha_2 \frac{A_r/r_*}{Q_r}\beta^2\right)\frac{\partial^2 c}{\partial \Psi_\ell^2} \qquad (3.60)$$

When the dispersed zone around the interface is small compared with the distance, r_*, from the origin, the two convective terms on the left hand side of Eq. (3.59) will cancel near the interface, $r = r_i$. The second term in brackets in the longitudinal dispersion term will also be negligible under these conditions because it involves a lower order of differentiation than the first. This type of approximation can be formally justified, as done by Gelhar and Collins (1970), using perturbation methods and can be verified from the result of the present analysis. It is also consistent to replace the coefficients (A/r) in the dispersive terms by A/r_*. The coefficient in this equation can be eliminated by the introduction of a new variable, ξ.

$$\xi = \int_0^{\Psi_*} \left[\frac{\alpha_1 Q_r r_*}{A_r} + \frac{\alpha_2 A_r}{Q_r r_*}\beta^2\right] d\Psi_* \qquad (3.61)$$

The function, ξ, is evaluated from the known flow field, based on the immiscible displacement model, Eqs. (3.35) and (3.31).

$$\xi = \left[\frac{\alpha_1}{3r_*} + \frac{\varepsilon_r^2}{h^2}\frac{r_*}{5}\alpha_2\right] 4\Psi_*^2 \qquad (3.62)$$

With this new variable, Eq. (3.60) transforms to

$$\frac{\partial c}{\partial \xi} = \frac{\partial^2 c}{\partial \Psi_\ell^2} \tag{3.63}$$

The initial condition corresponding to a vertical interface at the origin (Ψ=0) is

$$t = 0 \qquad c = c_o \qquad \Psi > 0$$

$$c = 0 \qquad \Psi < 0$$

and the boundary conditions are

$$t > 0 \qquad c = c_o \qquad \Psi \to \infty$$

$$c = 0 \qquad \Psi < -\infty$$

The solution of Eq. (3.63), subject to these conditions, is

$$\frac{c}{c_o} = \frac{1}{2} + \frac{1}{2} \operatorname{erf} \frac{\Psi_\ell}{\sqrt{4\xi}} \tag{3.64}$$

The dispersed zone width, in volumetric coordinates Δ, may be defined as

$$\Delta = \sqrt{4\pi\xi} = 4\Psi_* \sqrt{\frac{\alpha_1 \pi}{3 r_*} + \frac{\varepsilon_r^2}{H^2} \frac{r_*}{5} \alpha_2 \pi} \tag{3.65}$$

and the approximate radial width of the dispersed zone, δ, may be defined as

$$\delta = \frac{\Delta}{2\pi n H r_*} = 2 r_* \sqrt{\frac{\alpha_1 \pi}{3 r_*} + \frac{\varepsilon_r^2}{H^2} \frac{r_*}{5} \alpha_2 \pi} \tag{3.66}$$

As the width of the dispersed zone, δ, becomes large, dynamic effects of grain dispersion are expected, and the dynamics of the mixing are not given by the immiscible displacement model. The ratio, $\Delta/\Delta\Psi$, where $\Delta\Psi$ is given by Eq. (3.31) and Δ is given by Eq. (3.65), is proposed as a criterion to estimate the importance of grain dispersion in the radial flow problem during recharge

$$\left.\frac{\Delta}{\Delta\Psi}\right|_r = \left[\frac{4\alpha_1 \pi}{3\varepsilon_r^2 r_*} \left(1 + \frac{3\varepsilon_r^2}{5} \frac{r_*^2}{H^2} \frac{\alpha_2}{\alpha_1}\right)\right]^{1/2} \tag{3.67}$$

Equation (3.67) indicates that the lateral dispersion becomes important for

$$\frac{3\varepsilon_r^2}{5}\frac{r_*^2}{H^2}\frac{\alpha_2}{\alpha_1} > 1 \tag{3.68}$$

The concentration distribution described by Eq. (3.64) is expected to be accurate when $\Delta << \Delta\Psi$. However, as Δ approaches $\Delta\Psi$, it is necessary to consider the interaction of grain dispersion and density differences in the mixing dynamics.

Withdrawal Cycle Under the assumptions outlined at the beginning of this section, the convective dispersion equation (Eq. 3.55) during withdrawal for $A = -A_w$ is

$$\frac{\partial c}{\partial t} + u_i \frac{\partial c}{\partial r} = +\alpha_1 \frac{A_w}{r}\frac{\partial^2 c}{\partial r^2} + \alpha_2 \frac{A_w}{r}\frac{\partial^2 c}{\partial y^2} \tag{3.69}$$

where the subscript refers to withdrawal. Using the same method of analysis described for the recharge period, this equation can be transformed to the volumetric coordinate system, Ψ_ℓ, measured from the interface.

$$\frac{\partial c}{\partial \Psi_*} - \frac{u_i}{A_w/r}\frac{\partial c}{\partial \Psi_\ell} + \frac{u_i}{A_w/r_i}\frac{\partial c}{\partial \Psi_\ell} = \frac{-\alpha_1}{A_w/r}\left[Q_w \frac{\partial^2 c}{\partial \Psi_\ell^2} - \frac{\partial (A_w/r)}{\partial r}\frac{\partial c}{\partial \Psi_\ell}\right] \tag{3.70}$$

$$- \alpha_2 \frac{A_w/r}{Q_w}\beta^2 \frac{\partial^2 c}{\partial \Psi_\ell^2}$$

For withdrawal, Ψ_* is given by (see Section 3.1)

$$\Psi_* = \Psi_o - Q_w(t-t_o) \tag{3.71}$$

while Ψ_ℓ and Ψ_i are defined as before, in terms of Ψ_* (Eqs. (3.57) and (3.58)). Using the same approximations used to obtain Eq. (3.60) from Eq. (3.59), Eq. (3.70) reduces to

$$\frac{\partial c}{\partial \xi} = \frac{\partial^2 c}{\partial \Psi_\ell^2} \tag{3.72}$$

where

$$\xi = -\int \left[\frac{\alpha_1 Q_w}{A_w/r_*} + \beta^2 \frac{\alpha_2 (A_w/r_*)}{Q_w}\right] d\Psi_* + C_5 \tag{3.73}$$

and C_5 is an arbitrary constant to be determined by matching with the concentration field at $t=t_o$. The appropriate solution of Eq. (3.72) is of the form

$$\frac{c}{c_o} = \frac{1}{2} + \frac{1}{2} \operatorname{erf} \frac{\Psi_\ell}{\sqrt{4\xi}} \tag{3.74}$$

where ξ can be evaluated from the known value of β found for the withdrawal period using immiscible displacement theory (Eq. (3.46) with $\Delta\Psi=\beta H$ or Eq. (3.50)). Substituting this value of β into Eq. (3.73) yields

$$\xi = \frac{-4}{(\pi nH)^{1/2}} \left[\frac{\pi nH}{3} \alpha_1 \Psi_*^{3/2} + \frac{\varepsilon_w^2}{H^2} \alpha_2 \Psi_*^{1/2} \left(C_2 - \frac{\Psi_*^2}{5}\right)\right] + C_5 \tag{3.75}$$

If the form of C_2 implied in Eq. (3.50) is used, and C_5 is evaluated in terms of the initial volumetric width of the dispersed zone, $\Delta_o = \sqrt{4\pi\xi}$, when $t=t_o$ and $\Psi_*=\Psi_o$, the variable ξ is given by

$$\xi = \frac{-4}{(\pi nH)^{1/2}} \left[\frac{\pi nH}{3} \alpha_1 (\Psi_*^{3/2} - \Psi_o^{3/2}) + \frac{\varepsilon_w^2 \alpha_2}{H^2} \left\{ \left(\frac{\beta_o^2 H^2}{4\varepsilon_w^2} + \Psi_o^2 \right) (\Psi_*^{1/2} - \Psi_o^{1/2}) \right.\right.$$

$$\left.\left. + \frac{1}{5} (\Psi_o^{5/2} - \Psi_*^{5/2}) \right\}\right] + \frac{\Delta_o^2}{4\pi} \tag{3.76}$$

As in recharge, the ratio Δ to $\Delta\Psi$ represents the relative importance of grain dispersion. The volumetric width of the dispersed zone $\Delta = \sqrt{4\pi\xi}$ is given by Eqs. (3.75) or (3.76), and $\Delta\Psi$ is obtained from Eqs. (3.46) or (3.50). Thus the ratio $\Delta/\Delta\Psi$ can be expressed as

$$\frac{\Delta}{\Delta\Psi} = \frac{1}{\varepsilon_w} \left[\frac{\pi\xi}{(C_2 - \Psi_*^2)} \right]^{1/2} = \left[\frac{4\pi\xi}{4\varepsilon_w^2 (\Psi_o^2 - \Psi_*^2) + H^2 \beta_o^2} \right]^{1/2} \tag{3.77}$$

In this solution it has been assumed that the mixing dynamics are given by the immiscible displacement theory. Therefore, $\Delta/\Delta\Psi$ must be small for the solution to be valid.

Storage Cycle When the net convective motion in the aquifer is zero, the additional mixing due to grain dispersion is negligible. Physically, this is implied from the fact that the volumetric length of the interface, $\Delta\Psi$, must be small compared with the mean volumetric distance to the interface, Ψ_*, for the solution during storage (Eq. 3.41) to be valid. Since the width of the dispersed zone generally is proportional to the square root of the distance traveled by the interface, and the length of the interface is, under these implied limitations, small compared with the distance from the origin, the additional dispersion during

storage will generally be small. Thus it is consistent to assume that the volumetric thickness of the dispersed zone around the interface does not change during storage. For extremely large storage periods (e.g. several years) it may, however, be necessary to include the broadening of the dispersed zone as a result of molecular diffusion.

3.3 Interaction Between Grain Dispersion and Density Induced Mixing

In Section 3.2, the additional mixing due to grain dispersion was analyzed, assuming that the dynamics of the mixing is described by the immiscible displacement model (Section 3.1). As the mixing due to grain dispersion becomes large, the immiscible displacement model no longer describes the fluid motion. To determine the influence of the grain dispersion on the motion, the mass and momentum equations must be solved simultaneously. When the mass and momentum equations are coupled for the entire flow field, a practically intractable system of nonlinear partial differential equations is obtained. However, as in the linear case, a useful approximation can be developed by coupling these equations at the mean interfacial position, $\Psi=\Psi_i$.

The governing dynamic equations (Darcy equations) are

$$v_r = \frac{-k}{n\mu}\frac{\partial p}{\partial r} \tag{3.78}$$

$$v_y = \frac{-k}{n\mu}\left(\frac{\partial p}{\partial y} + \rho g\right) \tag{3.79}$$

in which v_r and v_y refer to radial and vertical seepage velocities respectively, p is the pressure, k is the permeability and μ is the dynamic viscosity. The governing mass conservation equation is

$$\frac{\partial c}{\partial t} + v_r\frac{\partial c}{\partial r} + v_y\frac{\partial c}{\partial y} = \frac{1}{r}\frac{\partial}{\partial r}\left(D_1 r\frac{\partial c}{\partial r}\right) + \frac{\partial}{\partial y}\left(D_2\frac{\partial c}{\partial y}\right) \tag{3.80}$$

which is simplified by the same assumptions appearing in Section 2.2.

$$\frac{\partial c}{\partial t} + u_i\frac{\partial c}{\partial r} = \alpha_1\frac{|A|}{r}\frac{\partial^2 c}{\partial r^2} + \alpha_2\frac{|A|}{r}\frac{\partial^2 c}{\partial y^2} \tag{3.81}$$

The interface is assumed to be linear in the volumetric coordinate system (Eq. 3.58) and δ is an unknown time-dependent function which represents the inverse volumetric interfacial slope.

The dynamic equations are manipulated in the same fashion as their linear counterparts (Section 2.3). The Dupuit approximation implies a hydrostatic pressure distribution,

$$\frac{\partial p}{\partial y} = -\rho g$$

and thus from Eq. (3.78) it follows that

$$\frac{\partial v_r}{\partial y} = \frac{kg}{n\mu}\frac{\partial \rho}{\partial r} = \frac{K}{n}\frac{1}{\rho}\frac{\partial \rho}{\partial r} \tag{3.82}$$

where K is hydraulic conductivity.

Equation (3.82) can be applied at the interface

$$\left.\frac{\partial v_r}{\partial y}\right|_{r=r_i} \simeq \frac{\partial u_i}{\partial y}$$

when the thickness of the dispersed zone, Δ, is much larger than the horizontal projected length of the wedge, $\Delta\Psi$. The analogous approximation for the linear case is examined in Appendix A. The result of this approximation is

$$\frac{\partial u_i}{\partial y} = \frac{\partial^2 r_i}{\partial y \partial t} = \frac{1}{2\pi nH}\frac{\partial}{\partial y}\left(\frac{1}{r_i}\frac{\partial \Psi_i}{\partial t}\right) = \left.\frac{K}{n}\frac{1}{\rho}\frac{\partial \rho}{\partial r}\right|_{r=r_i} \tag{3.83}$$

Using the linearity between density and concentration changes (Eq. 2.21), this becomes

$$\frac{\partial u_i}{\partial y} = \frac{K}{n}\frac{\Delta\rho}{\rho}\left(\frac{\partial c/c_o}{\partial r}\right)_{r=r_i} \tag{3.84}$$

Recharge Cycle The solution to Eq. (3.81) during recharge is obtained by the approximate method used in Section 3.2, and is given by Eq. (3.64) in which ξ is given by Eq. (3.61). However, in this case β is an unknown function of time. Differentiating c/c_o with respect to r and evaluating the result at the interface gives

$$\left.\frac{\partial (c/c_o)}{\partial r}\right|_{r=r_i} = \frac{2\pi nH\, r_i}{\sqrt{4\pi\xi}}$$

This result is used to evaluate the right hand side of Eq. (3.84), and the left hand side of Eq. (3.84) is, after multiplying by r_i^{-1}, written as

$$\frac{1}{r_i}\frac{\partial}{\partial t}\left(\frac{\partial r_i}{\partial y}\right) = \frac{1}{r_i}\frac{\partial}{\partial t}\left(\frac{1}{2r_i}\frac{\partial r_i^2}{\partial t}\right) = \frac{1}{2\pi nHr_i}\frac{\partial}{\partial t}\left(\frac{\beta}{r_i}\right)$$

where $\beta = \partial\Psi_i/\partial y$ has been introduced. It is consistent with the approximation of the convective dispersion equation (see Section 3.2, Eq. 3.60) to approximate r_i by r_* in the last expression. Equation (3.84) then reduces to

$$\frac{1}{2\Psi_*^{1/2}} \frac{d}{d\Psi_*}\left(\frac{\beta}{\Psi_*^{1/2}}\right) = \frac{\varepsilon_r^2}{H\sqrt{4\pi\xi}} \tag{3.85}$$

Equation (3.85) must be solved simultaneously with Eq. (3.61) in differential form,

$$\frac{d\xi}{d\Psi_*} = \left[\alpha_1 \frac{Q_r}{A_r/r_*} + \beta^2 \alpha_2 \frac{A_r/r_*}{Q_r}\right] \tag{3.86}$$

In order to simplify the simultaneous solution of these two equations, a new variable, $\theta = \beta/\Psi_*^{1/2}$, is introduced. Equations (3.85) and (3.86) then become

$$\frac{d\theta}{d\Psi_*} = \frac{\varepsilon_r^2 \Psi_*^{1/2}}{H\sqrt{\pi\xi}} \tag{3.87}$$

$$\frac{d\xi}{d\Psi_*} = \left[2\alpha_1(\pi nH)^{1/2} + \frac{\alpha_2}{2(\pi nH)^{1/2}} \theta^2\right]\Psi_*^{1/2} \tag{3.88}$$

which can be solved simultaneously to give

$$\xi^{1/2} = \left[2\alpha_1(\pi nH)^{1/2}\,\theta + \frac{\alpha_2}{6(\pi nH)^{1/2}} \theta^3\right] \frac{H\sqrt{\pi}}{2\varepsilon_r^2} \tag{3.89}$$

This result is substituted into Eq. (3.87) in order to find the inverse slope, $\beta = \Psi_*^{1/2}\theta$, for the initial condition $\beta=0$ at $t=0$,

$$\alpha_1(\pi nH)^{1/2}\,\beta^2 + \frac{\alpha_2}{24(\pi nH)^{1/2}} \frac{\beta^4}{\Psi_*} = \frac{4}{3} \frac{\varepsilon_r^4 \Psi_*^{5/2}}{\pi H^2} \tag{3.90}$$

The volumetric width of the dispersed zone, $\Delta = \sqrt{4\pi\xi}$, can be found from Eq. (3.89)

$$\Delta = \left[\frac{2\alpha_1}{r_*} + \frac{\alpha_2 r_*}{6\Psi_*^2} \beta^2\right] \frac{\beta\pi H}{\varepsilon_r^2} \tag{3.91}$$

and the ratio of Δ to $\Delta\Psi$ is

$$\frac{\Delta}{\Delta\Psi} = \frac{\Delta}{\beta H} = \left[\frac{2\alpha_1}{r_*} + \frac{\alpha_2 r_*}{6\Psi_*^2}\beta^2\right] \frac{\pi}{\varepsilon_r^2} \tag{3.92}$$

Equation (3.90) can be approximated for both large and small interfacial slopes, noting that α_1 is usually an order of magnitude greater than α_2. For larger slopes (β small), lateral dispersion is negligible and Eq. (3.90) reduces to

$$\beta = \frac{2\varepsilon_r^2 \Psi_*^{5/4}}{H}\left(\frac{1}{3\alpha_1 \pi (\pi n H)^{1/2}}\right)^{1/2} \tag{3.93}$$

The volumetric width of the mixed zone is

$$\Delta = 4\Psi_*^{3/4}\sqrt{\frac{\pi(\pi n H)^{1/2}\alpha_1}{3}} \tag{3.94}$$

and the ratio Δ to $\Delta\Psi$ is,

$$\frac{\Delta}{\Delta\Psi} = \frac{2\pi\alpha_1}{\varepsilon_r^2}\frac{(\pi n H)^{1/2}}{\Psi_*^{1/2}} \tag{3.95}$$

For small interfacial slopes (large β), longitudinal dispersion is negligible and Eq. (3.90) simplifies to

$$\beta = 2\varepsilon_r \Psi_*^{7/8}\left[\frac{2}{H\alpha_2}\sqrt{\frac{n}{\pi H}}\right]^{1/4} \tag{3.96}$$

In this case the ratio of Δ to $\Delta\Psi$ is given by

$$\frac{\Delta}{\Delta\Psi} = \frac{2}{3}\left[\frac{2\pi\alpha_2}{H^2(\pi n H)^{1/2}}\right]^{1/2}\Psi_*^{1/2} \tag{3.97}$$

Storage Cycle As explained in Section 3.2, the additional mixing during storage due to grain dispersion is negligible. Suppose that at the start of the storage period the volumetric length of the interface, $\Delta\Psi$, is much smaller than the width of the dispersed zone, Δ. Then the rate of tilting of the wedge will be governed by a coupled analysis which accounts for the interaction of the density difference and the given dispersed zone.

In this case it is assumed that the volumetric width of the dispersed zone remains constant and equal to its initial value, Δ_o, throughout the storage cycle. From the definition of Δ,

$$\Delta_o^{-1} = \frac{\partial}{\partial \Psi}\left(\frac{c}{c_o}\right) = \frac{1}{2\pi nHr}\frac{\partial}{\partial r}\left(\frac{c}{c_o}\right)$$

and from this expression the right hand side of Eq. (3.84) is evaluated to yield

$$\frac{\partial u_i}{\partial y} = \frac{K}{n}\frac{\Delta\rho}{\rho}\frac{2\pi nH}{\Delta_o} r_i \qquad (3.98)$$

The velocity gradient is represented by

$$\frac{\partial u_i}{\partial y} = \frac{\partial}{\partial t}\left(\frac{\partial r_i}{\partial y}\right) = \frac{1}{2\pi nH}\frac{\partial}{\partial t}\left(\frac{\beta}{r_i}\right)$$

where $\beta = \partial \Psi_i/\partial y$ and $\Psi_i = \Psi_o + \beta(y-H/2)$. Equation (3.98) then becomes

$$\frac{1}{\pi nHr_i}\frac{\partial}{\partial t}\left(\frac{\beta}{r_i}\right) = \frac{4\pi nD}{\Delta_o} \qquad (3.99)$$

and by introducing the approximation analogous to that preceding Eq. (3.85), i.e., $r_i \cong r_o$ or $\Psi_i \cong \Psi_o$, this reduces to

$$\frac{d\beta}{dt} = \frac{4\pi nD\Psi_o}{\Delta_o}$$

If β_o is the inverse volumetric slope of the interface at the start of the storage cycle, $t=t_o$, then

$$\beta = \beta_o + \frac{4\pi nD\Psi_o}{\Delta_o}(t-t_o) \qquad (3.100)$$

which remains valid as long as $\beta H = \Delta\Psi \ll \Psi_o$.

Withdrawal Cycle The coupled solution for the withdrawal period utilizes the convective dispersion equation found in Section 3.2 (Eq. 3.69) and its solution (Eq. 3.74). The analysis parallels that described for the recharge period, and yields two equations analogous to Eqs. (3.85) and (3.86) for the recharge period. The governing equations differ only by signs, and the details of the development are omitted. The result for the equation describing the flow dynamics (the equivalent of Eq. (3.85)) is

$$\frac{1}{\Psi_*^{1/2}}\frac{d}{d\Psi_*}\left(\frac{\beta}{\Psi_*^{1/2}}\right) = \frac{-\varepsilon_w^2}{H\sqrt{\pi\xi}} \qquad (3.101)$$

and the equation expressing dispersion (equivalent to Eq. (3.86)) becomes

$$-\frac{d\xi}{d\Psi_*} = \frac{\alpha_1 Q_w}{A_w/r_*} + \beta^2 \alpha_2 \frac{A_w/r_*}{Q_w} \tag{3.102}$$

In these equations Ψ_* is given by

$$\Psi_* = \Psi_o - Q_w(t-t_o)$$

The simultaneous solution to these equations is found as in the recharge case and

$$\xi^{1/2} = \left[\frac{2\alpha_1}{r_*} + \frac{\alpha_2 r_*}{6} \frac{\beta^2}{\Psi_*^2} \right] \frac{\beta H\sqrt{\pi}}{2\varepsilon_w^2} + C_6 \tag{3.103}$$

where C_6 is a constant used to match with the previous cycle. The inverse slope, β, is found by substituting Eq. (3.103) into Eq. (3.101) and integrating

$$\alpha_1(\pi nH)^{1/2} \frac{\beta^2}{\Psi_*} + \frac{\alpha_2}{24(\pi nH)^{1/2}} \frac{\beta^4}{\Psi_*^2} + \frac{2\varepsilon_w^2}{H\sqrt{\pi}} \frac{\beta}{\Psi_*^{1/2}} C_6 = -\frac{4\varepsilon_w^4}{3\pi H^2} \Psi_*^{3/2} + C_7 \tag{3.104}$$

The constant, C_7, is dependent on the initial slope, β_o.

When considering multiple cycles, it may be convenient to evaluate the constants C_6 and C_7 in terms of the initial dispersed zone thickness, Δ_o, and the initial inverse slope, β_o. Using $\Psi_o = \pi n H r_o^2$, the dispersed zone thickness becomes

$$\Delta = (4\pi\xi)^{1/2} = \frac{\pi H}{\varepsilon_w^2}\left[2\alpha_1\left(\frac{\beta}{r_*} - \frac{\beta_o}{r_o}\right) + \frac{\alpha_2}{6}\left(\frac{r_*\beta^3}{\Psi_*^2} - \frac{r_o\beta_o^3}{\Psi_o^2}\right)\right] + \Delta_o \tag{3.105}$$

and the general expression for the inverse interfacial slope, β, is

$$\alpha_1(\pi nH)^{1/2}\left[\frac{\beta^2}{\Psi_*} - \frac{\beta_o^2}{\Psi_o}\right] + \frac{\alpha_2}{24(\pi nH)^{1/2}}\left[\frac{\beta^4}{\Psi_*^2} - \frac{\beta_o^4}{\Psi_o^2}\right]$$

$$+ \left[\frac{\varepsilon_w^2\Delta_o}{\pi H} - \beta_o\left(\frac{2\alpha_1}{r_o} + \frac{\alpha_2 r_o}{6}\frac{\beta_o^2}{\Psi_o^2}\right)\right]\left[\frac{\beta}{\Psi_*^{1/2}} - \frac{\beta_o^2}{\Psi_o^{1/2}}\right]$$

$$= \frac{-4\varepsilon_w^4}{3\pi H^2} [\Psi_*^{3/2} - \Psi_o^{3/2}] \qquad (3.106)$$

The concentration field is obtained by using Eq. (3.105) in the general solution as given by Eq. (3.74). The interpretation and application of these results are discussed in the following sections.

3.4 Discussion of the Theoretical Results

In the previous portions of this Section, theoretical models were presented to describe the mixing of two fluids in a radial flow system, due to density difference and grain dispersion. The first model presented in Section 3.1 was based on an immiscible displacement process in which the only mixing mechanism was the density difference. A nonlinear partial differential equation (Eq. 3.11) describing the interfacial shape and position for either recharge, storage or withdrawal was derived. An equivalent equation was used by Perrine and Gay (1964) in their investigation of secondary recovery of oil. However, they were primarily interested in the effects of large viscosity differences on the interface and did little analysis of those situations in which the density difference is the predominant effect.

A solution of Eq. (3.11) was first developed for the recharge process. It was found that the interface is described by a straight line in volumetric coordinates when the volumetric length of the interface, $\Delta\Psi=\beta H$, is small in comparison to the volumetric distance of the convected front from the origin, Ψ_*. This is the case when ε_r (Eq. 3.17) is small compared to unity. For an initially vertical interface at the well this ratio, $\Delta\Psi/\Psi_*$, remains constant throughout recharge (Eq. 3.31) and the interface is adequately described by the straight line interface at all times during the recharge period if ε_r is sufficiently small. When there is some amount of tilting at the start of recharge (Eq. 3.52), such as would occur after a recharge, storage, withdrawal sequence, the ratio $\Delta\Psi/\Psi_*$ decreases as Ψ_* increases. Thus the description of the interface by a straight line will improve with time.

In order to improve upon the linear interfacial solution found for recharge, perturbation techniques were used to investigate the curvature of the interface. The results of this perturbation analysis, as shown in Figure 3.2, indicate that there is only a small departure from the linear interface, even for relatively large values of ε_r. It is seen that for large ε_r the lower end of the interface has advanced into the aquifer farther than it would for a linear interface. In the subsequent analysis of the recharge process, it will be assumed that the interface is linear in the volumetric coordinate system.

One of the primary characteristics of the immiscible model is the volumetric length of the interface. For the linear interface (lowest order form of Eq. (3.31)),

$$\Delta\Psi = \beta H = 2\varepsilon_r \Psi_* \qquad (3.107)$$

is shown in Figure 3.3 as a dimensionless plot of $\beta D/Q_r H = \Delta V D/Q_r H^2$ versus $2\varepsilon_r \tau$. The parameter τ is a dimensionless time,

$$\tau = \frac{K}{n}\frac{\Delta\rho}{\rho}\frac{t}{H} = \frac{Dt}{H^2}$$

It is also useful to consider the interface as it appears to an observer in a single observation well at a radius r. This is often the type of information which may be gathered in the field. The observer would record depth averaged relative concentration in the aquifer, $\bar{c}/c_o$, as a function of time

$$\frac{\bar{c}}{c_o} = \frac{1}{H}\int_o^H \frac{c}{c_o}\, dy \qquad (3.108)$$

Because the fluids are considered immiscible for the purpose of this model, the value of $\bar{c}/c_o$ is identical to the dimensionless height of the interface, η/H. A simple method of representing these results is the time slope at $\bar{c}/c_o = \eta/H = 0.5$ (i.e., $V = V_*$) which is, from Eq. (3.51),

$$\left.\frac{\partial \eta/H}{\partial t}\right|_{\eta/H=0.5} = (\Delta t)^{-1} = -Q_r/\beta H$$

where Δt is the inverse of the rate of change of relative concentration. It is convenient to present this result in terms of the dimensionless variable

$$\Delta\tau \equiv \frac{K}{n}\frac{\Delta\rho}{\rho}\frac{\Delta t}{H} = -2\varepsilon_r\tau \qquad (3.109)$$

as obtained from Eq. (3.107). This result is shown graphically in Figure 3.4.

Equation (3.11) was also solved for storage and withdrawal processes. During storage the interface is described by a straight line in volumetric coordinates when ΔV is small compared to the initial volume, V_o (Eq. 3.41). The requirement of small $\Delta V/V_o$ must be met for the initial condition at the start of storage. However, unlike the recharge process examined earlier, the ratio $\Delta V/V_o$ is a function of time, V_o is a constant and $\Delta V = \beta H$ is increasing with time (Eq. 3.49). If storage is continued long enough, ΔV will eventually become large compared to V_o and the approximation of a linear interface may become inappropriate. A reasonable limit on the application of the linear interface solution (Eq. 3.41) is the condition $\Delta V/V_o < 1$. From the results for recharge, it would be expected that interface curvature will become important for $\Delta V/V_o$ near unity. Analysis of these curvature effects is suggested as a topic for future study.

The withdrawal phase also yielded a linear volumetric interfacial solution when the volumetric interfacial length, ΔV (Eq. 3.50), is small compared to the volumetric distance of the convected front from the origin, V_*. A necessary, but not sufficient, condition for this solution is that ε_w be small compared to unity ($\varepsilon_w << 1$). The initial condition inherited from the previous recharge or storage process must also be considered. Thus $\beta_o H/V_o$

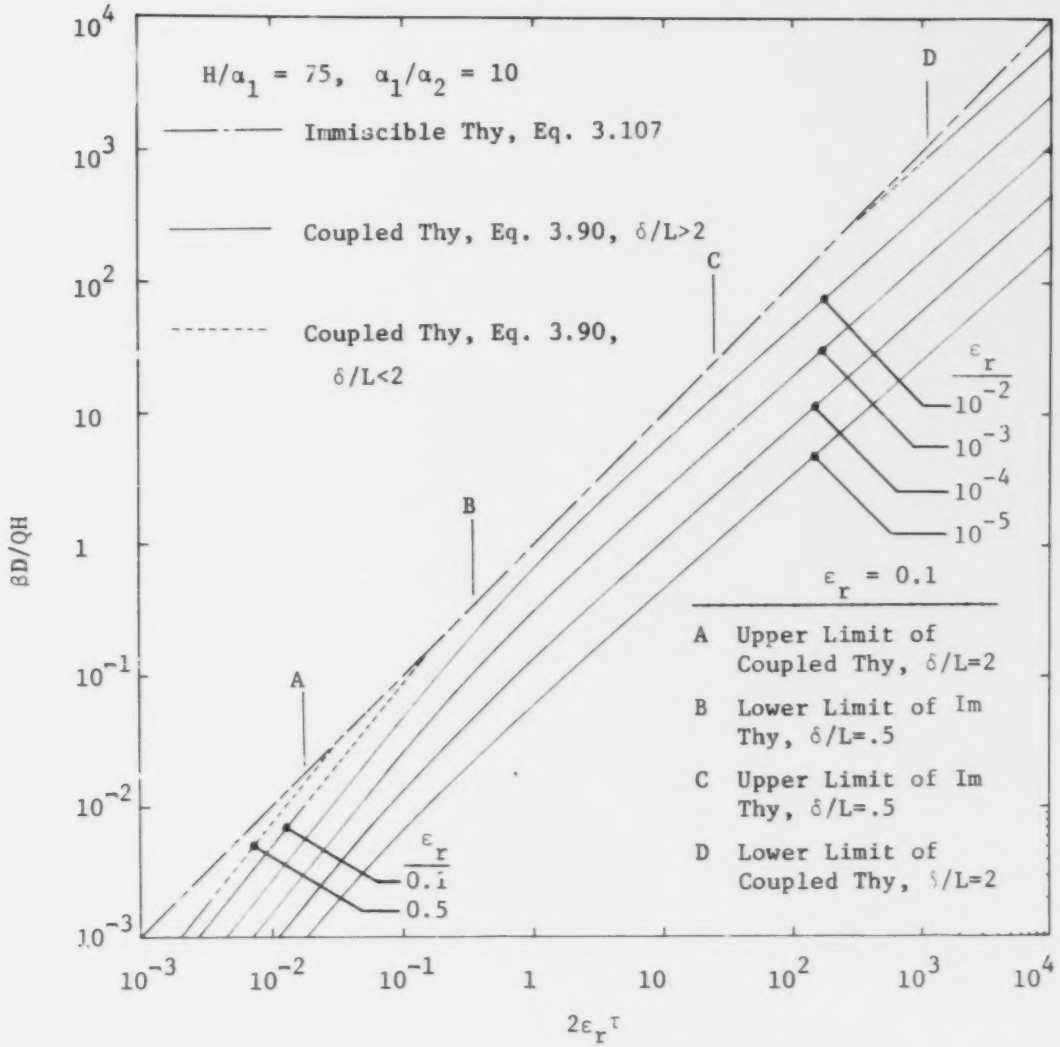

Figure 3.3 Inverse Interface Slope, β, as a Function of Time during Recharge

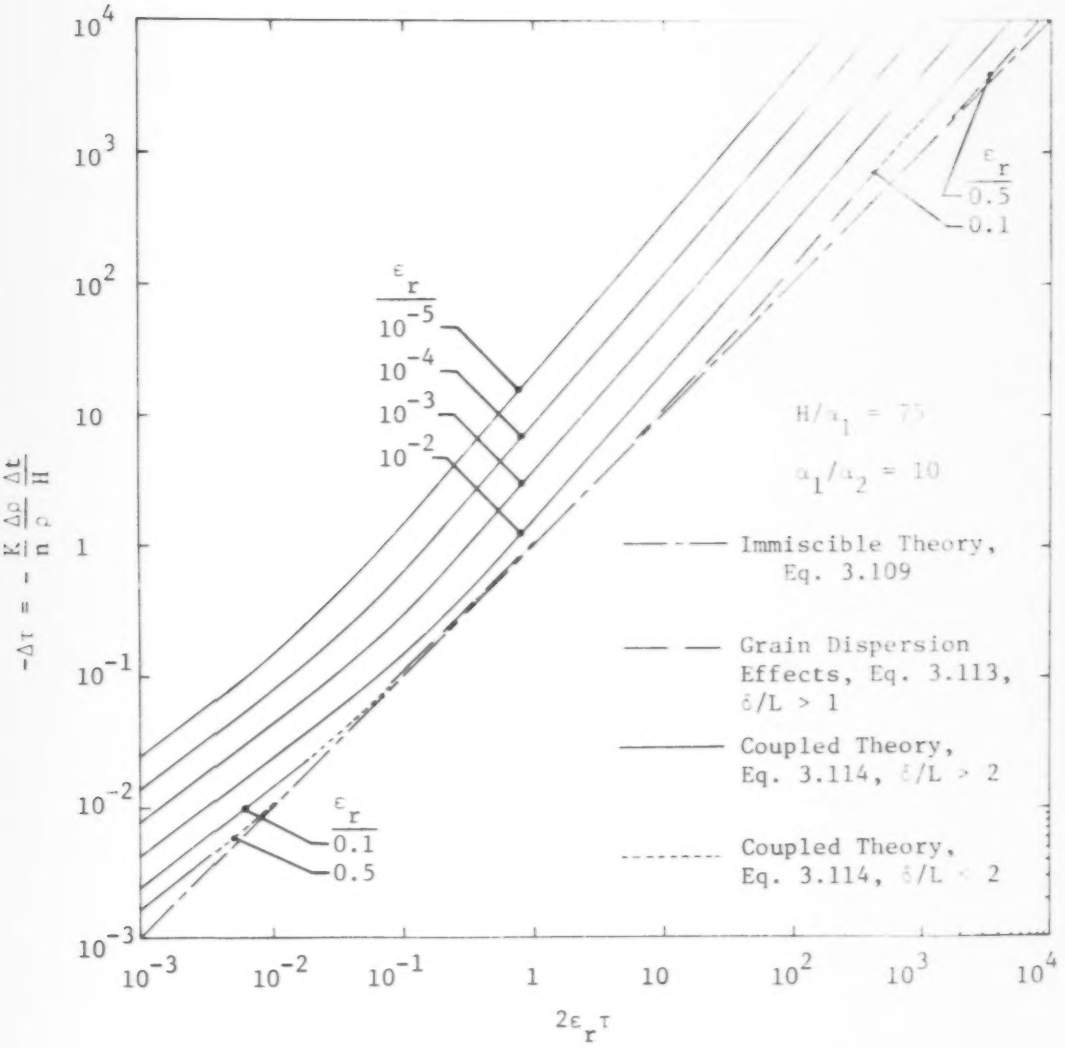

Figure 3.4 Inverse Rate of Change of Relative Concentration, Δt, as a Function of Time during Recharge

must be small compared to unity at the start of withdrawal. Finally, it is important to examine the temporal conditions under which the linear interfacial solution is valid. The ratio $\Delta\Psi/\Psi_*$ can be expressed as (Eq. 3.50)

$$\frac{\Delta\Psi}{\Psi_*} = \frac{\beta H}{\Psi_*} = \frac{\beta_o H}{\Psi_*} \left[1 + \left(\frac{2\varepsilon_w}{\beta_o H}\right)^2 \left(\Psi_o^2 - \Psi_*^2\right)\right]^{1/2} \qquad (3.110)$$

As Ψ_* decreases to zero during withdrawal, the ratio $\Delta\Psi/\Psi_*$ increases and the linear interface solution eventually becomes invalid. As in the storage case, the limit for this solution may be taken as $\Delta\Psi/\Psi_*<1$. Using this condition in Eq. (3.110) there is the implied lower limit on the application of the linear interface result during withdrawal,

$$\Psi_* > \Psi_o \left[\frac{\left(\beta_o H/\Psi_o\right)^2 + 4\varepsilon_w^2}{1 + 4\varepsilon_w^2}\right]^{1/2}$$

When Ψ_* approaches this limit, it would be expected that interface curvature effects may become significant. If a linear interface is assumed, the lower end of the interface reaches the well when $\Delta\Psi/2=\Psi_*$. For this condition $\Delta\Psi/\Psi_*>1$ and thus significant errors may be introduced when the linear interface theory is applied at the well. The possible effects of interface curvature as the interface approaches the well should be analyzed in future studies.

The effects of grain dispersion were analyzed in Section 3.2 by assuming the grain dispersion to have no influence upon the flow dynamics. The dynamics are given by the immiscible model (Section 3.1) where the interface is now idealized as the line of 50% relative concentration. The volumetric interfacial length, $\Delta\Psi$, was assumed to be small compared to the distance from the origin, Ψ_* or Ψ_o, and a linear volumetric interface was obtained. An estimate for the volumetric width of the dispersed zone, Δ, was found for recharge (Eq. 3.65) and withdrawal (Eq. 3.76). The ratio of the dispersed zone width to the volumetric interfacial length, $\Delta/\beta H$, was proposed as the criterion to estimate the importance of grain dispersion during radial flow. For recharge this is given by Eq. (3.67) and for withdrawal by Eq. (3.77).

As described in Section 3.2, this model is valid when $\Delta/\beta H$ is small compared to unity. Figure 3.5 shows the ratio, $\Delta/\beta H$, versus dimensionless time, τ, for several values of ε_r during a recharge operation with an initially vertical interface. This graph was constructed by assuming a typical ratio of dispersivities ($\alpha_1/\alpha_2=10$) and by taking the ratio of aquifer height, H, to longitudinal dispersivity, α_1, as a constant equal to 75, a typical field value. $\Delta/\beta H$ is large for small time indicating that interaction between density difference and longitudinal grain dispersion may be important near the well. $\Delta/\beta H$ decreases at first, but it

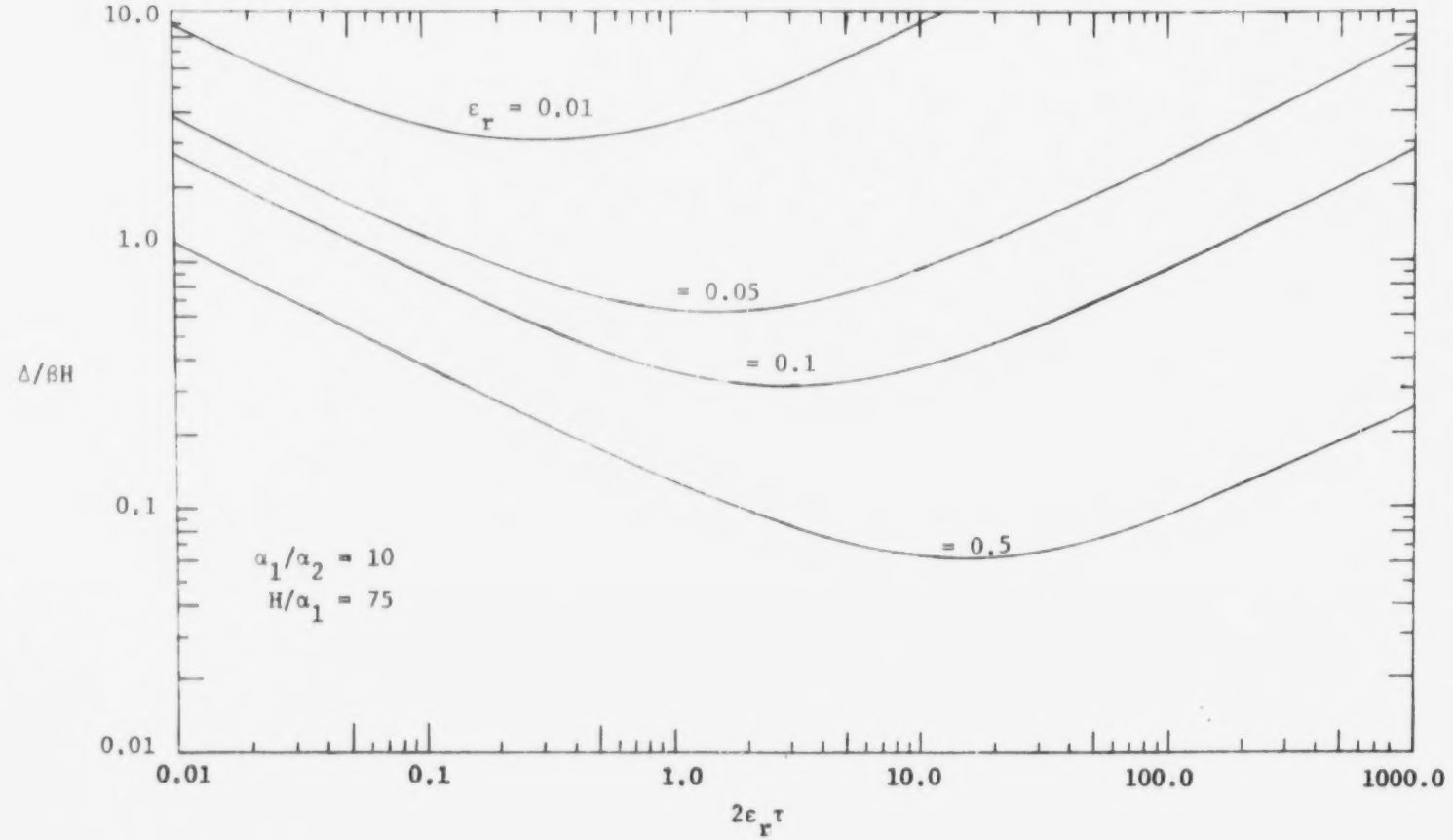

Figure 3.5 Δ/βH as a Function of Time During Recharge for the Case of No Dynamic Effects of Grain Dispersion

eventually increases as lateral dispersion becomes important (Eq. 3.67). It can be expected that even for large values of ε_r, mixing due to grain dispersion will eventually become as important as density induced mixing. The exact limits of applicability of the immiscible model cannot be specified, but as was demonstrated in Section 2.4 reasonable estimates may be obtained by assuming the limiting values of $\Delta/\beta H$ at a fixed number less than one. $\Delta/\beta H=1/2$ will be chosen here. For a given value of ε_r, the indicated range of dimensionless time, τ, for which the immiscible analysis is valid is found from Figure 3.5 or Eq. (3.67). For example, when $\varepsilon_r=0.1$ the minimum $2\varepsilon_r\tau$ is shown in Figure 3.5 as 0.35 and the maximum is 25. Between these two values the immiscible theory can be expected to apply.

The dimensionless length of time, $\Delta\tau$, as defined in Eq. (3.109), is found by differentiating the depth averaged concentration (Eq. 3.108) with respect to time. The depth averaged concentration is obtained by integrating Eq. (3.64),

$$\frac{\bar{c}}{c_o} = \frac{1}{2}\left[1+\frac{\sqrt{4\xi}}{\beta H}\left\{\mu_2 \operatorname{erf}\mu_2 - \mu_1 \operatorname{erf}\mu_1 + \frac{1}{\sqrt{\pi}}\left(e^{-\mu_2^2}-e^{-\mu_1^2}\right)\right\}\right] \qquad (3.111)$$

where

$$\mu_n = [\bar{\Psi}+(-1)^n\beta H/2]/\sqrt{4\xi}$$

The derivative of (Eq. 3.111) with respect to time is evaluated at $\Psi_*=V$ ($\bar{\Psi}=0$).

$$\left.\frac{\partial \bar{c}/c_o}{\partial t}\right|_{\bar{\Psi}=0} \equiv (\Delta t)^{-1} = -\frac{1}{\beta H}\frac{\partial \Psi_*}{\partial t}\operatorname{erf}\left(\frac{\sqrt{\pi}}{2}\frac{\beta H}{\Delta}\right) \qquad (3.112)$$

For the recharge case ($\partial\Psi_*/\partial t=Q_r$) with an initially vertical interface, βH is given by Eq. (3.107) and $\Delta/\beta H$ by Eq. (3.67). Thus $\Delta\tau$ becomes

$$\Delta\tau = \frac{K}{n}\frac{\Delta\rho}{\rho}\frac{t}{H} = -2\varepsilon_r\tau\left[\operatorname{erf}\frac{3\sqrt{\pi}\,k_1(2\varepsilon_r\tau)^{1/4}}{4\left[1+\frac{3}{5}\frac{\alpha_2}{\alpha_1}\frac{(2\varepsilon_r\tau)}{\varepsilon_r}\right]^{1/2}}\right]^{-1} \qquad (3.113)$$

where

$$k_1 = \left(\frac{H}{\alpha_1}\frac{1}{3\pi}\right)^{1/2}\varepsilon_r^{1/4}$$

This result is shown graphically in Figure 3.4. Note that for some mid-range values of time there is effectively no increase in $\Delta\tau$ due to the addition of grain dispersion over the value predicted by the immiscible model.

During the storage cycle, the additional mixing due to grain dispersion was neglected. This assumption is consistent with the conditions necessary to derive the immiscible model with a linear volumetric interface.

The model requires that the dispersed zone width, Δ, be small compared to βH at the beginning of any process to which it is applied. During storage βH must also be small compared to Ψ_o for the model to apply. The dispersed zone width at the start of storage, Δ, is proportional to the distance traveled by the interface, Ψ_o. During storage the interface will tilt about its midpoint, with the result that the interfacial endpoints would travel the most and undergo the greatest amount of dispersion. But this travel must still be small compared to Ψ_o in order for $\Delta\Psi/\Psi_o$ ratio to remain small. Thus it is consistent to neglect this additional dispersion.

In the third model, presented in Section 3.3, the combined effects of density difference and grain dispersion were analyzed by an approximate coupling of the mass and momentum equations based on large $\Delta/\beta H$. It was assumed that the interface remained linear for this development. The interfacial slope for a recharge process with an initially vertical interface is given by Eq. (3.90) and can be represented by a family of curves relating the volumetric inverse slope, β, and Ψ_* for various values of ε_r, α_1/α_2 and H/α_1. Equation (3.90) is shown in Figure 3.3 as a dimensionless plot for several values of ε_r with $\alpha_1/\alpha_2=10$, and the ratio $H/\alpha_1=75$. As noted in Section 3.3, the coupled analysis is valid when $\Delta/\beta H>>1$. The ratio $\Delta/\beta H$ (Eq. (3.92) with Eq. (3.90) substituted for β) is shown in Figure 3.6 for a number of values of ε_r. The range of applicability of the coupled model (Eq. 3.90) can be analyzed by setting an approximate limit on the value of $\Delta/\beta H$. For this discussion the condition $\Delta/\beta H>2$ is assumed for the coupled model to apply. For example, when $\varepsilon_r=0.1$ the coupled model is applicable up to $2\varepsilon_r\tau=0.018$ during which longitudinal dispersion is important. Later when $2\varepsilon_r\tau$ exceeds 1000, the coupled analysis again becomes applicable with lateral dispersion as the predominant mixing mechanism. Figure 3.3 indicates these regions of validity and if closely examined, it can be seen that the regions of validity for the immiscible model (Eq. 3.107) and the coupled model (Eq. 3.90) are mutually exclusive for a given value of ε_r. In general, there will be intermediate time ranges during which neither model is applicable. In the example, $\varepsilon_r=.1$, these intermediate ranges are $0.018<2\varepsilon_r\tau<0.35$ and $25<2\varepsilon_r\tau<1000$. The actual behavior of the wedge in these ranges is not known, but a smooth transition between the models is expected.

The curves representing Eq. (3.90) in Figure 3.3 are shown as dashed lines for $\Delta/\beta H<2$. It can be seen that, even for large values of ε_r, longitudinal dispersion will influence the tilting near the well, and if recharge continues long enough, lateral dispersion will influence the tilting. As ε_r decreases, interfacial tilting becomes less and as lateral dispersion becomes important, the rate of tilting decreases. The point of intersection of the immiscible theory and the coupled theory can be found by solving equations (3.90) and (3.107) simultaneously. That expression can in turn be solved for the value of ε_r for which the coupled theory is tangential to the immiscible theory at the point of intersection, $\varepsilon_r=(2\alpha_1/H)(3\alpha_2/2\alpha_1)^{1/2}=3.26\times10^{-2}$ for Figure 3.3. For values of ε_r greater than this, there will be an intersection of the two theories; for values of ε_r less than this, the immiscible theory is never valid during recharge.

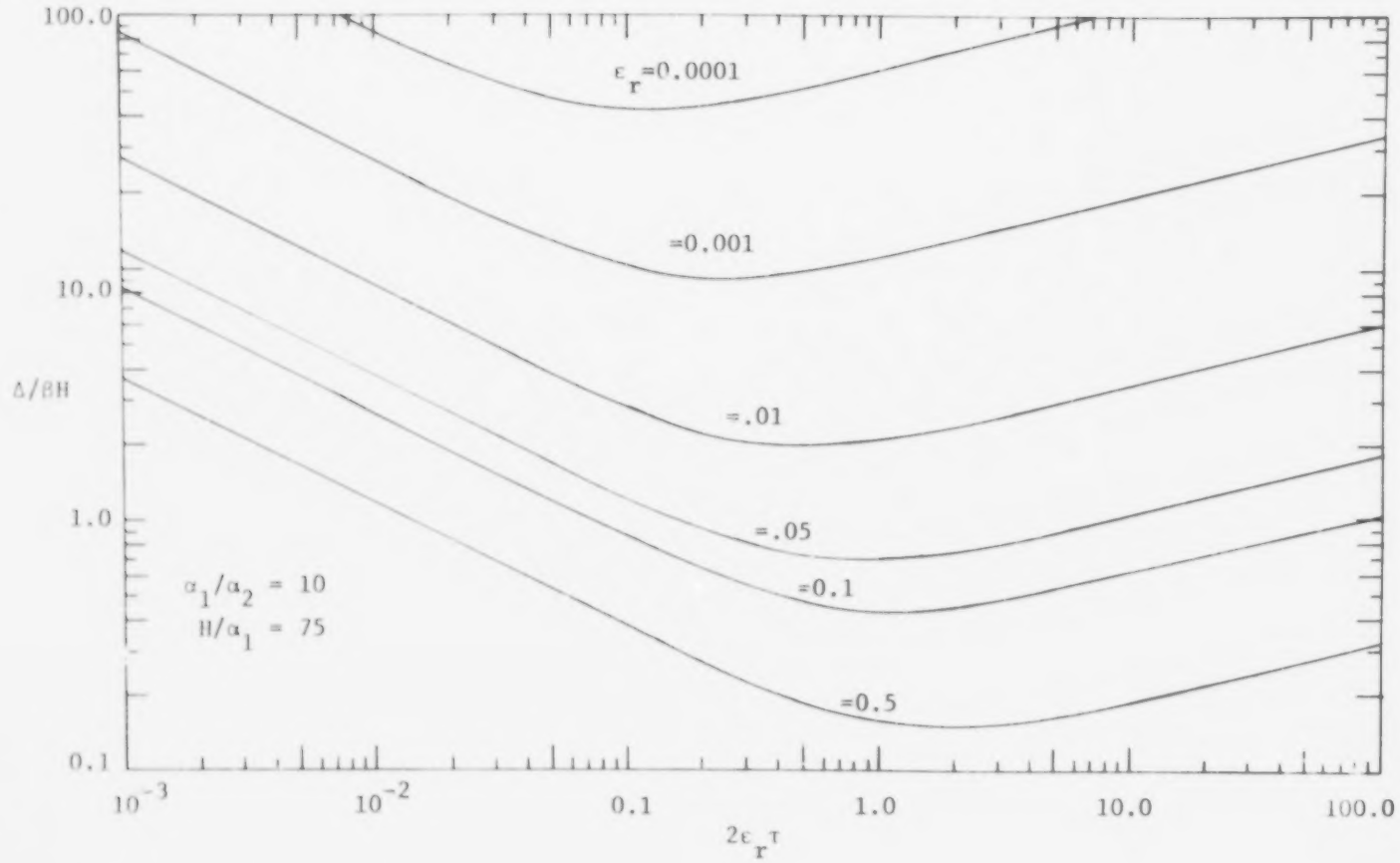

Figure 3.6 Δ/βH as a Function of Time During Recharge for the Case of Interaction Between Grain Dispersion and Density Induced Mixing

The ratio $\Delta/\beta H$ indicates the relative importance of the two mixing mechanisms, grain dispersion and density difference. When $\Delta/\beta H$ is small (Section 3.2), grain dispersion has no effect on the interface and the dynamics are given by the immiscible model. When $\Delta/\beta H$ is large, the combined effects of the two mechanisms are important (see Appendix A for analogous development in plane flow) and the coupled analysis governs the mixing. The coupled solution does not reduce to the immiscible solution when $\alpha_1, \alpha_2 \to 0$ because the regions of validity of the two solutions do not overlap.

The length of time, Δt, defined by the inverse time derivative of $\bar{c}/c_o$ (Eqs. (3.108) and (3.111)) at $\bar{\Psi}=0$ is given by Eq. (3.112) for both the coupled and immiscible dynamic theories. For recharge ($\partial\Psi_*/\partial t = Q_r$) in which interaction between grain dispersion and density difference is significant βH is given by Eq. (3.90) and Δ is given by Eq. (3.91). Then the dimensionless form of Δt can be written as

$$\Delta\tau = \frac{K}{n}\frac{\Delta\rho}{\rho}\frac{\Delta t}{H} = -\frac{\beta D}{Q_r H}\left[\operatorname{erf}\frac{3\sqrt{\pi}\, k_1^2\,(2\varepsilon_r\tau)^{1/2}}{4\left(1+\frac{2k_1^2}{k_2^4}\frac{(\beta D/Q_r H)^2}{(2\varepsilon_r\tau)}\right)}\right]^{-1} \qquad (3.114)$$

where

$$k_2 = \left(\frac{2}{\pi}\frac{H}{\alpha_1}\frac{\alpha_1}{\alpha_2}\right)^{1/4}\varepsilon_r^{3/8}$$

This expression is presented graphically in Figure 3.4 for several values of ε_r. For values of $\Delta/\beta H$ less than 2, the curves are shown by dashed lines. Note that for large values of ε_r there is effectively no increase in $\Delta\tau$, for some midrange values of τ, over that predicted by the immiscible theory, Eq. (3.109).

The combined effects of density difference and grain dispersion were also investigated for the storage and withdrawal cycles. During storage the change in dispersed zone thickness, Δ, was assumed to be negligible and the rate of interfacial tilting was described by Eq. (3.100). For withdrawal, expressions were presented which described the inverse slope of the interface (Eq. 3.106) and the volumetric width of the dispersed zone (Eq. 3.105). Some general features of these results may be noted. If lateral dispersion predominates during withdrawal (Eq. 3.106 with $\alpha_1=0$), then it can be shown that $\Delta/\beta H$ always increases with time and the coupled analysis can definitely become applicable. The same trend is noted for the immiscible theory (Eq. 3.77), thus indicating that a transition from immiscible dynamics to coupled dynamics can occur. If longitudinal dispersion is of primary importance during withdrawal, $\Delta/\beta H$ may increase or decrease depending on magnitude of Ψ_o, β_o and Δ_o (Eq. 3.106 with $\alpha_2=0$). If $\Psi_o >> \beta_o H$, the indication is that $\Delta/\beta H$ increases.

The analysis of the interaction between density difference and grain

dispersion, as presented in Section 3.3, has certain implicit limitations. One of these is that $\Delta/\beta H$ be large compared to unity. This restriction is explained in Appendix A for the case of linear two-dimensional flow and the same restriction is implied for radial flow. As pointed out in Appendix B, there is implied, from these approximate solutions, a relaxation of the no-flux boundary conditions at the upper and lower boundaries of the aquifer when $\Delta/\beta H$ is large. The possible effects of these boundary conditions should be investigated in future studies.

3.5 Applications of the Radial Theory

One of the objectives of this research is to make it possible to forecast the amounts and quality of fresh water which can be removed after storage in a saline aquifer under various operational schemes. Procedures by which the theoretical results in the previous sections can be combined to simulate complex operational conditions will be outlined. These procedures should also be applicable to deep-well waste disposal operations in which there is a density difference between the injected wastes and the native water.

The immiscible theory (Section 3.1) can be used to construct simple, approximate results for many types of applications. To illustrate the use of this theory, a one sequence operation of recharge, storage, and withdrawal cycles will be analyzed. Additional sequences may be analyzed by matching the solutions between cycles described in Section 3.1.

Consider a recharge operation with a flowrate, Q_r, for time, t_r, storage for time, t_s, and withdrawal at a rate Q_w. For these conditions, we want to find the interface position as a function of time and the amount of water recovered. Utilizing the set of solutions described by a linear volumetric interface, the volumetric length of the interface during recharge, βH, is described by Eq. (3.52) with $\beta_o = \Psi_o = 0$. At the end of recharge when a volume $\Psi_o = Q_r t_r$ has been injected, the volumetric length of interface is $\beta H = 2\varepsilon_r \Psi_o$ which provides the initial value of β for the storage cycle. During storage the net flow is zero and the interface is described by Eq. (3.49), with $\beta_o = 2\varepsilon_r \Psi_o / H$ and after storage for a period t_s

$$(\beta H/\Psi_o)^2 = 4\varepsilon_r^2(1+2t_s/t_r)$$

Using this value of β as the initial value, β_o, in Eq. (3.50) for withdrawal, we find

$$(\beta H/\Psi_o)^2 = 4\varepsilon_r^2(1+2t_s/t_r) + 4\varepsilon_w^2[1-(\Psi_*/\Psi_o)^2] \qquad (3.115)$$

which can be used to evaluate the volume of water recovered.

For this analysis it will be assumed that withdrawal ends when the depth averaged relative concentration, $\bar{c}/c_o$, reaches some specific level $\bar{c}/c_o = b$, $0 \le b \le 1$, at the well. This level will depend on the intended uses of the recovered fresh water. For purely immiscible displacement, the depth average concentration is $\bar{c}/c_o = r/H$ and the analysis of withdrawal can be

based on geometric considerations of the interface as it reaches the well. From Figure 3.7 it can be seen that when $c/c_o=b$ at the well,

$$\Psi_* = \beta H(1-2b)/2 \tag{3.116}$$

The total volume of water recovered at that time is

$$\Psi_R = \Psi_o - \Psi_* \tag{3.117}$$

Note that this recovered volume includes some contaminated water with $c/c_o=b$. The recovery ratio, $R=\Psi_R/\Psi_o$, is, from Eqs. (3.116) and (3.117),

$$R = 1 - (1-2b)(\beta H/2\Psi_o) \tag{3.118}$$

The value of βH when withdrawal ends is found by solving Eqs. (3.115) and (3.116) simultaneously and with that result the recovery ratio becomes

$$R = 1 - (1-2b)\left(\frac{\varepsilon_w^2+\varepsilon_r^2(1+2t_s/t_r)}{1+(1-2b)^2\varepsilon_w^2}\right)^{1/2} \tag{3.119}$$

This simple result can form the basis for approximate comparisons of alternative recharge, storage and withdrawal schemes. As indicated in Section 3.4, some error may be introduced because of interface curvature near the well. However, the comparisons with experiments in Section 5 indicate that Eq. (3.119) provides reasonable estimates of R which are somewhat less than those observed.

Some characteristics of the result in Eq. (3.119) can be seen by considering $t_s=0$ and $b=0$, in which case the recovery ratio can be represented graphically as shown in Figure 3.8. Note that lines of constant R are roughly circular in the $\varepsilon_r,\varepsilon_w$ plane, hence, a given value of recovery ratio can be attained approximately by specifying a constant distance from the origin in this plane. The graph also illustrates the importance of the parameters ε_r and ε_w in determining the recovery ratio. Favorable recovery ratios are generally obtained with low values of ε_r and ε_w.

Some other features can be analyzed using the immiscible solutions. For multiple sequences of recharge-storage-withdrawal, interface movements and recovery ratios can be found by repeated application of Eqs. (3.49), (3.50) and (3.52) with appropriate matching between cycles. As a specific example of multiple recharge-withdrawal sequences, consider a well operation in which ε_r and ε_w are unchanged (i.e., the same flow rates) for several sequences and $t_s=0$. In each recharge cycle the same volume of water is injected and during withdrawal, water is pumped until the wedge first reaches the well (b=0). Under these conditions we find, using Eqs. (3.49), (3.50) and (3.52)with matching between cycles, the following recovery ratios for each sequence:

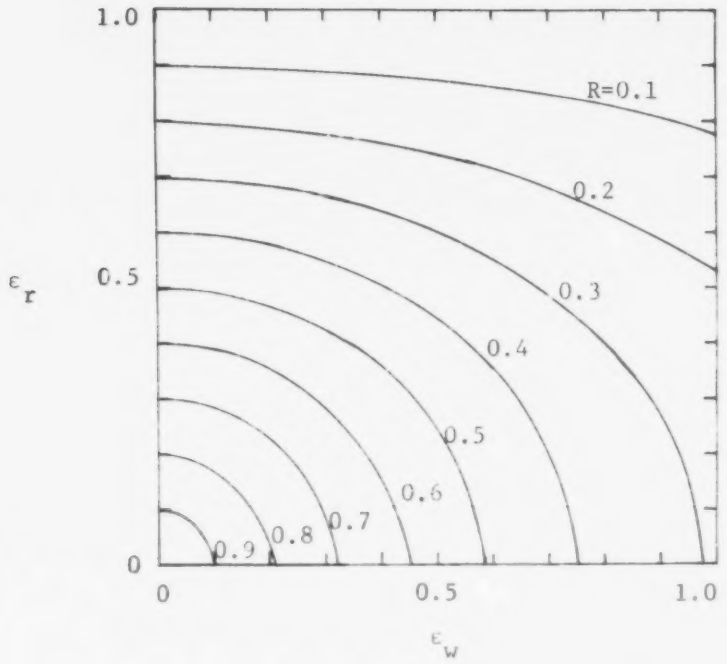

Figure 3.8 Recovery Ratio, R, as a Function of ε_r and ε_w (t_s=0)

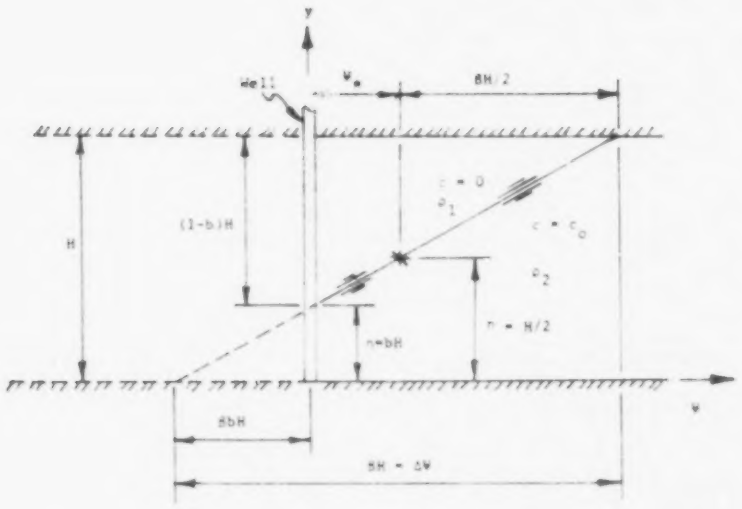

Figure 3.7 Sketch of the Interface at the End of Withdrawal

$$R_1 = 1 - \ell_1, \qquad \ell_1^2 = (\varepsilon_r^2+\varepsilon_w^2)/(1+\varepsilon_w^2)$$

$$R_2 = 1 + \ell_1 - \ell_2, \qquad \ell_2^2 = \ell_1^2 + \ell_1^2(1+2\ell_1)$$

$$R_3 = 1 + \ell_2 - \ell_3, \qquad \ell_3^2 = \ell_2^2 + \ell_1^2(1+2\ell_2)$$

$$R_n = 1 + \ell_{n-1} - \ell_n, \qquad \ell_n^2 = \ell_{n-1}^2 + \ell_1^2(1+2\ell_{n-1})$$

where recovery ratio R_n for the n^{th} sequence of cycles is defined as the ratio of the volume of water withdrawn during that sequence to the volume injected during recharge in that sequence. The following examples illustrate how the numerical values of the recharge ratio increase during repeated sequences:

Sequence no.	1	2	3	4	5
$\ell_1 = 0.141$:	0.859	0.928	0.942	0.949	0.953
$\ell_1 = 0.526$:	0.475	0.608	0.643	0.661	0.672

It can be seen that there is a significant increase in recovery ratio during the first few sequences but that an upper limit on the recovery ratio is approached asymptotically after several sequences. However, it should be recognized that dispersive effects are cumulative and thus are likely to alter these immiscible results after several sequences.

When the effects of dispersion are included, prediction procedures are more complex and general analytical representations are not possible. As discussed in Section 3.4, there are two different theories - immiscible dynamics with superimposed dispersion (Section 3.2) or coupled dynamics (Section 3.3) - which may be applicable depending on whether the ratio of dispersed zone thickness to interface length, $\Delta/\beta H$, is respectively much less than or much greater than unity. In addition, there will be some transition region in which neither of the theories is strictly correct and transition from one theory to the other could concievably occur several times during a recharge-storage-withdrawal sequence.

For purposes of specific prediction during a sequence, it will be assumed that the immiscible model applies when $\Delta/\beta H<1$ and the coupled model when $\Delta/\beta H>1$. Thus, the values of Δ and βH are computed from the appropriate equations in Sections 3.2 or 3.3 and final values from the previous cycle provide the initial values of the dispersed zone width, Δ_o, and the inverse slope, β_c, for the current cycle. The ratio $\Delta/\beta H$ is monitored throughout the computation and the appropriate model (immiscible or coupled) is selected using the current value of that variable.

Table 3.1 summarizes the various equations that are used in the computational procedure for a recharge-storage-withdrawal sequence. The table is essentially complete, but those recharge equations marked with an asterisk are restricted for the particular initial condition of a vertical interface, $\Psi_o = 0$ with $\Delta_o = 0$. More general forms would be required in some cases. For example, when an initial dispersed zone width, Δ_o, is specified during recharge with an initial radius, r_o, and volume, Ψ_o, Eq. (3.63) is generalized to

$$\Delta^2 = \Delta_o^2 + \frac{16\pi\alpha_1}{3}\left(\frac{\Psi_*^2}{r_*} - \frac{\Psi_o^2}{r_o}\right) + \frac{16\pi\varepsilon_r^2\alpha_2}{H^2}\left\{\left(\frac{\beta_o^2 H^2}{4\varepsilon_r^2} - \Psi_o^2\right)(r_* - r_o) + \left(\frac{\Psi_*^2 r_* - \Psi_o^2 r_o}{5}\right)\right\} \qquad (3.120)$$

The computational procedure outlined above is used in Section 5.6 to develop comparisons between the miscible theories and the laboratory experiments.

TABLE 3.1 SUMMARY OF EQUATIONS APPLICABLE TO A RECHARGE, STORAGE, WITHDRAWAL OPERATION

	$\Delta/\beta H<1$			$\Delta/\beta H>1$		
	Immiscible Model (Sections 3.1 & 3.2)			Coupled Model (Section 3.3)		
	Recharge	Storage	Withdrawal	Recharge	Storage	Withdrawal
β $(\Delta\Psi/H)$	Eq. 3.52	Eq. 3.49	Eq. 3.50	Eq. 3.90*	Eq. 3.100	Eq. 3.106
Δ $(\sqrt{4\pi\xi})$	Eq. 3.65* or Eq. 3.120	Δ_o	Eq. 3.76	Eq. 3.91*	Δ_o	Eq. 3.105
$\frac{\Delta}{\beta H}$	Eq. 3.67*	Δ_o/Eq. 3.49	Eq. 3.77	Eq. 3.92	Δ_o/Eq. 3.100	Eq.3.105/Eq.3.106

*For the case $\Psi_o = \Delta_o = 0$; a more general form (e.g., Eq. 3.120) is required in some cases.

4. LINEAR FLOW EXPERIMENTS

The objectives of this part of the experimental investigation were to evaluate the theoretical results for linear flow and determine any limits of their validity. Experiments designed to evaluate the immiscible displacement model were successfully conducted. Due to model capabilities and the availability of materials for the porous media, experiments to evaluate the theory for the interaction between grain dispersion and density induced mixing were not conducted. Additionally, experiments were run to obtain data on the behavior of the interface for small τ.

4.1 Experimental Equipment

The linear experiments were conducted in a lucite box which contained the porous media in a section 120 inches long, 3 inches wide and 6 inches deep (Figure 4.1). The porous medium was placed in the test section through the top of the box. A sponge rubber strip was placed between the medium and the top plate. The sponge rubber could expand to prevent short circuiting along the top in the event that the medium settled with time. The medium was kept in place by brass screens at the ends of the box. Beyond the screens, the inlet and outlet reservoirs, which were free of porous media, provided constant heads over the cross section. Inflow and outflow of the inlet and outlet reservoirs, respectively, were connected to constant head devices in order to maintain steady flow rates during experiments.

Piezometer taps were located in the side wall at distances of 4.75 cm, 149 cm and 296 cm from the upstream or inlet screen. The upstream screen was taken as the origin of the coordinate axes, with the x-axis horizontal and at the mid-height of the medium. Three electrical conductivity probes were located at $x_1 = 62.4$ cm, $x_2 = 182.9$ cm and $x_3 = 274.2$ cm. The probes consisted of two parallel stainless steel rods, 1/8 inches in diameter, spaced 3/8 inches on centers. The probes averaged the conductivity over the depth of the medium to give a one-dimensional record of concentration.

4.2 Procedure

After a careful packing, the porous medium was saturated with water, before the rubber strip and top plate were installed, to prevent trapping of air in the medium. In place measurements of hydraulic conductivity were made using fresh and salt water before and after each series of runs.

Preliminary experiments were conducted to determine the longitudinal grain dispersion coefficient for each medium used. Salt solutions of specific gravity 1.0005, were used as tracers. For the initial condition

$$t = 0, \quad c = 0 \quad x > 0$$

$$c = c_o \quad x < 0$$

Preceding page blank

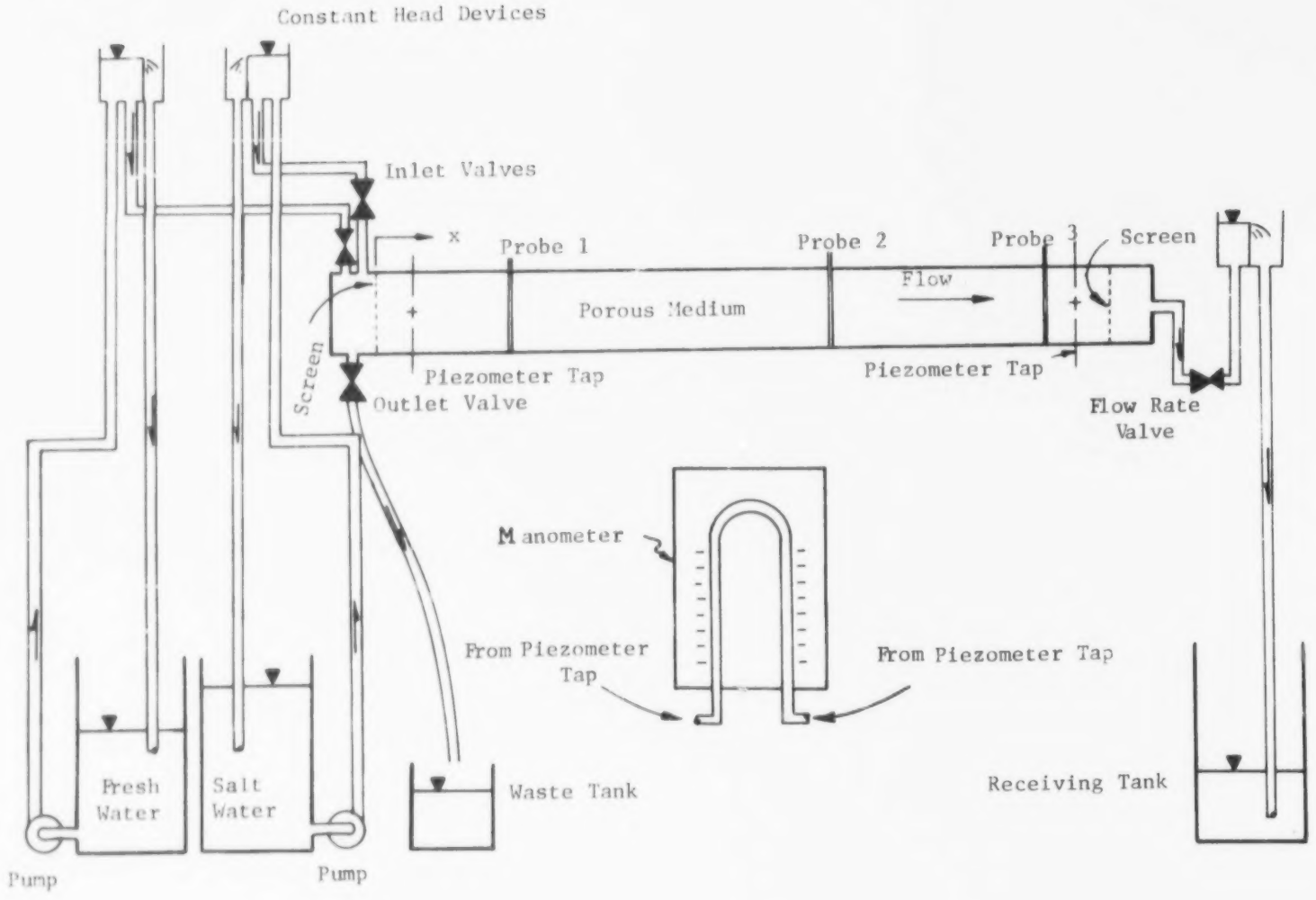

Figure 4.1 View of the Linear Sand Box Model

the dispersion coefficient could be determined using the solution

$$\frac{c}{c_o} = \frac{1}{2} \operatorname{erfc} \left(\frac{x-Ut}{\sqrt{4D_1 t}} \right) \tag{4.1}$$

where U is the steady seepage velocity. The slope of the concentration versus time curve, for a constant x, at $t = x/U = t_{50}$, is used to determine D_1 from

$$D_1 = \frac{U^2}{4\pi\, t_{50}\, S_{50}^2}$$

where

$$S_{50} = \frac{1}{c_o} \left. \frac{\partial c}{\partial t} \right|_{t=t_{50}}$$

To satisfy the initial condition, the experimental model was initially filled with fresh water, c = 0, and the flow rate set by observing the manometer and adjusting the constant head devices. Then, the fresh water flow was shut off and the salt water inlet valve and the reservoir outlet valve were opened simultaneously. The fresh water in the inlet reservoir was replaced by the salt tracer solution. Next, the reservoir outlet valve was closed and the flow rate valve was opened to start the experiment. This procedure was successful in introducing an initially vertical interface, corresponding to the initial condition.

The conductivity probes were connected through an AC Wheatstone bridge to a recording oscillograph to produce a continuous time record of conductivity. Since conductivity was approximately a linear function of tracer concentration, the conductivity records were interpreted directly as concentration records and the necessary information was obtained from them.

For the actual experiments, the model initially contained salt water of known density ρ_2 and salt concentration c_o. Again the flow rate was set by observing the manometers and adjusting the constant head devices. The initially vertical interface was introduced by the procedure used for the grain dispersion experiments, except in this case dyed fresh water replaced the salt water initially in the inlet reservoir. Records of conductivity were obtained in the same manner as for the dispersion experiments. For runs with a density difference, the interface posi- was observed visually and recorded periodically on the front of the box with a china marker. These visual markings were recorded and the horizontal projection of the interface, L, was determined for each marking.

A series of experiments was conducted with the box containing a crushed quartz sand having a mean grain diameter, d_{50}, of 0.069 cm, and a uniformity coefficient of 1.37. The inplace hydraulic conductivity was 0.10 cm/sec and the porosity was 0.35.

4.3 Experimental Results for Linear Flow

Preliminary experiments to determine the longitudinal grain dispersion coefficient produced results indicating that local heterogeneities were present in the medium. The dispersion coefficients determined from conductivity records at probe 3 were larger than those determined from records at probe 2 which were in turn larger than those determined from records at probe 1. Visual observations indicated thin layers having higher hydraulic conductivity than the surrounding media. Thus, the measured dispersion coefficients reflected the effects of this layering. The largest indicated dispersion coefficient was used to characterize the longitudinal dispersion coefficient, D_1, for the medium.

A number of experimental runs were made for specified values of the density difference, $\Delta\rho$, and the seepage velocity, U. The parameters for these experiments are given in Table 4.1 along with the computed value of $\bar{E}/D_1$ for each run. Smaller values of $\bar{E}/D_1$ could not be obtained because of limiting model capabilities. The horizontal interface projections, as determined by visual observations, are shown as a function of time on the dimensionless plot in Figure 4.2. Also shown are the theoretical expressions for L/H versus τ given by Eq. (2.19) and the interpolation equation (Eq. 2.72) given by Gardner, et al., (1962). The result given by Keulegan (1954)

$$L/H = \sqrt{2\tau} \tag{4.2}$$

to represent his experimental results for an unconfined system with no net flow is also shown in Figure 4.2. It appears that the presence of a free surface reduces the rate of interface tilting. Gardner, et al., (1962) also reported experimental results for models with no net flow which confirmed their theoretical result (Eq. 2.72).

The experimental results of the current study show that, in this range of $\bar{E}/D_1$, the rate of interface tilting is not affected by the net seepage velocity in these experiments. The current experimental results do not provide a direct confirmation of the coupled analysis in Section 2.3 (Eq. 2.63) but are consistent with that theory. That is, for each value of the parameter $\bar{E}/D_1$ the range in dimensionless time τ is such that the immiscible solution (Eq. 2.19) should be valid as discussed in Section 2.4 and indicated in Figure 2.3. It was found that, using this porous medium, it is not possible to operate this experimental equipment in the range where grain dispersion becomes important. A model of greater length or larger dispersivity would be required to observe these effects.

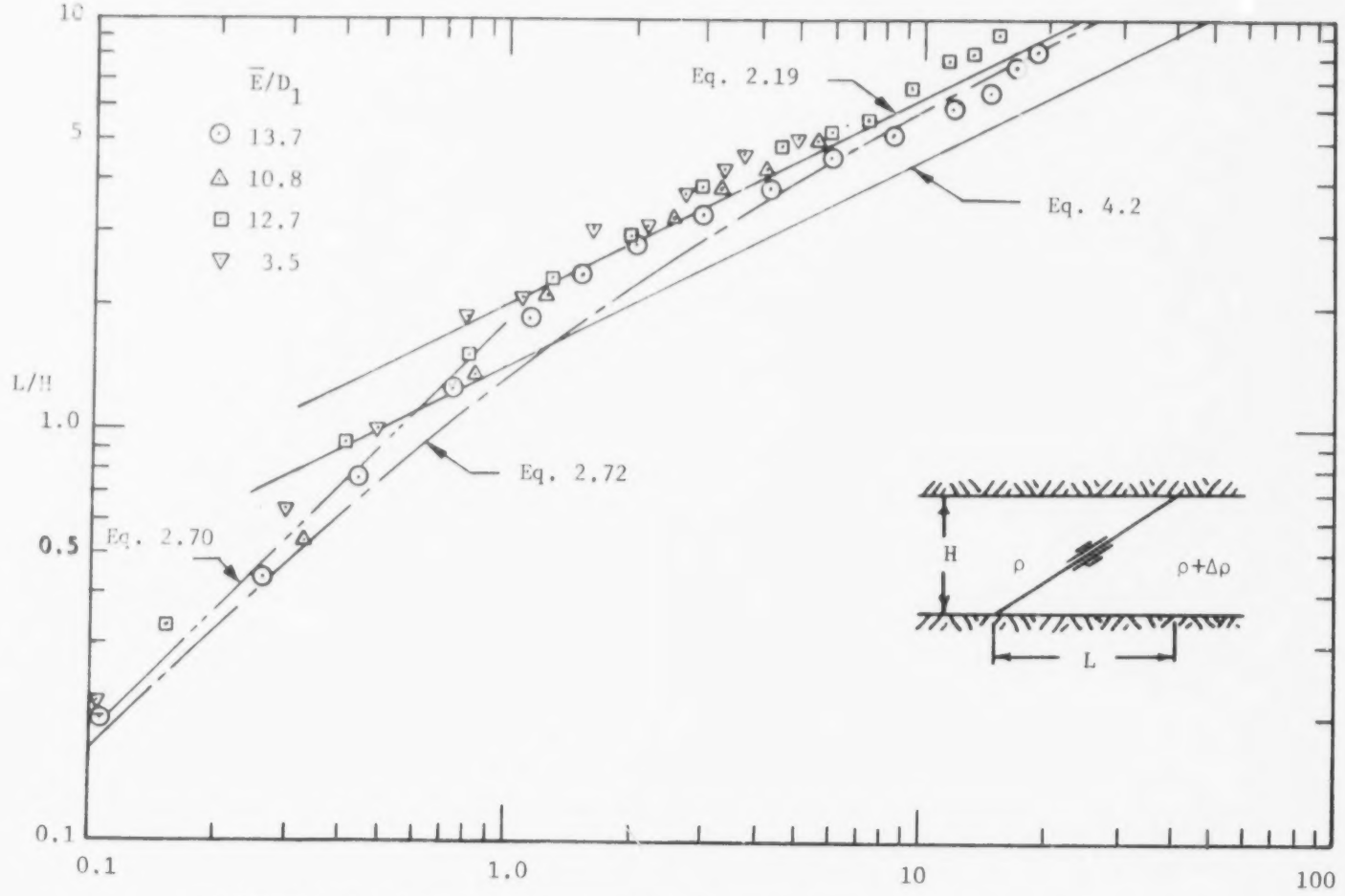

Figure 4.2 Horizontal Projection of Interface, L, as a Function of Time

U (cm/sec)	$\frac{\Delta\rho}{\rho}$	$\bar{E}$ (cm^2/sec)	$\bar{E}/D_1$
.008	0.030	0.0218	13.7
.0101	0.030	0.0218	10.8
.0085	0.030	0.0218	12.7
.0309	0.030	0.0218	3.5

$a_1 = 0.2$ cm, $D_1 = Ua_1$, $\bar{E} = \frac{K}{n}\frac{\Delta\rho}{\rho}\frac{H}{6}$

Table 4.1: Range of Test Results for the Linear Model

One-dimensional concentration, $\bar{c}$, was recorded as a function of time at the three conductivity probes, for each experimental run. A typical experimental curve of c/c_o versus τ is shown, compared with the approximate one-dimensional concentration model given by Eq. (2.33) in Figure 4.3. A comparison of the results indicates a reasonable degree of agreement between theory and experiment especially when it is noted that Eq. (2.33) was based on an average dispersion coefficient over the mixed zone.

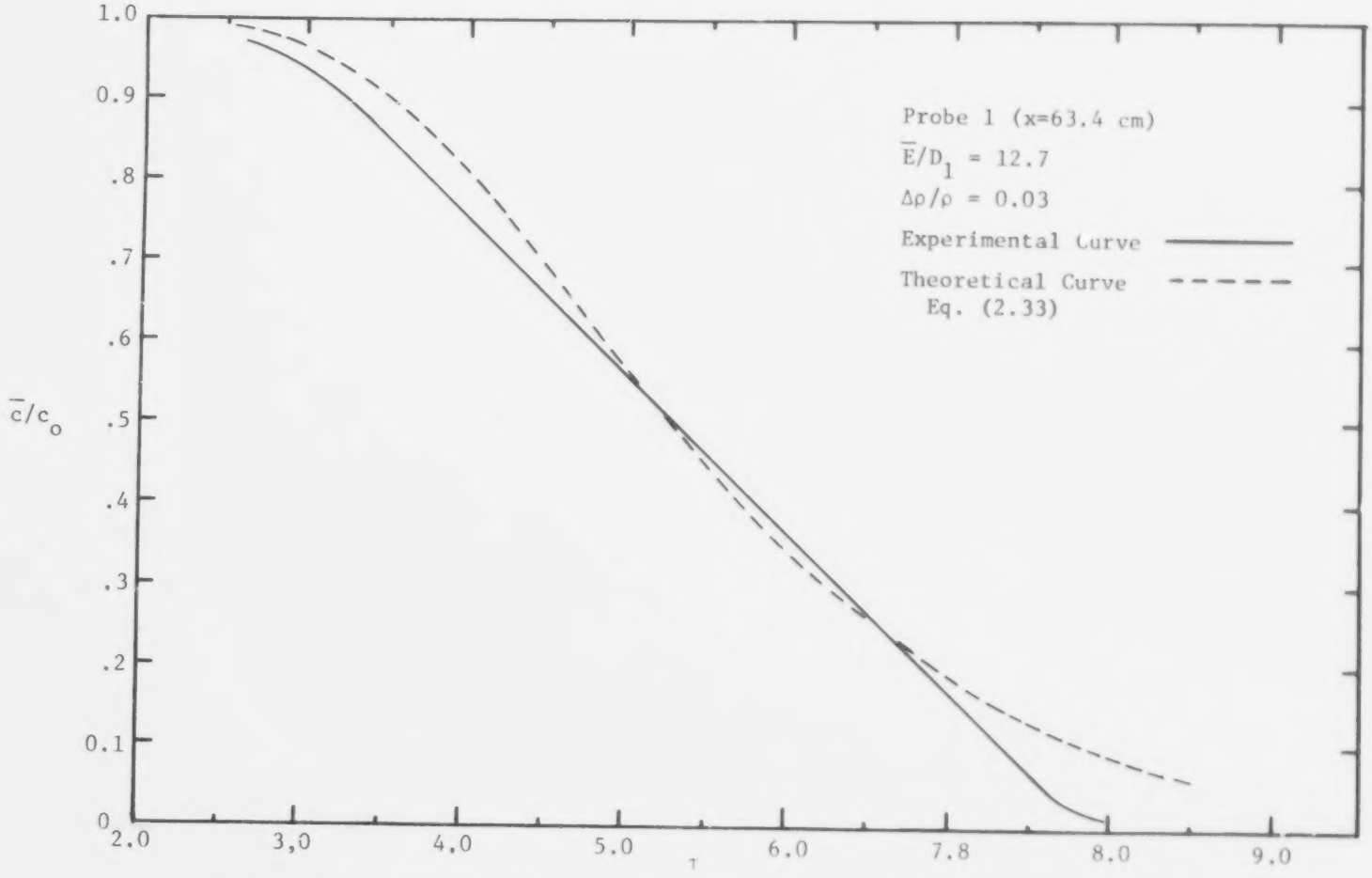

Figure 4.3 A Typical Linear Flow, Experimental Breakthrough Curve Compared with Theory

5. RADIAL FLOW EXPERIMENTS

There were two principal objectives of the radial flow experiments: (1) to construct a model with radial flow characteristics capable of modeling real aquifer field situations; and (2) to evaluate the theoretical results and to determine the limits of their validity. The theoretical results initially were to be evaluated for the immiscible displacement model including evaluation of the separate topics of injection, storage and withdrawal. Other tests were needed to evaluate the effects of grain dispersion on the immiscible model and the combined effects of density and grain dispersion on the total mixing process.

5.1 Model Construction and Equipment

The construction and operation of the radial model was more complex than the linear model because radial flow from a line source is more difficult to achieve than uniform flow in a constant area model. Also, experience during operation of the linear model indicated that the choice of media and the method of packing were important for measurement of dispersive effects.

Considerable care was taken to determine the model dimensions and media to be used. Several porous media including porous foam rubber, crushed quartz sand, and a consolidated media formed from plastic beads mixed with epoxy resin were tested in a small linear model. The plastic beads mixed with epoxy resin forming a rigid porous media were found to be most suitable considering homogeneity and ease of construction. The dimensions of the model were determined from practical considerations. The necessity of packing the model uniformly while still leaving a model thickness large enough to allow accurate interface measurements indicated that a model thickness of three inches was desirable. Using this depth and considering estimated interfacial tilting rates, it was determined that the model should have an eight foot radius. To keep the model manageable with this radius, it was necessary to construct a sector model with a 15 degree included angle. These dimensions enabled the modeling of a variety of real aquifer situations by varying the density difference of the fluids and the flowrate.

Once the dimensions and choice of media were determined, the model was constructed as shown in Figures 5.1 and 5.2. The model consisted of a 1/8 inch thick plexiglass sheet fastened to a 1 inch thick piece of plywood, 2-1/2 feet by 8 feet, which acted as the base. The two radial sides of the model were 1/2 inch thick plexiglass sheets, three inches high, that allowed visual observation of dyed fluids in the model. The sheets were placed at a 15 degree angle with the apex having a 1/8 inch opening, simulating the well. Piezometer taps, 1/8 inch in diameter, were drilled at ten locations in the model, including one within the well itself (see Figure 5.1). The piezometer taps were connected with plastic tubing to a piezometer board and a manometer. The piezometer board consisted of open-ended plastic tubes (1/4"ID) fastened to a board with paper marked at 1 mm intervals as a background. The manometer was

Preceding page blank

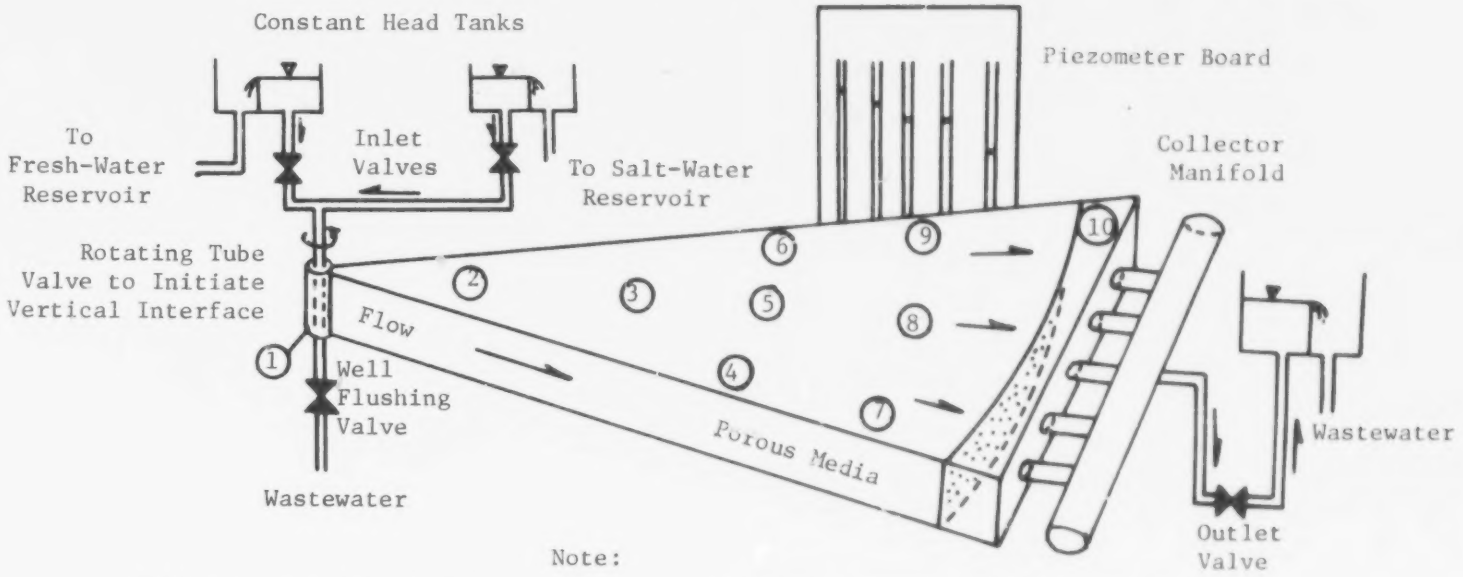

Note:

Well radius = 0.5 inches
Media radius = 7 ft 10 in
Media angle = 15 degrees

Total model length = approx. 10 ft
Model thickness = 3 inches
(1) e.g., Location of piezometer number 1

Piezometer Number	1	2	3	4	5	6	7	8	9	10
Radius (cm)	1.27	31.3	61.8	123.1	123.1	123.1	199.5	199.5	199.5	239.0

Figure 5.1 View of the Radial Model

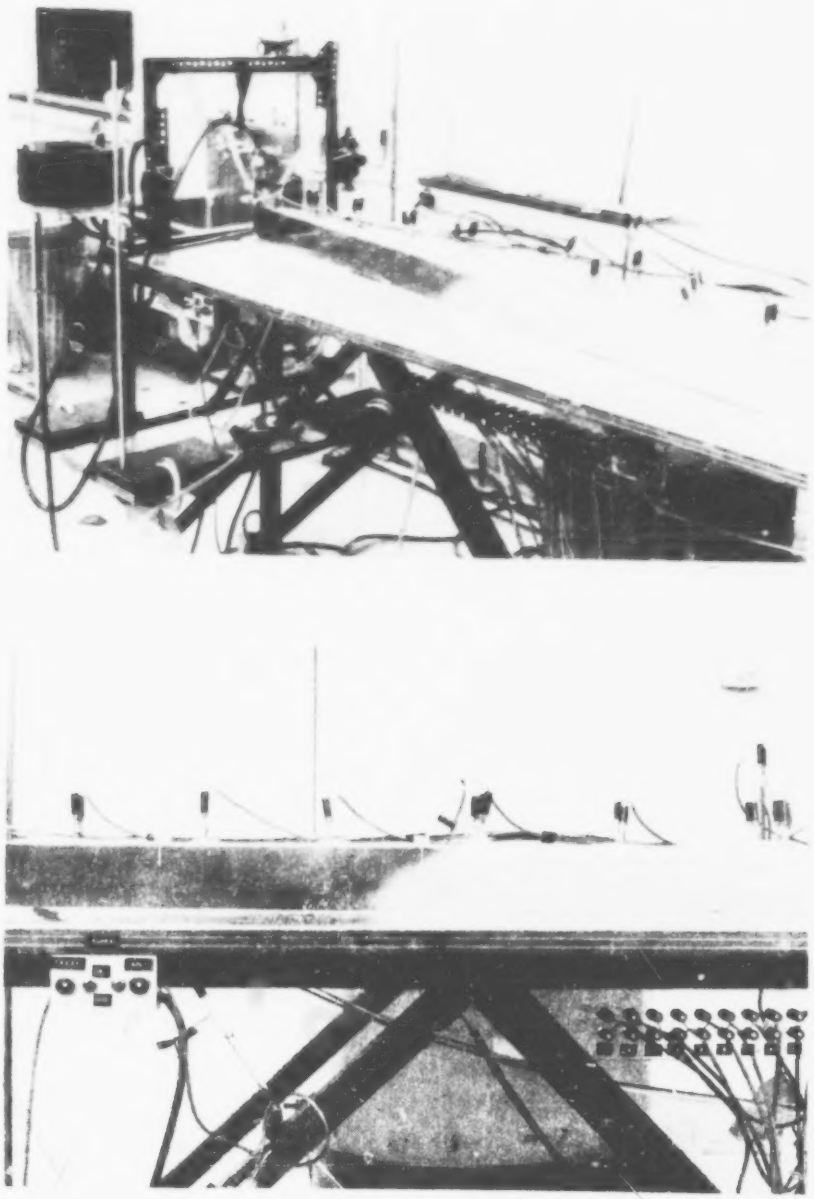

Figure 5.2 Photographs of the Radial Model During Operation

graduated in hundredths of a foot and could be read to a thousandth of a foot accuracy with a vernier scale. Since it was more accurate than the piezometer board, the manometer was used in all tests where piezometer difference was measured. The apparatus was designed so that the manometer could be connected between any two piezometer taps. The piezometer board was used to give an overall measurement of the piezometric head and to simultaneously compare the head at different locations.

With the piezometer taps drilled, the model was ready for packing. Glass beads about one millimeter in diameter were sieved through a U.S. Standard Sieve Series. Only those beads held by the no. 20 sieve after passing the no. 18 sieve (1000 micron mesh) were used. This insured uniformity of the media and gave a mean diameter (d_{50}) of about 1 mm and a uniformity coefficient of approximately 1.0. The beads were mixed with epoxy resin (1 part resin to 25 parts beads by volume) and hand-packed into the model. While the epoxy was hardening, 21 conductivity probes were inserted vertically into the media (see Figure 5.3). The probes consisted of two hypodermic needles (24 gauge stainless steel tubing) located 3/4 inch apart on a circumferential line at various radii from the well. A resistance measuring circuit, consisting of a carrier amplifier system (Sanborn Co. Model 350-1100C), was connected to the probes and then to a recording oscillograph (Sanborn Co. Model 296). The probes were inserted through the entire thickness of media; hence, the recorder gave the depth averaged change in conductance as a function of time at the location of each probe. These probes are hereafter referred to as "averaging probes". One of these averaging probes was inserted inside the well. This probe served to indicate if the start of a test had a step input with a vertical interface. During withdrawal tests this probe indicated the time at which saltwater first reached the well. This information was used later in determining the percentage of water recovered during the test.

What shall be referred to as "point" probes were also inserted into the top of the model. These probes consisted of two very short hypodermic needles (16 gauge) inserted just through the top coat of the model, 1/16 inch apart. They were located at the same radius and adjacent to averaging probes #6 and #10. These point probes were also connected to a resistance measuring circuit and then to a recorder.

The 3/4 inch spacing of the averaging probes was originally chosen from consideration of two factors. First, it was felt that they should be this far apart so that during insertion of the probes the media between them wouldn't be highly disturbed. Secondly, this spacing yielded satisfactory current between the probes for anticipated salt concentrations (1% to 2.5%). Experimentation showed that it would have been better if the averaging probes were moved closer together. There was apparently little disturbance to the media during probe insertion. In addition, salt concentrations much lower than anticipated (less than 0.1% by weight) were used for the tests. This meant that the current was less than expected. Finally, a third factor was the radial width of the electric field generated between the probes. With 3/4 inch spacing

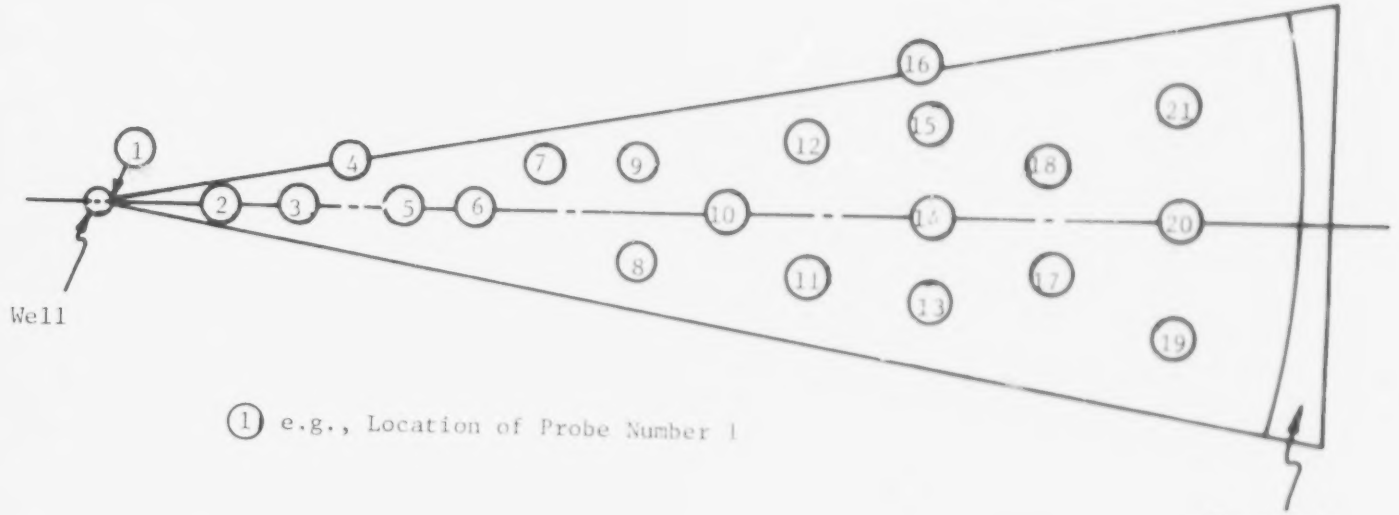

(1) e.g., Location of Probe Number 1

Probe Number	1	2	3	4	5	6	7	8	9	10	11
Radius (cm)	1.27	19.6	34.9	45.7	50.0	67.7	87.0	104.5	104.2	122.9	142.0

Probe Number	12	13	14	15	16	17	18	19	20	21
Radius (cm)	142.0	165.0	165.0	165.0	167.0	193.5	193.5	218.0	218.0	218.0

Figure 5.3 Location of Conductivity Probes

between the probes, the electric field width (area that is sensitive to the approaching interface) became significant and the probes read not as points but as zones. This caused what can be termed electronic dispersion of the recorder output. For example, a vertical immiscible interface approaching and passing the probes would yield a characteristic "S" shaped dispersion curve output rather than a step change as desired. If the probes were moved closer together, the thickness of this zone of influence would be lessened and electronic dispersion decreased. Probably 3/8 inch spacing of the probes would have been preferable. A potential theory analysis of the electronic dispersion for the 3/4 inch spacing, however, showed it to be approximately an order of magnitude less than hydrodynamic dispersion and it was disregarded during most data analysis.

With the probes in place, the top surface of the model could be constructed. It was made by spreading a 1/8 inch thick epoxy coat onto the exposed media. Prior to application the epoxy was allowed to become very viscous so that it wouldn't flow into the media. It hardened into a translucent top surface, bound to the media, eliminating short circuiting of the fluid flow along the top. The model was to be 7.62 cm high, but due to seepage of the epoxy top coat in certain small areas, the height was somewhat less. Visual observation of the seepage through the side plates made it possible to estimate an average height of 7.46 cm for the model.

The well end of the model consisted of concentric plastic tubes with slots cut into them that acted as a valve during tests (see Figure 5.4). This system was designed to insure a vertical interface between the fresh and saltwater at the start of a test.

The well tube was connected through a "T" fitting and valves to saltwater and freshwater constant head tanks (see Figure 5.1). The constant head tanks could be raised above or below the well level in order to simulate injection or withdrawal from the well. The valves and "T" connection allowed a rapid change from freshwater to saltwater feeding of the well, or vice versa.

The end of the model opposite from the well consisted of the media ending in a circular arc of 7 foot 10 inch radius followed by a large reservoir (see Figure5.1). The reservoir was connected through a manifold to a constant head tank. During an injection cycle, water was drained from this tank, but during withdrawal fluid was constantly supplied in order to maintain the head. The system of constant head tanks at either end of the model produced hydrostatic conditions within the well and the reservoir.

5.2 Experimental Procedure

Preparation of the Model for Operation Once the model was constructed, it was tilted at an angle to the floor and saturated slowly from the well. By tilting the model, air within the media had a chance to escape through

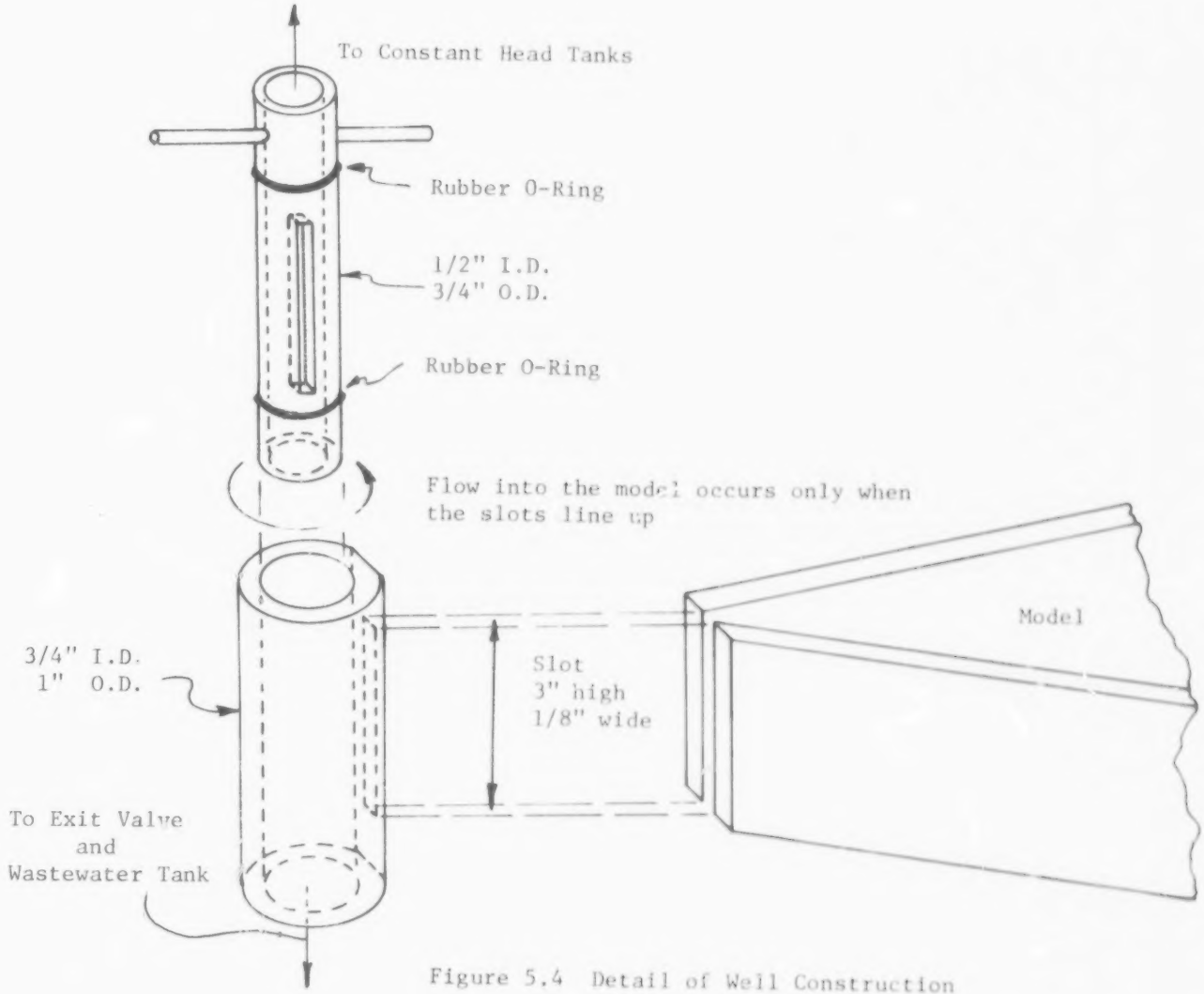

Figure 5.4 Detail of Well Construction

the reservoir end as the water entering slowly displaced it. After the model was saturated, it was leveled and prepared for experiments.

Deaerated water was used to saturate the model and run tests. This was done to minimize the likelihood of gas coming out of solution in the model forming air pockets. Deaeration was accomplished by pumping the water through a chamber under a vacuum until the dissolved oxygen level was around 3 mg/l. The water was also sand filtered and passed through a demineralizer that removed anions and cations from the water. Finally, to avoid the growth of either bacteria or algae in the model, a disinfectant, zephiran chloride, was added to the water.

Model Operation during Tests To start a test, a solution of sugar, salt and water that had the desired density and conductivity was pumped into the model. The freshwater constant head tank was set at the proper height for the desired flowrate. About 30 seconds before the start of the test, valves were opened allowing the freshwater to go from the constant head tank into the well, flushing the saltwater out through an exit valve (see Figure5.1). At time t = 0 the valve within the well was turned so that the slots lined up and flow into the model could occur. At the same time, the well exit valve was closed and a valve at the reservoir end of the model was opened to allow flow through the model. Flow was continued as long as desired, stopped for a period if necessary, and could be reversed by changing the relative position of the constant head tanks. This procedure was used to model recharge, storage and withdrawal cycles.

Methods of Data Collection There were three types of measurements made during tests: (1) measurement of flowrate; (2) visual measurement of the interface shape and location; and (3) measurements made with the conductivity probes. Flow measurements were made by using a 1000 ml graduated cylinder and a stopwatch. Several readings were taken during a test and the average of the readings was used as the flowrate.

Visual measurement of the interface consisted of periodic marking of the interface location with a china marker on the clear plexiglass sidewalls. The time of each marking was recorded. It was found that as long as the density difference was in the range of principal interest (from 1% to 2.5%), the dyed fluid made a distinct interface that could be observed and whose location could easily be marked. When the density difference between the fluids was less than 1% by weight, the interface was no longer sharply defined. Apparently, as the density difference between the two fluids decreased, the relative importance of dispersion and the effects of slight inhomogeneities in the model construction increased. Since the experiments normally had higher density differences than 1%, visual observation of the interface was possible.

In addition to the visual observation of the interface position, measurement of the interface was made with the averaging conductivity probes. In order to obtain a linear relationship between salt concentration and output from the recorder, salt concentrations less than 0.1%

by weight had to be used (see Figure 5.5). In order to achieve the desired density difference of 1% to 2.5%, sugar was also added to the salted water. The sugar was a nonelectrolyte and hence increased the water density without affecting its conductivity. The sugar, however, did have some affect on the viscosity of the denser fluid. Viscosity increases of 2.5 to 7 percent are found for sugar concentrations of from 1% to 2.5% by weight.

5.4 Determination of Model Parameters

The porosity of the model was determined in two ways. First, a value of 0.337 was determined using a small test cylinder that had been packed at the time of model construction. Its porosity was determined from comparison of the volume of water required to saturate the cylinder versus the gross volume of the cylinder. Since the test specimen was packed in a similar manner to the model, with the same bead and epoxy mixture, its porosity should be the same as that of the model. The second method for determining the porosity was done using the in situ model media. By measuring the travel time of fluid flow between conductivity probes at different radii, an average porosity of 0.34 was determined. This value is used in subsequent calculations.

The hydraulic conductivity of the media was also determined in two ways. First, a cylindrical permeameter (1-1/2" diameter, 10" long) which had been packed at the time of model construction was tested. Hydraulic conductivity tests were made using this cylinder with the flow perpendicular to the packed surface. The hydraulic conductivity from these tests approximated the results that would be obtained by vertical flow through the actual model. Consequently, the hydraulic conductivity of the test cylinder was an approximation of the vertical conductivity of the radial model. The average vertical conductivity from these tests was 0.48 cm/sec at 60°F.

The horizontal conductivity of the model was determined from tests run on the in situ media. The tests consisted of measuring piezometric head and flow rate in order to calculate the hydraulic conductivity from the well equation for a confined aquifer between two constant head reservoirs. The equation is:

$$K = \frac{Q}{2\pi sH}\left(\ln \frac{r_1}{r_2}\right) \qquad (5.1)$$

where: K = horizontal hydraulic conductivity (cm/sec)
Q = flowrate (cm^3/sec)
s = piezometric difference between the radii r_1 and r_2 (cm), ($r_1 > r_2$)
H = thickness of the aquifer (cm)

The average horizontal conductivity derived from the use of this equation was 0.43 cm/sec at 60°F (see Table 5.1). The fact that the conductivity

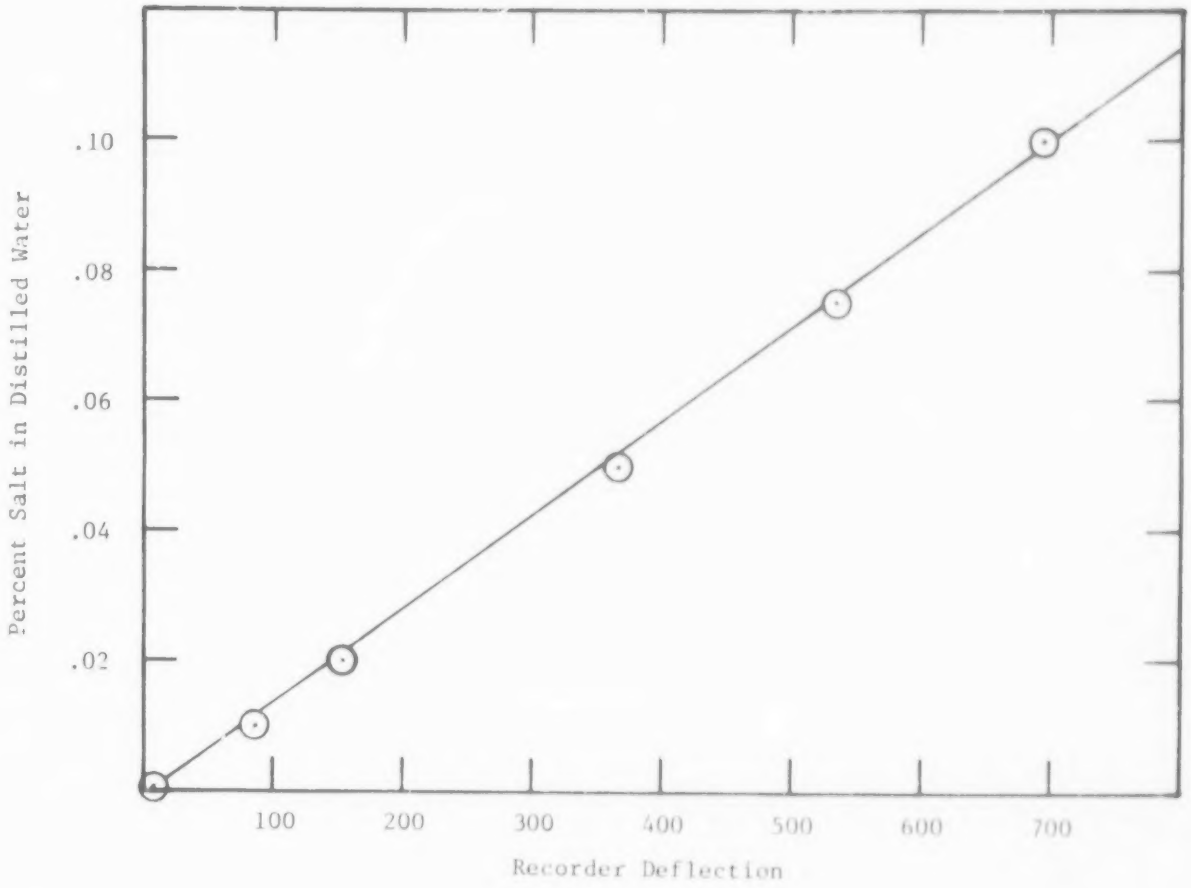

Figure 5.3 Calibration of Averaging Conductivity Probes

TABLE 5.1

HORIZONTAL HYDRAULIC CONDUCTIVITY

Note: The governing equation for the model:

$$K = \frac{Q'}{(2\pi/24)sH} \ln(r_1/r_2); \quad r_1 > r_2$$

Temperature of the water for all runs = 75°F

From the table below, the average K = 0.52 $\frac{cm}{sec}$ @ 75°F

Average K = 0.43 $\frac{cm}{sec}$ @ 60°F

Location (Number refers to piezometer)	Discharge* $Q'(cm^3/sec)$	K (cm/sec)
1 to 10	0.569	0.502
	2.4	0.514
	3.63	0.500
	6.14	0.49
1 to 8	2.23	0.509
	3.93	0.501
1 to 5	1.56	0.515
	4.80	0.495
1 to 3	1.18	0.504
	4.18	0.488
1 to 2	2.03	0.496
	4.92	0.474
2 to 8	2.34	0.563
	3.36	0.606
	4.82	0.531
2 to 5	2.34	0.572
	3.36	0.628
	4.82	0.532
3 to 8	2.34	0.563
	3.36	0.569
	4.82	0.548

*This is the sector model discharge; i.e., $Q = 240'$

measured in the test cylinder was very close to the in situ horizontal conductivity of the model indicated that the media was reasonably isotropic.

Since the model was to be used to study the effects of dispersion on the mixing process between the two fluids at the interface, a measurement of the media's dispersivity was required. The dispersivity was determined through the use of the conductivity probes already mentioned. As the interface between the two fluids passed a probe, the reading from the recorder plotted the change in salt concentration versus time at that point. There are several theories that mathematically describe the concentration c/c_o at a particular radius for flow from a well. One recent study (see Gelhar and Collins, 1971) can be used to estimate the longitudinal dispersivity of the media by considering the slope of the curve c/c_o versus time at the point $c/c_o = 0.5$ for the case of no density difference between the two fluids. Gelhar and Collins derived the following equation assuming that the dispersivity, a_1, is a constant:

$$\frac{c}{c_o} = \frac{1}{2}\left[1 + \operatorname{erf}\left\{\frac{r^2 - r_*^2}{\left[\frac{16}{3}a_1(r_*^3 - r_\omega^3) + \frac{D_m}{A}\left(\frac{r_*^4 - r_\omega^4}{4}\right)\right]^{1/2}}\right\}\right] \qquad (5.2)$$

where: c = concentration of tracer at radius r
c_o = original concentration of the tracer in the model
a_1 = longitudinal dispersivity
t = time
r = radius to point in question
r_* = radius to the 50% point ($=\sqrt{2At}$)
r_ω = radius of the well
D_m = coefficient of molecular diffusion in the porous medium
$A = \frac{Q}{2\pi nH}$ where n = porosity, H = depth of aquifer, Q = flowrate

The effects of molecular diffusion and the radius of the well are small in magnitude compared to other terms and Eq. (5.2) reduces to

$$\frac{c}{c_o} = \frac{1}{2}\left[1 + \operatorname{erf}\frac{r^2 - r_*^2}{\left(\frac{16}{3}a_1 r_*^3\right)^{1/2}}\right] \qquad (5.3)$$

Taking the derivative of Eq. (5.3) with respect to time and evaluating at $c/c_o = 0.5$ remembering that $r^2 - r_*^2 = 0$ at $c/c_o = 0.5$,

$$\left.\frac{\partial(c/c_o)}{\partial t}\right|_{c/c_o=.5} = \frac{1}{t}\sqrt{\frac{3}{16\pi}\frac{r_*}{a_1}} = S_{50} \qquad (5.4)$$

Since $t = r_*^2/2A$, we can solve for a_1 in terms of the slope at the

point $c/c_o = 0.5$ and r_*:

$$\alpha_1 = \frac{3}{4\pi r_*^3} [A/S_{50}]^2 \qquad (5.5)$$

Experimentally, r_*, is the radius to the probe in question and the slope at $c/c_o = 0.5$ is determined from the recorder output.

Using this method of analysis, the dispersivity was determined from several of the averaging probes as summarized in Table 5.2 and Figure 5.6. The longitudinal dispersivity generally falls in the range between 0.1 and 0.2 cm although at the larger radii, a few observations indicate higher values. These large values of the dispersivity may be associated with inhomogenieties of the media. The very small density difference (see Table 5.2) may also have affected the results; however, for these values of ε this effect is indicated to be negligible using the results of the coupled analysis in Section 3.3. The so-called electronic dispersion associated with the averaging probes may have introduced some error in the dispersivity determination for some probes near the origin, but, as discussed in Appendix C, this effect is unimportant over most of the model.

A few determinations of dispersivity made using the more closely spaced point probes were found to be of the same magnitude ($0.075 \text{ cm} < \alpha_1 < 0.18 \text{ cm}$) as those found with the averaging probes. In all subsequent calculations, the longitudinal dispersivity is taken to be constant throughout the medium and equal to 0.15 cm.

5.5 Model Verification

The model was tested to see if radial flow was in fact occurring. Observations from the piezometers were used to obtain the distribution of drawdown versus radius from the well. The results are plotted in Figure 5.7 and compared with the solution of the well equation, Eq. (5.1). Comparisons of piezometric head for the taps at the same radius showed no measurable differences thus indicating a purely radial flow. The observations of piezometric head distribution in the model generally indicate that the desired radial flow was attained and that the model was homogeneous with respect to hydraulic conductivity.

To further check the flow situation, observations of travel times were made with practically zero density difference between the two fluids. A small amount of salt was added to one fluid (0.02% salt by weight) in order to obtain a measurable output from the conductivity probes. By comparing the readings from probes located at the same radius, it could be seen that the saltwater was reaching radial points at approximately the same time. Also visual observation of the semiclear top coat of the model during density tests showed that the injected fluid moved

TABLE 5.2

DETERMINATION OF DISPERSIVITY FROM AVERAGING PROBES

Run Number		C-1	I-2	1	3	5
Discharge Q'cm^3/sec**		2.27	4.66	4.94	2.96	3.40
Density difference $\Delta\rho/\rho$		0*	0	0.001	0	0.001
ε		0	0	0.039	0	0
Probe Number	Radius cm	Longitudinal Dispersivity α_1 - cm				
2	19.6	0.153				
3	34.9	0.108	0.105	0.095		
5	50.5	0.110			0.115	0.0927
6	67.7	0.151	0.144	0.163	0.142	
7	87.0	0.150	0.148		0.125	0.146
8	104.5	0.293	0.293	0.172		
9	104.2					
10	122.9	0.318			0.106	0.157
11	142.0				0.162	
12	142.0			0.14	0.152	
14	165.0				0.173	0.405
17	193.5				0.2	
18	193.5			0.175	0.217	
21	218.0			0.355		

*The condition $\Delta\rho/\rho = 0$ indicates cases in which the density of the liquids was matched using sugar and salt solutions to within ±0.0002 relative density difference.

**This is the sector model discharge; i.e., $Q = 24Q'$

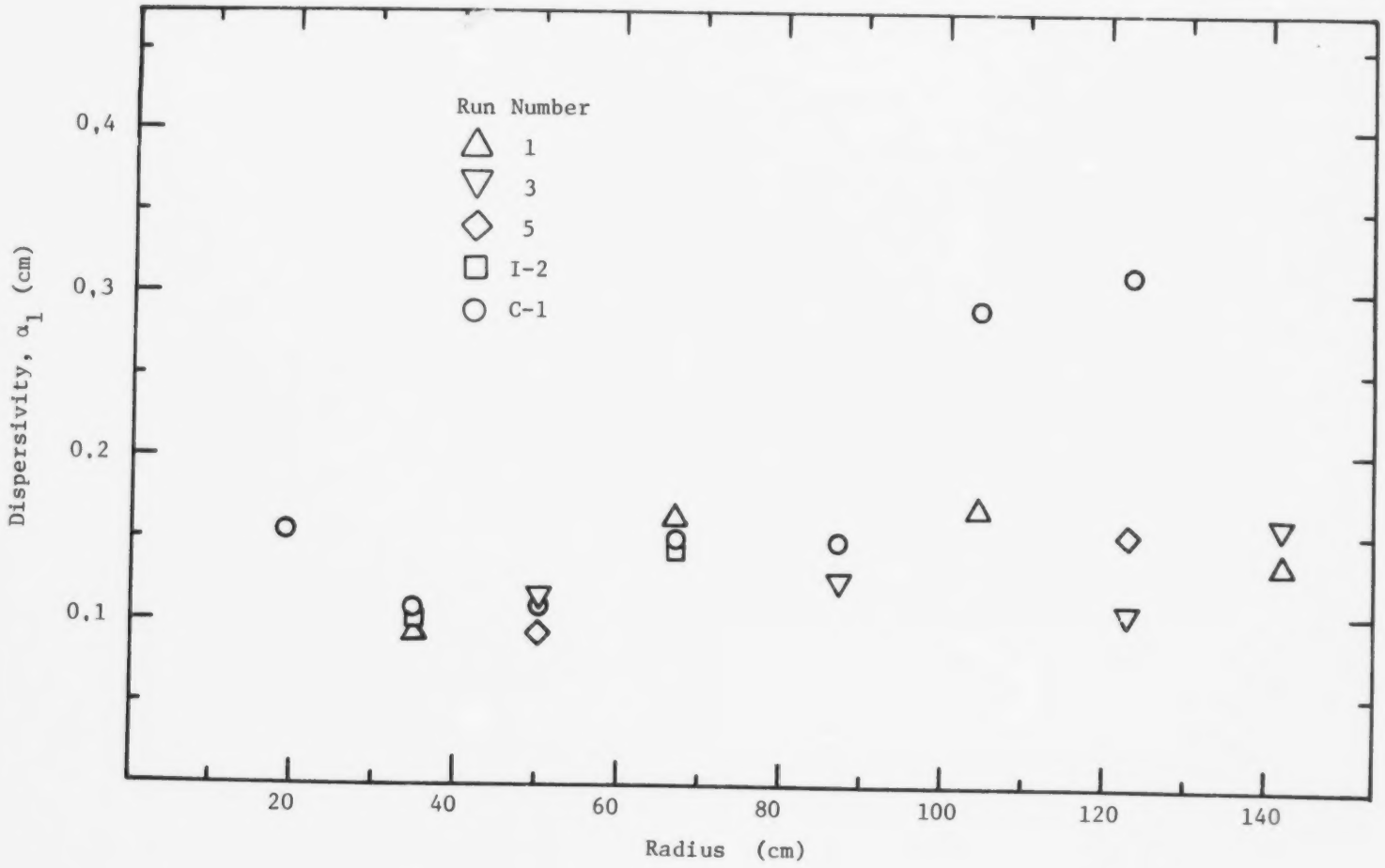

Figure 5.6 Media Dispersivity Calculated From the Averaging Probes

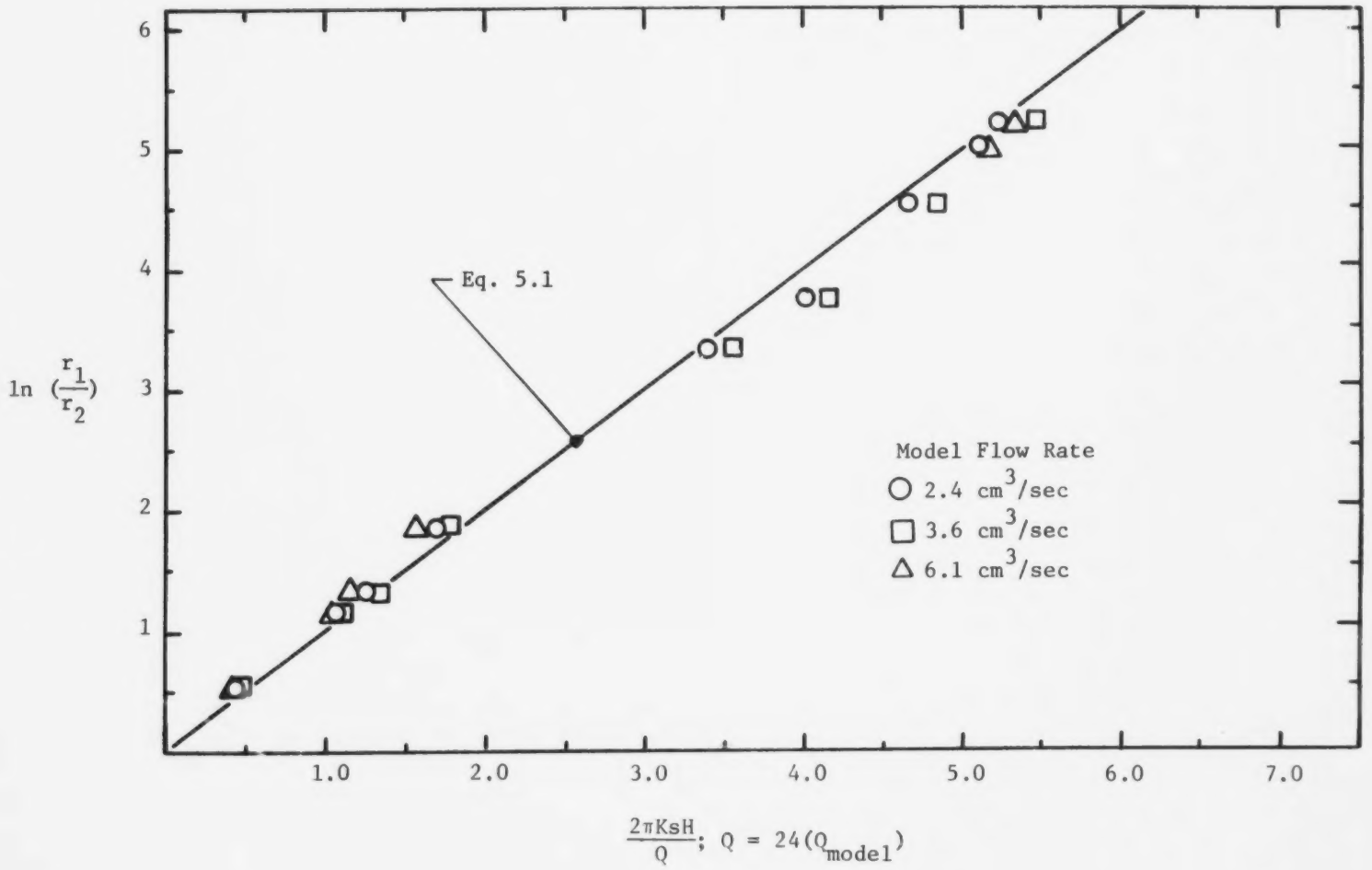

Figure 5.7 Piezometric Head Distribution in the Model

radially into the model with a velocity independent of angular position.

To correlate the effectiveness of visual observation of the interface location with the depth-averaging conductivity probe measurements, the following comparison was made. The interface position was marked on both of the side walls as the interface passed a conductivity probe. A comparison was made of η/H as determined from the visual markings of the interface with the relative concentration, $\bar{c}/c_o$, from the probe output. These values were recorded at several different times as the interface passed the probe. The results for a run with a relatively large density difference ($\Delta\rho/\rho=0.020$) are shown in Figure 5.8. This figure indicates a good correlation between the probe reading and the visual recordings.

5.6 Experimental Results for Radial Flow

A series of experiments was undertaken to investigate the behavior of density induced mixing in aquifers using the previously described visual and electronic methods of data collection. Table 5.3 summarizes the experimental parameters along with the computed values of ε_r and ε_w for each run. In some experiments, only recharge tests were conducted, while in other experiments complete recharge, storage and withdrawal cycles were investigated. When an item is not given in the table, it was not measured during that particular run. A summary of model characteristics, as used in data reduction, is given for convenience:

Model Height	$H = 7.46$ cm
Porosity	$n = 0.34$
Longitudinal Dispersivity	$\alpha_l = 0.15$ cm

The hydraulic conductivity, K, was determined for each run using the average viscosity of the two fluids (see Table 5.3).

The parameters ε_r and ε_w were found in Section 3 to characterize the recharge and withdrawal processes. In Figure 5.8 the results of a recharge run with a relatively large value of ε_r (=0.422) using both visual and electronic interface measurements are compared with the predicted interface position of the immiscible theory with a linear interface in volumetric coordinates (Eq. 3.107). The theory, which is based on small ε_r, compares well with the experimental data. The indication is that the interface tilting is governed predominantly by immiscible displacement under these conditions and that the curvature of the interface is unimportant even for this relatively large value of ε_r.

Electronic data were obtained in the form of breakthrough curves (see Figure 5.12) for various conductivity probes during recharge and withdrawal. A method was developed for interpreting these data based on the measured rate of change of depth averaged concentration at $\bar{c}/c_o=0.5$. This information was used to characterize the various breakthrough curves and was expressed in terms of the parameter Δt:

TABLE 5.3 EXPERIMENTAL CONDITIONS FOR THE RADIAL MODEL

Run	$\Delta\rho/\rho_1$*	Q_r'* $\frac{cm^3}{sec}$	Q_w'* $\frac{cm^3}{sec}$	Fluid Temp. ^oF	Average ν centi-stokes	Average K $\frac{cm}{sec}$	ε_r	ε_w	Recharge Time sec	Storage Time sec
1	0.001	4.94		≃71	0.995	0.49	0.020			
2	0.001	3.87		≃71	0.995	0.49	0.043			
I-1	0.005	2.49		75	0.940	0.52	0.123			
A-1	0.005	3.70	5.74	70	0.985	0.49	0.098	0.079	1500	75
A-2	0.005	3.70	5.55	71	0.977	0.50	0.099	0.080	1500	49
A-3	0.005	0.76		69.5	0.985	0.49	0.216			
A-4	0.0215	4.79		≃70	1.012	0.48	0.177			
A-5	0.0215	1.32		≃70	1.012	0.48	0.337			
A-6	0.021	0.48	6.07	≃70	1.012	0.48	0.556	0.155	6000	240
A-7	0.021	2.43	4.70	71	0.995	0.49	0.248	0.179	2423	157
A-8	0.021	2.30		69	1.020	0.47	0.250			
A-9	0.020	0.78		70	1.012	0.48	0.422			
A-10	0.020	0.26		67	1.050	0.46	0.726			
B-1	0.018	2.55	2.70	69.5	1.012	0.48	0.222	0.216	1440	480
B-2	0.018	1.64	1.86	≃69	1.010	0.48	0.277	0.260	1440	720
B-3	0.018	5.04	5.39	≃69	1.010	0.48	0.158	0.153	1440	1200
B-4	0.018	1.86	1.96	68	1.020	0.47	0.257	0.251	2100	10900
C-1	0.00014	2.28		67	1.050	0.46	0.020			

*ρ_1=1.000 gm/cm^3 for all runs; ≃ denotes estimated temperature; Q_r', Q_w'=model flowrates, i.e., $Q = 24\ Q'$

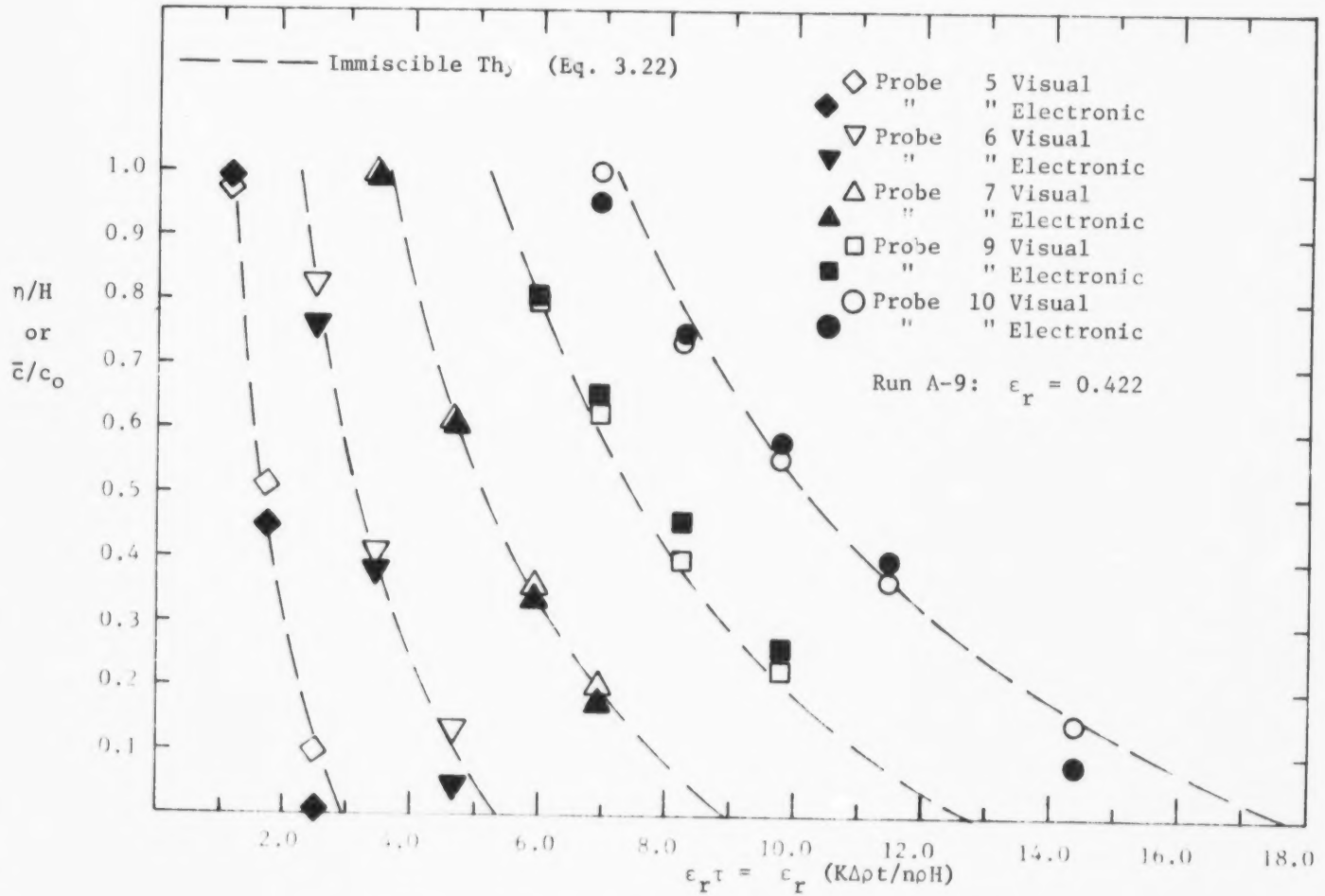

Figure 5.8 Comparison of Visual and Electronic Measurement of the Interface with Immiscible Displacement Theory

$$(\Delta t)^{-1} = \left.\frac{\partial(c/c_o)}{\partial t}\right|_{\bar{c}/c_o=0.5}$$

For a linear interface in volumetric coordinates $\bar{c}/c_o=0.5$ coincides with $\forall_p=\forall_*$ ($r_p=r_*$), where the subscript "p" refers to the probe at which the measurement is being made. The dimensionless form of Δt (Eq. 3.109) found from the recharge experiments is shown in Figure 5.9 as a function of dimensionless time, τ (Eq. 2.14) and is compared with the theoretical results presented in Section 3 (Eq. 3.109). The range of ε_r and τ is such that the ratio of the dispersed zone width to interface length in volumetric coordinates, $\Delta/\mathcal{H}$, is small. Therefore only the immiscible theory should apply for the most part. At low $2\varepsilon_r\tau$ however, there may be some effects of dispersion as noted by the dashed line for $\varepsilon_r=0.1$. Figure 5.9 shows excellent agreement between theory and experiment, although some systematic differences are noted in the early part of those runs with larger values of ε_r. Figure 5.10 shows a comparable visual measurement of the length of the interface in volumetric coordinates, $\Delta\forall=\mathcal{H}$ (Eq. 3.28), versus time for three runs with large ε_r. Only the immiscible theory (Eq. 3.31) is shown, as ε_r and τ were in the range in which only density difference governs the mixing dynamics. Excellent agreement between theory and experiment is again found, although some systematic decrease in $\mathcal{H}$ for smaller values of $2\varepsilon_r\tau$ is indicated. A glance at Figure 3.3 or Figure 3.4 indicates that this difference in Δt or $\mathcal{H}$ for lower values of $2\varepsilon_r\tau$ during runs of relatively high ε_r cannot be attributed to dispersive effects. Similar differences were observed for the linear experiments presented in Section 4.3 and are attributed to the influence of vertical velocities for small times, and the limited applicability of the Dupuit assumption under those conditions. Figures 5.9 and 5.10 also show that, for this range of ε_r and τ, the rate of interface tilting is not affected by dispersion and thus provide a direct confirmation of immiscible displacement theory (Sections 3.1 and 3.2) and are consistent with the coupled theory (Sections 3.3).

Figures 3.3 and 3.4 of Section 3.4 indicate that density difference and grain dispersion will interact to govern the mixing dynamics for small time when longitudinal dispersion will be important or for very large time when lateral dispersion will be important. It was found that it is not possible to operate this experimental equipment in the range of $2\varepsilon_r\tau$ where lateral grain dispersion becomes important for recharge. A model of greater length or larger dispersivity would be required. However, several experimental runs were conducted for small ε_r over the range of times ($2\varepsilon_r\tau$) in which the coupled theory should apply. The results are presented in Figure 5.11; good agreement between theory and experiment is indicated. The value $\alpha_l=0.15$ cm was used for the plots of the coupled theory. It is interesting to note that these runs were made with a very small density difference (Table 5.3), and that several of them were also analyzed to determine longitudinal dispersivity by ignoring this small density difference (Table 5.2). In light of the importance of density difference as indicated in Figure 5.11, it is possible that several of the larger dispersivities found in Table 5.2 may be due in part to the density effect.

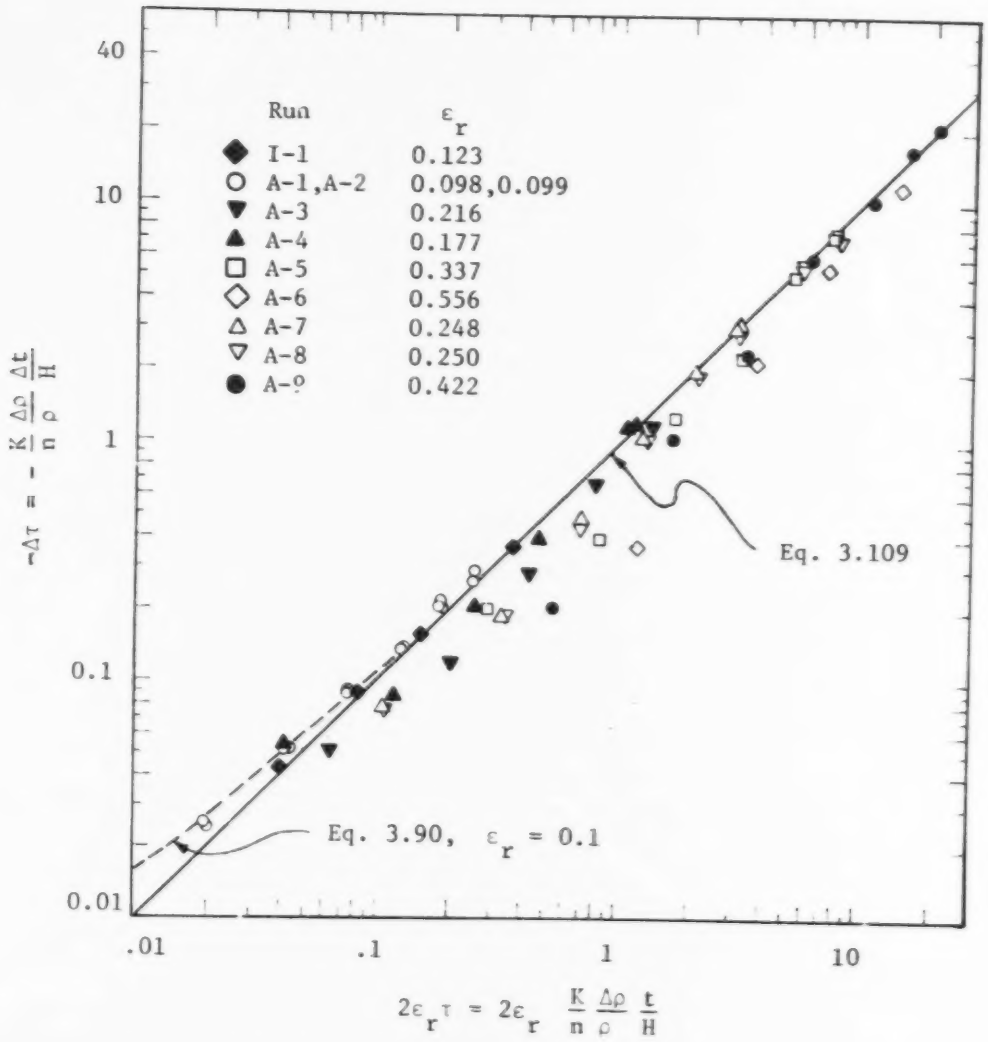

Figure 5.9 Comparison of Theory and Experimental Time Dependent Concentration Slopes During Recharge

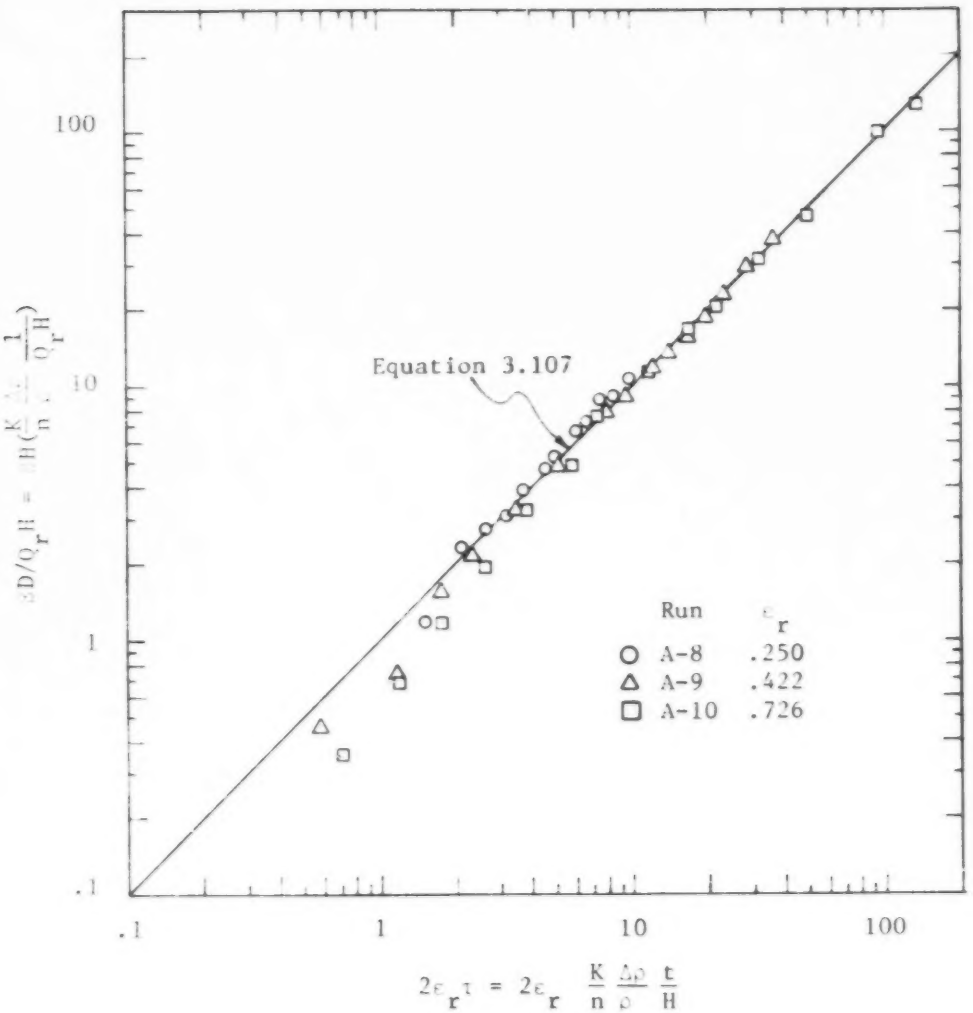

Figure 5.10 Volumetric Length of the Interface, $\Delta H=\Delta V$, As a Function of Time

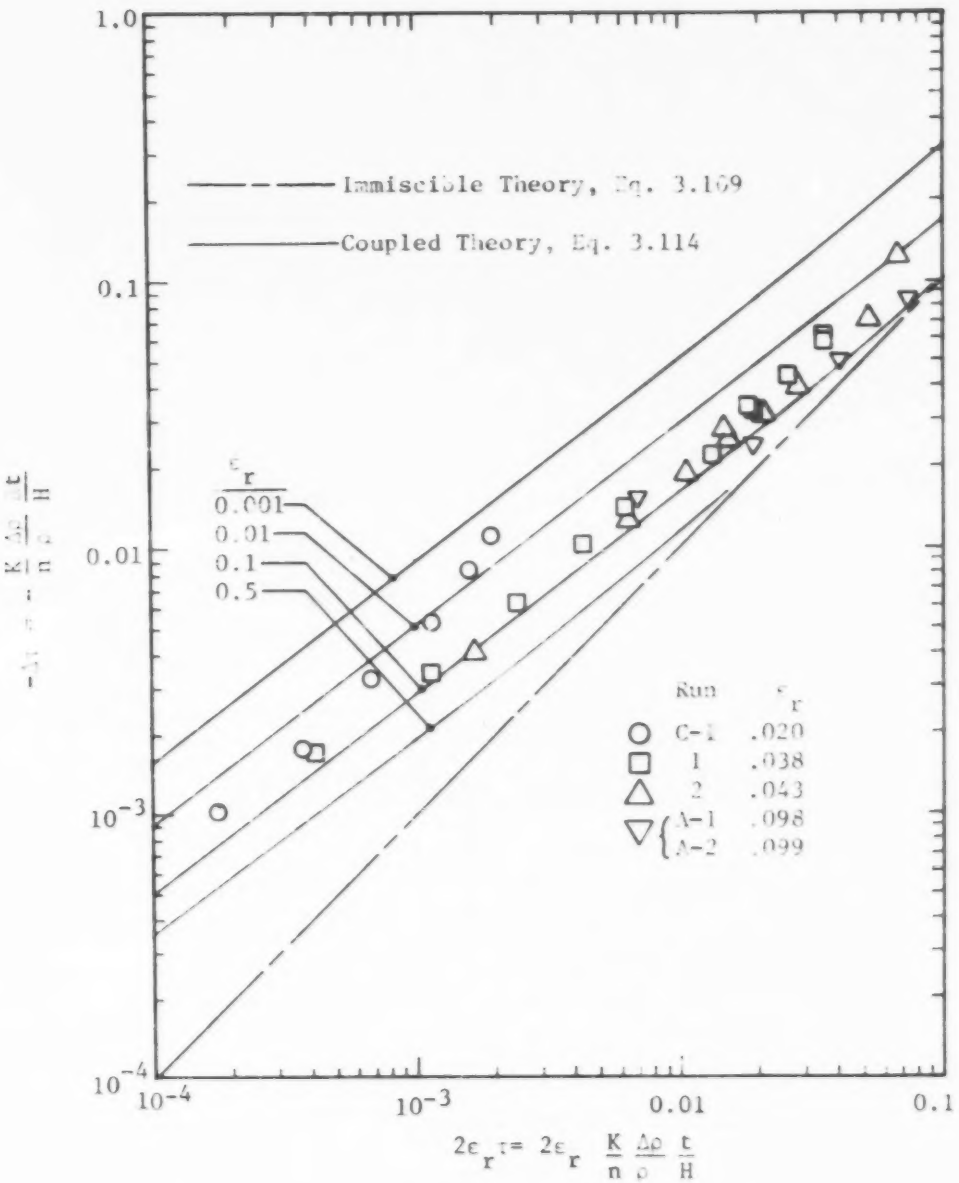

Figure 5.11 Comparison of the Coupled Theory and Experimental Time Dependent Concentration Slopes During Recharge

It has been shown that simple direct comparisons between experiment and theory are possible for the recharge cycle with an initially vertical interface and that excellent agreement is found. However, during storage and withdrawal direct comparisons are more difficult because of the complex dependence on conditions in previous cycles of the recharge-storage-withdrawal sequence. The depth averaged concentration was monitored at the various probes and at the well during withdrawal. Visual observations proved to be inadequate for these runs, which generally involved a low value of ε_r. In Figure 5.12 some typical breakthrough curves at the well are shown in dimensionless form where V_o is the net injected volume. The curves are skewed, and the 50 percent point occurs earlier than would be expected with a linear interface in volumetric coordinates. These features may reflect some effects of interface curvature and local mixing in the well.

A series of breakthrough curves for several probe locations during a complete recharge-storage-withdrawal sequence (Run B-2) is shown in Figure 5.13. The depth average concentration, c/c_o, is plotted in terms of a dimensionless time coordinate, $(V_p-V_*)/V_o$, where V_p is the pore volume between the origin and the probe. The increasing length of the mixed zone is obvious for the recharge portion of the sequence, but during the withdrawal process this trend is not clear.

Figures 5.14, 5.15 and 5.16 present a comparison of several observed recharge and withdrawal breakthrough curves with theoretical results from Section 3 at various radii. The theoretical curves in Figures 5.14 and 5.15 represent recharge with an initially vertical interface. The initial period during which the coupled analysis applies ($\Delta/\beta H>1$) is short and was neglected in the calculation. Therefore, the theoretical curve represents the immiscible displacement theory with superposed dispersion (Eq. 3.111 with βH given by Eq. 3.107 and $\sqrt{4\tau}$ given by Eq. 3.65). There is excellent comparison between the theory and experiment at Probe 7 (Figure 5.15), especially for the leading edge of the curve ($V_*<V_p$). However, the breakthrough curve for Probe 3 (Figure 5.14), reflects discrepancies similar to those noted in Figure 5.9 near the well when ε_r is relatively large. As indicated earlier, these differences probably reflect limitations of the Dupuit assumption under these conditions. Figure 5.16 represents a comparison between theory and experiment for withdrawal during the same experimental run. The theoretical curve shown here is derived by matching the immiscible displacement theory with superposed dispersion at the end of recharge and at the end of storage as described in Section 3.5. Except for a period at the beginning of recharge, $\Delta/\beta H$ remained less than one. It can be seen that the theory predicts a larger mixed zone than that observed. This difference was noted for all breakthrough curves during withdrawal. The characteristics of several breakthrough curves during a recharge-storage-withdrawal sequence are conveniently summarized in terms of the variable Δt (Eq. 3.112) as shown in Figure 5.17 for Run A-2. The solid line represents the theoretical curve obtained by the method outlined above. As expected there is excellent agreement during recharge, but as withdrawal proceeds major differences develop. Theoretically, Δt is expected to increase slightly during withdrawal, reflecting the increasing length of the interface and width

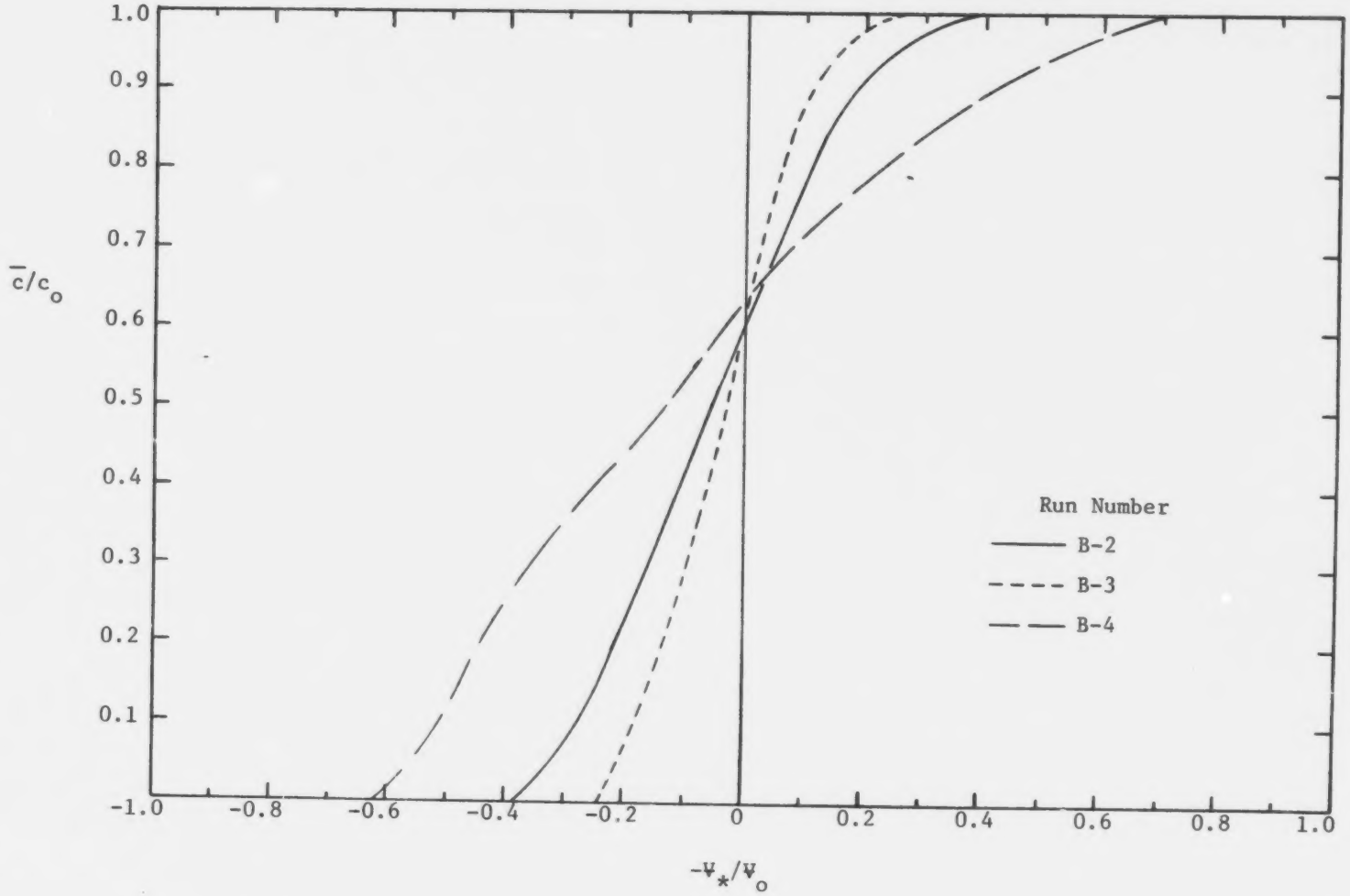

Figure 5.12 Experimental Breakthrough Curves at the Well

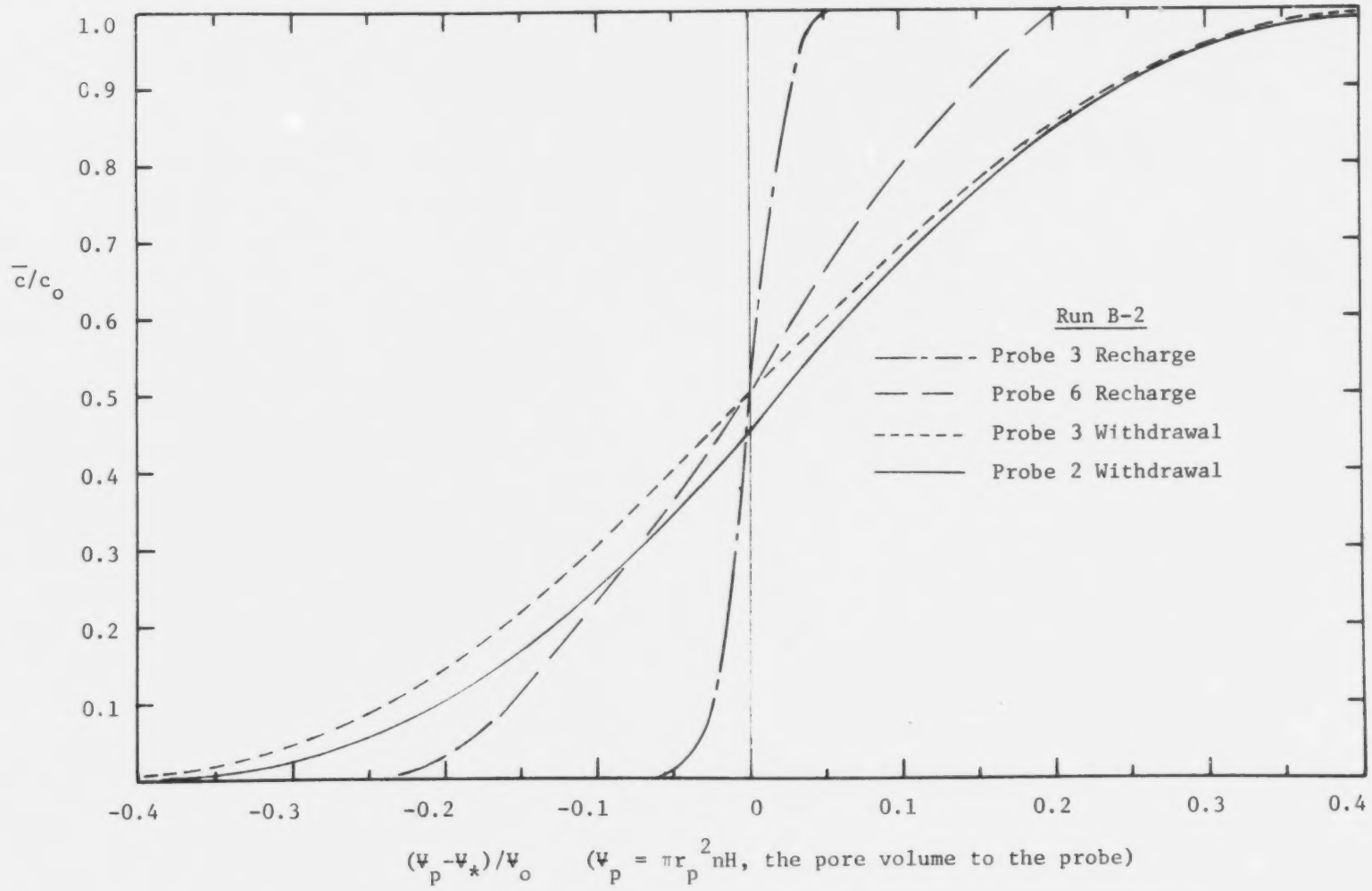

Figure 5.13 Experimental Breakthrough Curves During Recharge and Withdrawal

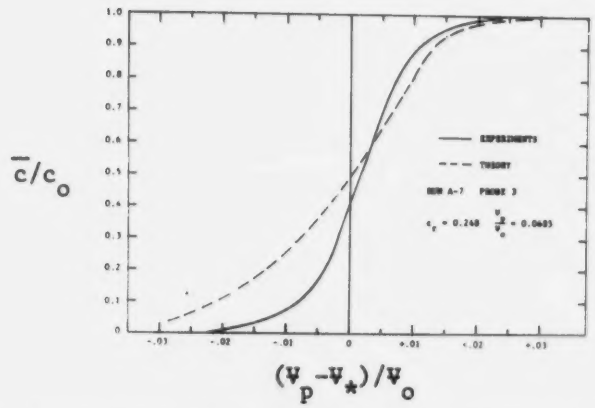

Figure 5.14 Comparison of Experimental and Theoretical Breakthrough Curves During Recharge

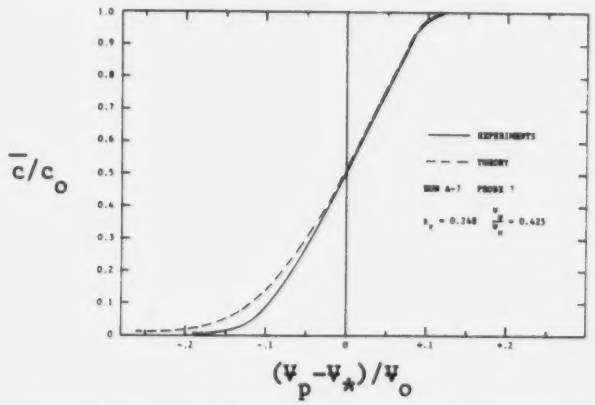

Figure 5.15 Comparison of Experimental and Theoretical Breakthrough Curves During Recharge

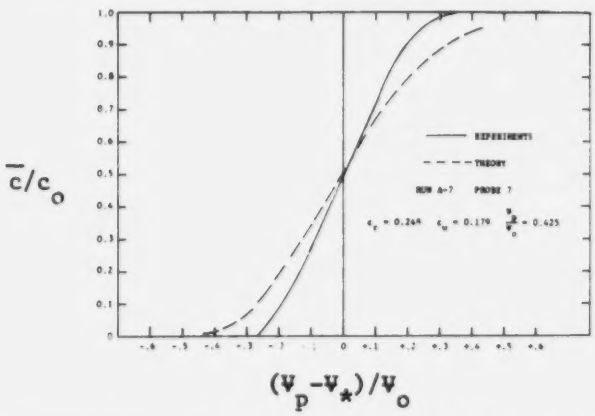

Figure 5.16 Comparison of Experimental and Theoretical Breakthrough Curves During Withdrawal

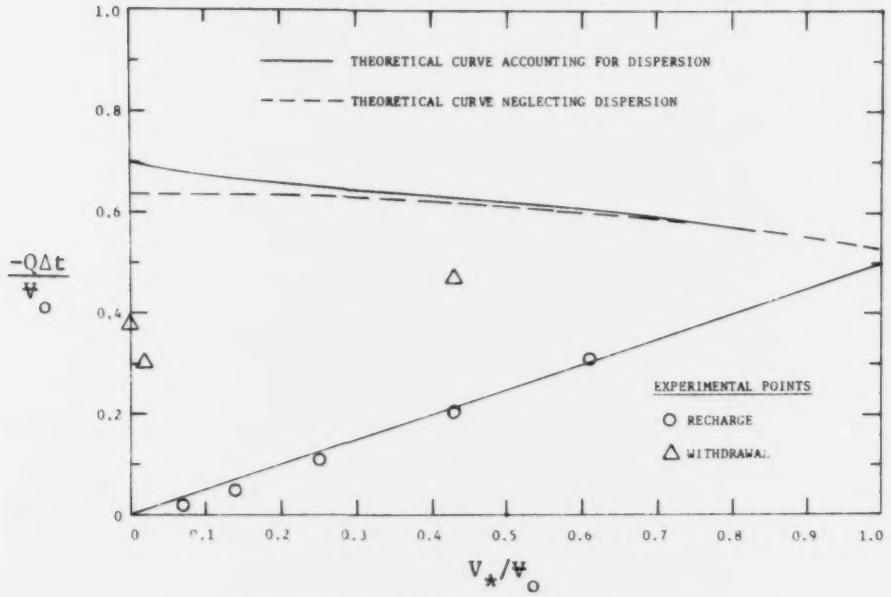

Figure 5.18 Δt as a Function of Time During a Recharge-Storage-Withdrawal Sequence, Run A-7

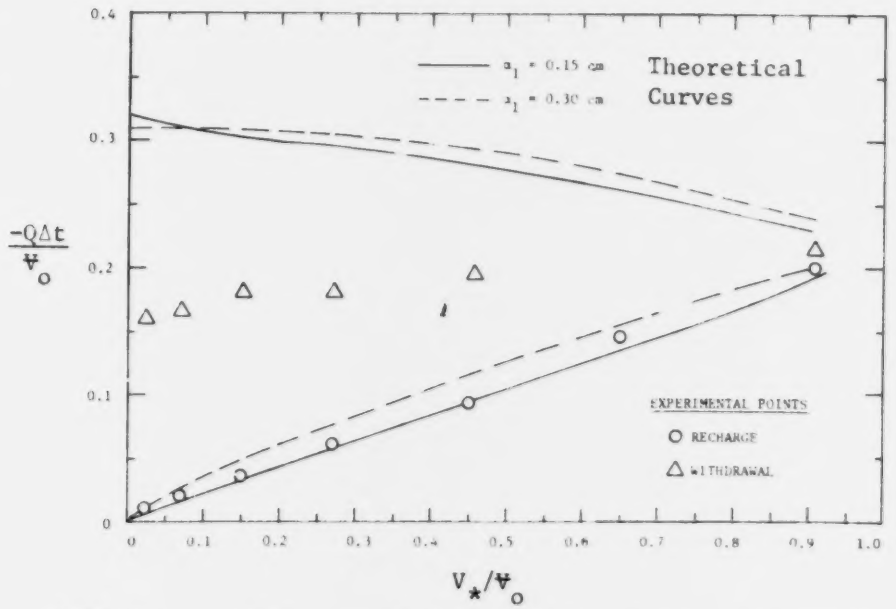

Figure 5.17 Δt as a Function of Time During a Recharge-Storage-Withdrawal Sequence, Run A-2

of the dispersed zone. However, it is observed that Δt decreases systematically. A possible explanation for this decrease is the interaction of density difference and grain dispersion. As shown in Section 3.3, this interaction could decrease the rate of interface tilting, thus lower Δt. This possibility was examined for Run A-2 in Figure 5.17. The longitudinal dispersivity, α_l, was doubled to a value of 0.3 cm and the theoretical curve recalculated. For this value of α_l and for the given parameters of Run A-2, $\Delta/\beta H$ remained at a value greater than one for the entire recharge, storage and withdrawal process reflecting the importance of longitudinal dispersion. The theoretical analysis is now based on the coupled theory (Eq. 3.114) and is shown as a dashed line in Figure 5.17. It appears that the additional dispersion makes little difference in the general trend of the theory, and that the decrease in Δt during withdrawal must be due to some other factor.

It is of interest to evaluate the theoretical results of the immiscible displacement dynamics with and without superimposed grain dynamics. Figure 5.18 presents two theoretical curves, one accounting for the superposition of dispersion (solid line) and one neglecting dispersion (dashed line) for Run A-7. In fact, since both predict the same interface length, it should be expected that the superposed curve would give higher values of Δt. In both cases, predicted values of Δt during withdrawal are substantially larger than those observed. Other experimental values of Δt are tabulated in Table 5.4.

These discrepancies between theoretical and experimental data during the withdrawal cycle may be related to several factors. However, it is unlikely that dispersive effects can account for the difference, for those effects were evaluated in Figure 5.17 and were shown to be relatively small. Most likely, the primary factor is the increasing importance of the curvature of the interface as withdrawal proceeds. This is reflected in Figures 5.17 and 5.18 in which the difference between theory and experiment increases with time. The potential weakness of the theory with a linear interface in volumetric coordinates was identified and discussed in Section 3.4.

One of the ultimate purposes of this research is to predict the amount of freshwater that could be recovered in a recharge-storage-withdrawal sequence. The observed recovery ratios obtained by analyzing the breakthrough curves at the well will be compared with the theoretical results from Section 3.5. For an analysis of various breakthrough curves, it was found that 10% relative concentration at the well was a reasonable choice for the value determining the end of the withdrawal cycle. The observed recovery ratio, $R=V_R/V_o$, using $\bar{c}/c_o=0.1$ at the well is shown in Table 5.5 along with the recovery ratio predicted by the immiscible displacement theory (Eq. 3.119, $b=0.1$). Comparisons with the miscible theories (Sections 3.3 and 3.4) are also included. These computations were based on the matching procedure described in Section 3.5. Also included in Table 5.5 are experimental results reported by Kumer (1968). The predicted recovery ratios show trends similar to those observed in this study and by Kumer, but are somewhat lower. These results indicate

TABLE 5.4

OBSERVED VALUES OF $-Q\Delta t/V_o$ DURING WITHDRAWAL

Probe Number	Run Number					
	A-1	A-2	A-6	A-7	B-2	B-3
1				0.376	0.557	0.336
2	0.162	0.162	0.693	0.300	0.494	0.283
3	0.166	0.164	0.785		0.554	0.310
5		0.180	0.760			
6		0.182				
7	0.199	0.196		0.478		
8	0.211					
9	0.211					
10		0.216				

TABLE 5.5 A COMPARISON OF THEORETICAL RECOVERY RATIOS WITH EXPERIMENTS

Run Number	ε_r	ε_w	$\Delta\rho/\rho$	Q_r (cc/sec)	Q_w (cc/sec)	Average K (cm/sec)	Recovery Ratio, R		
							Observed	Immiscible Theory (Eq.3.119)	Miscible Theory
Present Experiments[1]									
A-7	0.248	0.179	0.021	58.32	112.80	0.49	0.790	0.748	0.700
B-1	0.222	0.216	0.018	61.20	64.80	0.48	0.795	0.717	0.680
B-2	0.277	0.260	0.018	39.24	44.64	0.48	0.728	0.631	0.595
B-3	0.158	0.153	0.018	120.96	129.36	0.48	0.820	0.762	0.720
B-4	0.257	0.251	0.018	44.64	46.80	0.47	0.482	0.291	0.265
Kumar (1968) Experiments[2]									
2	0.334	0.296	0.373	9.98	12.68	0.0081	0.647	0.545	0.515
3	0.459	0.309	0.223	3.05	6.73	0.00785	0.578	0.468	0.440
6	0.647	0.647	0.092	0.8	0.8	0.0099	0.085	0.141	0.132

[1]Recovery based on $\bar{c}/c_o = 0.1$ at the well. [2]Recovery based on $\bar{c}/c_o = 0.03$ at the well.

that dispersion actually decreases the predicted recovery ratio and does not account for the relatively large observed recovery. It appears that the interface curvature may be the important effect in these cases. If the behavior shown in Figure 3.2 for the recharge also occurs during withdrawal, the arrival of the wedge at the well would be delayed. This phenomenon during withdrawal could substantially increase the recovery ratio and account for the decreasing values of Δt observed in Figure 5.17.

ACKNOWLEDGMENTS

This investigation was conducted at the Ralph M. Parsons Laboratory for Water Resources and Hydrodynamics of the Department of Civil Engineering at Massachusetts Institute of Technology under a grant from the Office of Research and Monitoring, Environmental Protection Agency, Research Grant No. 16060ELJ.

The research was supervised by Dr. Lynn W. Gelhar, Associate Professor of Civil Engineering, and while Dr. Gelhar was on sabbatical leave by Drs. Donald R. F. Harleman and Keith D. Stolzenbach.

Mr. Roy Milley assisted in the construction of the laboratory models and Mr. Edward McCaffrey assisted with electronic instrumentation. Mrs. Pat Swan assisted in editorial work and typed the manuscript. The use of the M.I.T. Information Processing Center is acknowledged.

The support and assistance of the Office of Research and Monitoring, Environmental Protection Agency through Mr. Jack W. Keeley, Project Officer, is gratefully acknowledged.

REFERENCES

1. Bachmat, Y. and J. Bear, (1964), "The General Equations of Hydrodynamic Dispersion in Homogeneous Isotropic Porous Mediums", Journal of Geophysical Research, Vol. 69, No. 12, pp. 2561-7.

2. Bear, J. and G. Dagan, (1964), "Moving Interface in Coastal Aquifers", Journal of the Hydraulics Division, Proc. ASCE, Vol. 90, HY 4, pp. 193-215.

3. De Josselin de Jong, G., (1960), "Singularity Distributions for the Analysis of Multiple-Fluid Flow Through Porous Media", Journal of Geophysical Research, Vol. 65, No. 11, pp. 3739-58.

4. Esmail, O. J. and O. K. Kimbler, (1967), "Investigation of the Technical Feasibility of Storing Fresh Water in Saline Aquifers", Water Resources Research, Vol. 3, No. 3, pp. 683-95.

5. Gardner, G. H., J. Downie, and H. A. Kendall, (1962), "Gravity Segregation of Miscible Fluids in Linear Models", Society of Petroleum Engineers Journal, Trans. AIME, Vol. 225, pp. 95-104.

6. Gelhar, L. W. and M. A. Collins, (1971), "A General Analysis of Longitudinal Dispersion in Nonuniform Flow", Water Resources Research, Vol. 7, No. 6, pp. 1511-21.

7. Green, D. W. and R. Cox, (1968), "Storage of Fresh Water in Underground Reservoirs Containing Saline Water, Phase II", Kansas Water Resources Institute, Contribution No. 36.

8. Guymon, G. L., V. H. Scott and A. Hermann, (1970), "A General Solution of the Two Dimensional Diffusion-Convection Equation by the Finite Element Method", Water Resources Research, Vol. 6, No. 6, pp. 1611-17.

9. Hamrick, J. M., (1970), "Density Induced Mixing in Linear Flow Through Porous Media", M.I.T. Department of Civil Eng., MS Thesis.

10. Harleman, D. R. F., P. F. Melhorn, and R. R. Rumer, (1963), "Dispersion Permeability Correlation in Porous Media", Journal of the Hydraulics Division, Proc. ASCE, Vol. 89, HY 2, pp. 67-85.

11. Harleman, D. R. F. and R. R. Rumer, (1963), "Longitudinal and Lateral Dispersion in an Isotropic Porous Medium", Journal of Fluid Mechanics, Vol. 16, Part III.

12. Henry, H. R., (1960), "Salt Intrusion Into Coastal Aquifers", International Association of Sci. Hyd., Pub. No. 52, pp. 478-87.

Preceding page blank

13. Keulegan, G. H., (1954), "Ninth Progress Report on Model Laws for Density Currents; An Example of Density Currents in Permeable Media", National Bureau of Standards Report No. 3411, Washington, D.C.

14. Kohout, F. A., (1970), "Reorientation of Our Saline Water Resources Thinking", Water Resources Research, Vol. 6, No. 5, pp. 1442-48.

15. Kumer, Anil, (1968), "Dispersion and Gravity Segregation of Miscible Fluids in Porous Media for Stratified Radial Flow Systems", MS Thesis, Louisiana State University, Baton Rouge.

16. Kumer, A. and O. K. Kimbler, (1970), "Effect of Dispersion, Gravity Segregation, and Formation Stratification on the Recovery of Freshwater Stored in Saline Aquifers", Water Resources Research, Vol. 6, No. 6, pp. 1689-1700.

17. Li, W. H. and G. T. Yeh, (1968), "Dispersion at the Interface of Miscible Liquids in a Soil", Water Resources Research, Vol. 4, No. 2, pp. 369-77.

18. List, E. J. and N. H. Brooks, (1967), "Lateral Dispersion in Saturated Porous Media", Journal of Geophysical Research, Vol. 72, No. 10, pp. 2531-41.

19. Mercado, A., (1967), "The Spreading Pattern of Injected Water in a Permeability Stratified Aquifer", Symposium of Haifa, International Assoc. of Sci. and Hydrology, Pub. No. 72.

20. Moulder, E. A., (1970), "Freshwater Bubbles: A Possibility for Using Saline Aquifers to Store Water", Water Resources Research, Vol. 6, No. 5, pp. 1528-31.

21. Perrine, R. L. and G. M. Gay, (1964), "Radial Motion of a Surface Between Fluids Within a Porous Media", Journal of Canadian Petroleum Technology, Vol. 3, No. 1, pp. 33-38.

22. Reddel, D. L. and D. K. Sunada, (1970), "Numerical Simulation of Dispersion in Ground Water Aquifers", Colorado State Univ., Hydrology Paper No. 41.

23. Rose, D. A. and J. B. Passioura, (1971), "Gravity Segregation During Miscible Displacement Experiments", Soil and Science, Vol. 3, No. 4, pp. 258-65.

24. Rumer, R. R. and D. R. F. Harleman, (1963), "Intruded Salt-Wedge in Coastal Aquifers", Journal of the Hydraulics Division, Proc. ASCE, Vol. 89, HY 6, pp. 193-220.

25. Schiedegger, A. E., (1961), "General Theory of Dispersion in Porous Media", Journal of Geophysical Research, Vol. 66, No. 10, pp. 3273-8.

26. Shamir, U. Y. and G. Dagan, (1971), "Motion of the Seawater Interface in Coastal Aquifers; A Numerical Solution", Water Resources Research, Vol. 7, No. 3, pp. 644-57.

27. Shamir, V. Y. and D. R. F. Harleman, (1967), "Numerical Solutions for Dispersion in Porous Mediums", Water Resources Research, Vol. 3, No. 2, pp. 557-81.

28. Theis, C. V., (1967), "Aquifers and Models", Proc. National Symposium on Ground Water Hydrology, American Water Resources Assoc., pp. 138-48.

DEFINITION OF SYMBOLS

The primary symbols are defined below. A few additional special symbols are defined where used.

Symbol	Definition	Dimension
A	$Q/2\pi nH$	(L^2/T)
$A_{r,w}$	$Q_{r,w}/2\pi nH$	(L^2/T)
b	n/H at the well	
c	Concentration of material	
c_o	Concentration of material in liquid 2	
$\bar{c}$	Depth average of concentration	
C_n	Matching constant between cycles (n=1,2,...)	
d_{50}	Mean grain diameter	(L)
D	$K\Delta\rho H/n\rho$	(L^2/T)
D_1	Longitudinal grain dispersion coefficient	(L^2/T)
D_2	Lateral grain dispersion coefficient	(L^2/T)
D_m	Molecular diffusion coefficient	(L^2/T)
E	Density induced dispersion coefficient	(L^2/T)
E_1	A constant dispersion coefficient	(L^2/T)
$\bar{E}$	Average density dispersion coefficient	(L^2/T)
E_t	Total (gross) dispersion coefficient	(L^2/T)
f	Relative interface height (n/H)	(L/L)
$F(z),F(z')$	Dependent similarity functions (n/H)	
g	Gravitational constant	(L/T^2)
H	Aquifer height	(L)
$j(x,t)$	Constant of integration	
j_x	Mass flux of material relative to mean Linear flow	(M/TL^2)
$\bar{J}$	Mass flux of material relative to linear mean flow, for immiscible displacement	(M/TL^2)
k	Intrinsic permeability	(L^2)
K	Hydraulic conductivity	(L/T)
L	Interface length for linear flow	(L)
n	Porosity	
p	Pressure	(M/T^2L)

Preceding page blank

Symbol	Definition	Dimension
Q	Recharge (+) or withdrawal (-) rate in radial flow	(L^3/T)
Q_r, Q_w	Recharge rate, withdrawal rate magnitude	(L^3/T)
r	Horizontal radial coordinate	(L)
r_i	Radius to interface	(L)
r_*	Radius to convective front	(L)
r_p	Radius to probe	(L)
r_w	Well radius	(L)
R	Recovery ratio ($=V_R/V_o$)	
s	Piezometric difference between two points	
S	Interface slope for linear flow (=L/H)	
S_{50}	Slope of concentration breakthrough curve at $\bar{c}/c_o=0.5$	(T^{-1})
t	Time	(T)
t_o	Time at the start of a process	(T)
t_{50}	Time from the start of a process till $\bar{c}/c_o=0.5$ at radius r	(T)
u	Horizontal seepage velocity in linear flow	(L/T)
$u_{1,2}$	Horizontal seepage velocity in liquid 1,2	(L/T)
u_i	Velocity of the interface	(L/T)
$\bar{u}$	Seepage velocity relative to mean flow	(L/T)
U	Mean linear convective seepage velocity	(L/T)
v	Vertical seepage velocity in linear flow	(L/T)
v_r	Horizontal radial seepage velocity	(L/T)
v_y	Vertical seepage velocity in radial flow	(L/T)
V	Volumetric coordinate ($=\pi nHr^2$)	(L^3)
V_*	Volumetric distance to convective front	(L^3)
$\bar{V}$	$= V - V_*$	(L^3)
V_i	Volumetric distance to the interface from V origin	(L^3)
V_ℓ	$= V - V_i$	(L^3)
V_o	Net injected Volume at the start of a process	(L^3)
V_p	Volumetric distance to a probe in the model	(L^3)
V_R	Volume of liquid recovered	(L^3)

Symbol	Definition	Dimension
x	Horizontal coordinate in linear flow	(L)
x_i	Linear distance to interface	(L)
x_1	$= x - x_i$	(L)
$\bar{x}$	$= x - Ut$	(L)
y	Vertical coordinate	(L)
z, z'	Independent similarity variables	
α_1	Longitudinal dispersivity	(L)
α_2	Lateral dispersivity	(L)
β	Inverse slope of the interface = L/H in linear flow, = $\Delta\Psi/H$ in radial flow	(L^2)
β_o	Inverse slope at the start of a process in radial flow	(L^2)
δ	Width of the dispersed zone about the interface	(L)
Δ	Volumetric width of the dispersed zone	(L^3)
Δ_o	Volumetric width of the dispersed zone at the start of a process	(L^3)
Δt	$= 1/S_{50}$	(T)
$\Delta\Psi$	Volumetric length of the interface	(L^3)
$\Delta\rho$	Density difference between liquids 1 and 2	(M/L^3)
$\Delta\tau$	$= K\Delta\rho\Delta t/n\rho H$	
ζ	Distance to interface from top of aquifer	(L)
η	Distance to interface from bottom of aquifer	(L)
θ	$= \beta/\Psi_*^{1/2}$ in radial flow	($L^{1/2}$)
μ	Dynamic viscosity	(M/LT)
ν	Kinematic viscosity ($=\mu/\rho$)	(L^2/T)
ξ	Transformed time coordinate	
ρ	Density	(M/L^3)
$\rho_{1,2}$	Density of liquid 1,2	(M/L^3)
$\bar{\rho}$	Depth average density	(M/L^3)
τ	Dimensionless time ($=K\Delta\rho t/n\rho H$)	
ε	Parameter characterizing radial flow ($=\sqrt{D/A}$)	
$\varepsilon_{r,w}$	$=\sqrt{D/A_{r,w}}$	
$\phi_{1,2}$	Piezometric Head in liquid 1,2	(L)

APPENDICES

		Page No.
A.	Range of Validity of Approximation in Eq. 2.55	120
B.	A Note on Boundary Conditions	123
C.	An Estimate of Electronic Dispersion for the Averaging Probes	126

Preceding page blank

Appendix A

Range of Validity of Approximation in Eq. (2.55)

In Section 2.3 it was assumed that the interface would remain linear (Eq. 2.38), and that the net effect of grain dispersion would be to decrease the rate of interfacial tilting. Thereafter, the primary approximation used to develop the coupled solution involved the application of $\partial u/\partial y$ (Eq. 2.53) at the mean interfacial position in order to determine $\partial u_i/\partial y$ (Eq. 2.56). The approximation

$$\left.\frac{\partial u}{\partial y}\right|_{x=x_i} = \frac{\partial u_i}{\partial y} \tag{A.1}$$

was introduced in Eq. (2.55). The following analysis indicates when this approximation is valid.

If the interface $x_i(y,t)$ is of a linear form as given in Eq. (2.38) with β unspecified, the analysis of Section 2.2 applies and the density gradient can be obtained from Eqs. (2.21) and (2.48) as given in Eq. (2.58). Thus Eq. (2.53) can be written

$$\frac{\partial u}{\partial y} = \frac{K}{n}\frac{\Delta\rho}{\rho}\frac{1}{\sqrt{4\pi\xi}}\exp\left[-\frac{(x-x_i)^2}{4\xi}\right] \tag{A.2}$$

In this equation $x_i = x_i(y,t)$ is the only function of y, and the equation has the integrated form

$$u = \frac{K}{n}\frac{\Delta\rho}{\rho}\frac{1}{2\beta}\left[\operatorname{erf}\frac{x-Ut}{\sqrt{4\xi}} - \operatorname{erf}\frac{x-x_i}{\sqrt{4\xi}} + j(x,t)\right] \tag{A.3}$$

where $j(x,t)$ is a constant of integration.

From the continuity equation (Eq. 2.51)

$$v = -\int_{y=-H/2}^{y}\frac{\partial u}{\partial x}\,dy$$

which satisfies the condition $v = 0$ at $y = -H/2$. The requirement that $v = 0$ at $y = H/2$ implies that

$$\frac{\partial}{\partial x}\left[\int_{-H/2}^{H/2} u\,dy\right] = 0$$

Expressing the velocity in terms of the convective coordinate system,

$$\bar{u} = u - U$$

this flux condition becomes

$$\int_{-H/2}^{+H/2} \bar{u}\, dy = 0$$

This condition is used to evaluate $j(x,t)$, with the result

$$u = \frac{K}{n}\frac{\Delta\rho}{\rho}\frac{1}{2\beta}\left[\frac{1}{H}\int_{-H/2}^{+H/2} \operatorname{erf}\frac{x-x_i}{\sqrt{4\xi}}\, dy - \operatorname{erf}\frac{x-x_i}{\sqrt{4\xi}}\right] \tag{A.4}$$

Along the interface ($x=x_i$), the interfacial velocity relative to the convective front is defined at $\bar{u}_i$,

$$\bar{u}_i = u_i - U \equiv \bar{u}\Big|_{x=x_i} \tag{A.5}$$

which is combined with Eq. (A.4) to yield

$$\bar{u}_i = \frac{K}{n}\frac{\Delta\rho}{\rho}\frac{1}{2\beta H}\left[\int_{-H/2}^{+H/2} \operatorname{erf}\frac{x-x_i}{\sqrt{4\xi}}\, dy\right]_{x=x_i} \tag{A.6}$$

Equation (A.6) is evaluated using

$$\int \operatorname{erf} z\, dz = z \operatorname{erf} z + \frac{e^{-z^2}}{\sqrt{\pi}} + \text{const}$$

and can be expressed as

$$\bar{u}_i = \frac{K}{n}\frac{\Delta\rho}{\rho}\frac{\sqrt{4\xi}}{(-2\beta^2 H)}\left[\mu_1 \operatorname{erf}\mu_1 + \frac{e^{-\mu_1^2}}{\sqrt{\pi}} - \mu_2 \operatorname{erf}\mu_2 - \frac{e^{-\mu_2^2}}{\sqrt{\pi}}\right] \tag{A.7}$$

where

$$\mu_1 = \frac{\beta(y-H/2)}{\sqrt{4\xi}}$$

$$\mu_2 = \frac{\beta(y+H/2)}{\sqrt{4\xi}} \tag{A.8}$$

Differentiating this equation with respect to y yields

$$\frac{\partial \bar{u}_i}{\partial y} = \frac{K}{n}\frac{\Delta\rho}{\rho}\frac{-1}{2\beta H}[\mathrm{erf}\mu_1 - \mathrm{erf}\mu_2] \tag{A.9}$$

The approximation in Eq. (2.55) involves replacing quantity

$$\left.\frac{\partial u}{\partial y}\right|_{x=x_i} = \frac{K}{n}\frac{\Delta\rho}{\rho}\frac{1}{\sqrt{4\pi\xi}} \tag{A.10}$$

from Eqs. (2.54) and (2.60) by the expression in Eq. (A.9). This will be valid when

$$\mu_1, \mu_2 << 1 \tag{A.11}$$

in which case, using $\mathrm{erf}\mu_i = \frac{2}{\sqrt{\pi}}\mu_i$,

$$\frac{\partial u_i}{\partial y} = \frac{K}{n}\frac{\Delta\rho}{\rho}\frac{1}{\sqrt{4\pi\xi}} = \left.\frac{\partial u}{\partial y}\right|_{x=x_i} \tag{A.12}$$

The maximum absolute values of μ_1 and μ_2 occur at $y = \pm H/2$ and thus the restrictions on μ_1, μ_2 are seen to be equivalent to the requirement that

$$\frac{\beta H}{\sqrt{4\xi}} = \frac{L}{\sqrt{4\xi}} << 1$$

Since the approximate width of the dispersed zone about the interface, δ, is given by $\sqrt{4\pi\xi}$ (Eq. 2.47) the restriction implied by the approximation in Eq. (2.55) is $L << \delta$. Therefore, the result obtained in Section 2.3 is expected to be valid when the dispersed zone is wide in comparison to the wedge length.

Appendix B

A Note on Boundary Conditions

For a confined aquifer of constant thickness, the boundary condition to be satisfied by the solution of the convective dispersion equation at the upper and lower boundaries is

$$\frac{\partial c}{\partial y} = 0, \quad y = \pm H/2 \tag{B.1}$$

The approximate solution to the convective dispersion equation for the appropriate boundary conditions considered in Sections 2.2 and 2.3 was as given by Eqs. (2.44) or (2.58). For this solution

$$\frac{\partial}{\partial y}(c/c_o) = -\frac{\beta}{\sqrt{4\pi\xi}} \exp\left(\frac{-(x-x_i)^2}{4\xi}\right) \tag{B.2}$$

where $x-x_i = \bar{x}-\beta y$. At the lower boundary, $y = -H/2$, and Eq. (B.2) becomes

$$\frac{\partial}{\partial y}(c/c_o) = -\frac{\beta}{\sqrt{4\pi\xi}} \exp\left(\frac{-(x+\beta H/2)^2}{4\xi}\right) \tag{B.3}$$

The consequence of not satisfying the boundary conditions is the creation of an artificial mass flux through the aquifer in the vertical direction. At $y = -H/2$ this flux is proportional to Eq. (B.3).

The possible local effects of not satisfying this boundary condition can be evaluated by comparing the magnitude of the ficticious vertical flux to the horizontal dispersive mass flux at a given point. The ratio of these two fluxes is, from Eqs. (2.58) and (B.3),

$$D_2 \frac{\partial c}{\partial y} / D_1 \frac{\partial c}{\partial x} = \beta D_2/D_1 \tag{B.4}$$

Thus, it is seen that, even though the ratio D_2/D_1 is generally small (10^{-1} or less), the implied vertical flux of mass at the boundary will eventually become equal to or larger than the horizontal flux because β increases with time as indicated in Eqs. (2.63) and (2.68). The implication is that the effects of the no-flux condition at the boundaries may become important when $\beta > D_1/D_2$.

Another method of estimating the possible effects of the boundary conditions is to compare the horizontal and vertical components of the total mass transport through the aquifer. Hamrick (1970) computed the artificial vertical flux and compared it with the total horizontal flux

evaluated at its maximum, $\bar{x} = 0$. The total vertical dispersive mass flux is given by

$$J_y = - \int_{-\infty}^{+\infty} \rho D_2 \frac{\partial c}{\partial y} \, dx = \rho c_o D_2 \beta \tag{B.5}$$

and the maximum horizontal mass flux relative to the mean motion is, assuming ρ to be constant, at $\bar{x} = 0$,

$$J_x = -\rho D_1 \int_{-H/2}^{+H/2} \frac{\partial c}{\partial x}\bigg|_{\bar{x}=0} dy + \rho \int_{-H/2}^{H/2} (\bar{cu})\bigg|_{\bar{x}=0} dy \tag{B.6}$$

$$= - \frac{\rho c_o D_1}{\beta} [\mathrm{erf}(\frac{\sqrt{\pi} L}{2\delta}) + \frac{3}{2} \frac{\bar{E}}{D_1} \Phi(\frac{L}{\delta})]$$

where the integral

$$\Phi(\frac{L}{\delta}) = \int_0^1 \mathrm{erf}^2(\frac{Lw\sqrt{\pi}}{2\delta}) dw \; ; \quad w = \frac{2y}{H} \tag{B.7}$$

may be evaluated numerically. However, for small $\frac{Lw\sqrt{\pi}}{2\delta}$, the error function can be approximated by the first term of its series expansion and Φ is given approximately as

$$\Phi(\frac{L}{\delta}) \simeq \frac{1}{3}(\frac{L}{\delta})^2 \; ; \quad \frac{\beta y}{\delta} << 1 \tag{B.8}$$

At its maximum, within the aquifer

$$\frac{\beta y}{\delta} = \frac{1}{2} \frac{L}{\delta}$$

Under these conditions the error function in Eq. (B.6) is approximated by $\mathrm{erf}(\sqrt{\pi} L/2\delta \simeq L/\delta$. Thus, Eq. (B.8) is reasonably accurate for the range of δ/L for which the interaction solution is applicable ($\delta/L >> 1$). As a consequence J_x can be approximated by

$$J_x = - \frac{\rho c_o D_1}{\beta} [\frac{L}{\delta} + \frac{1}{2} \frac{\bar{E}}{D_1} (\frac{L}{\delta})^2] \tag{B.9}$$

The ratio of the absolute values of the total mass flux is given by

$$\left|\frac{J_y}{J_x}\right| = \frac{D_2}{D_1}\frac{\delta}{L}\left[\frac{\beta^2}{1+(3/2)(E/D_1)(L/\delta)}\right] \qquad (B.10)$$

Again, it is seen that the implied ratio of vertical to horizontal mass transport will eventually become large, in this case because both δ/L and β increase with time. Thus, from consideration of both local fluxes and total mass transport, there is the implication that the boundary conditions may, for sufficiently large times, influence interfacial tilting and overall mixing for the coupled analysis (Section 2.3).

Appendix C

An Estimate of Electronic Dispersion for the Averaging Probes

The following analysis is based on the solution for the concentration in a uniform linear flow with no density difference between the two fluids,

$$c/c_o = \frac{1}{2} + \frac{1}{2}\,\mathrm{erf}\left(\frac{x-ut}{\sqrt{4D_1 t}}\right) \tag{C-1}$$

in which x is the longitudinal coordinate, u is the seepage velocity and D_1 is the longitudinal dispersion coefficient. It will be assumed that a probe at $x = x_1$ measures the average concentration in a region $x_1 \pm a$ around the probe because of the generated electronic field. The indicated average concentration, $\hat{c}$, from the probe readout becomes

$$\frac{\hat{c}}{c_o} = \frac{1}{2}\int_{x=x_1-a}^{x=x_1+a} (1/2a)\left(1+\mathrm{erf}\,\frac{x-ut}{\sqrt{4D_1 t}}\right) dx \tag{C-2}$$

and after integration

$$\frac{\hat{c}}{c_o} = \frac{\sqrt{4D_1 t}}{4a}\left(\frac{x_1+a-ut}{\sqrt{4D_1 t}}\,\mathrm{erf}\,\frac{x_1+a-ut}{\sqrt{4D_1 t}} - \frac{x_1-a-ut}{\sqrt{4D_1 t}}\,\mathrm{erf}\,\frac{x_1-a-ut}{\sqrt{4D_1 t}} + \frac{e^{-(x_1+a-ut)^2/4D_1 t}}{\sqrt{\pi}} - \frac{e^{-(x_1-a-ut)^2/4D_1 t}}{\sqrt{\pi}} \right) \tag{C-3}$$

From Eq. (C-3) we find that

$$(\Delta \hat{t})^{-1} \equiv \left.\frac{\partial \frac{\hat{c}}{c_o}}{\partial t}\right|_{x_1=ut} = -\frac{u}{2a}\,\mathrm{erf}\,\frac{a}{\sqrt{4D_1 t}} \tag{C-4}$$

and as $a \to 0$, Eq. (C-4) reduces to

$$(\Delta t)^{-1} = \left.\frac{\partial \frac{c}{c_o}}{\partial t}\right|_{x_1=ut} = -\frac{u}{\sqrt{4\pi D_1 t}} \tag{C-5}$$

which corresponds to a point measurement with no electronic dispersion. The effects of electronic dispersion can be assessed by considering the ratio of the indicated and actual rates of change of concentration (Eqs. (C-3) and (C-4))

$$\Delta t/\Delta \hat{t} = (\delta/2a)\,\mathrm{erf}\,(a\sqrt{\pi}/\delta) \qquad \text{(C-6)}$$

where δ is the dispersed zone thickness defined by

$$\delta^{-1} = \left.\frac{\partial c}{\partial x}\right|_{x=ut} = (4\pi D_1 t)^{-1/2}$$

Figure C-1 shows this ratio as a function of a/δ. It can be seen that when $a/\delta < 0.2$, the indicated and average rates of change differ by less than 5%. The possible error in Δt is of importance because the values of Δt from experiments are used to determine dispersion coefficients.

This analysis can be adapted to the observations in radial flow if we determine δ during recharge from Eq. (5.3)

$$\delta^{-1} = \left.\frac{\partial}{\partial r}\left(\frac{c}{c_o}\right)\right|_{r=r_*} = (4\pi\alpha_1 r_*/3)^{-1/2}$$

and estimate that 2a is equal to the spacing of the probe electrodes (a=3/8 in.). Using these relationships and the estimated dispersivity from Section 5.4 (α_1=0.15 cm), the radius r_* corresponding to a given value of a/δ can be determined as shown in Figure C-1. Probe locations are also shown.

From Figure C-1 it can be seen that during recharge the distortion due to electronic dispersion will be significant for only the first few probes near the wall. For tests with a density difference or measurements during withdrawal, this distortion will be unimportant because the thickness of the dispersed zone will be larger under these conditions.

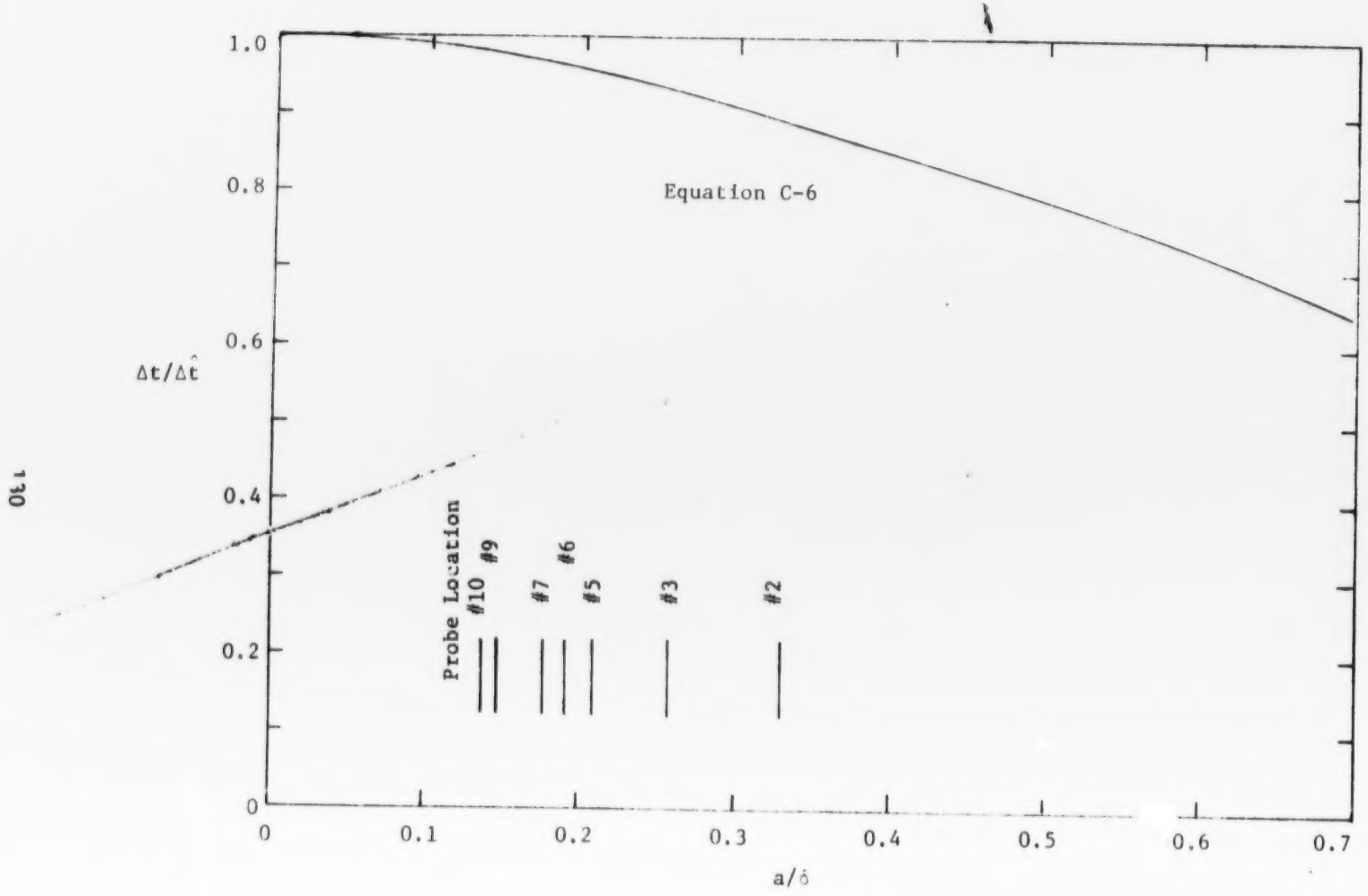

Figure C-1 Estimate of Electronic Distortion During Recharge

U.S. GOVERNMENT PRINTING OFFICE: 1974—484-484/274 1-3